IMPROVEMENTS IN MASS SPECTROMETRIC ANALYSES WITH DIFFERENTIAL ION MOBILITY SPECTROMETRY

Samantha L. Isenberg

A dissertation submitted to the faculty of the University of North Carolina at Chapel hill in partial fulfillment of the requirements for the degree of Doctor of Philosophy in the Department of Chemistry

Chapel Hill
2014

Approved by:

Gary L. Glish

James Jorgenson

Leslie Hicks

Paul Armistead

Marcey Waters

ABSTRACT

Samantha L. Isenberg: Improvements in Mass Spectrometric Analyses with Differential Ion Mobility Spectrometry
(Under the direction of Gary L. Glish)

Mass spectrometry (MS) based analyses of complex samples often require separations to improve signal-to-background and remove isobaric and isomeric interferences prior to mass analysis. Chromatographic and electrophoretic separations are commonly employed prior to ionization, but these separations can add minutes to hours to mass spectrometric analyses. Ion mobility spectrometry (IMS) has the ability to separate ions based on shape-to-charge rather than mass-to-charge, making IMS complementary to MS. IMS has been shown to improve signal-to-background and have the ability to separate isomeric/isobaric species.

There are several different variants of ion mobility spectrometers, including drift-tube IMS (DTIMS), travelling-wave IMS (TWIMS), trapped IMS (TIMS), and differential IMS (DIMS). DIMS is unique from other types of IMS because it is the only variant in which the electric field alternates between a low and high field. Thus, DIMS provides a separation of ions based on the difference in mobilities between two electric fields, whereas the others provide a separation that is based on only the low-field ion mobility. Low-field ion mobility is directly proportional to the collision cross-section (CCS) of an ion and is often closely correlated to the mass-to-charge ratio. As a differential ion mobility separation, DIMS is no longer directly correlated to CCS, and is therefore more orthogonal to mass spectrometry.

The work described in this dissertation focuses on the optimization of DIMS separations as well as the use of DIMS for biological and environmental applications. Fundamental studies with respect to improving the performance of DIMS are presented with the goal of maximizing both resolving power and sensitivity of the separations. Optimization of resolving power and sensitivity allows DIMS to be used for a wide variety of applications. DIMS allows for the examination of ion reactions including a charge-reduction in the ion transfer optics prior to mass analysis. When coupled to tandem mass spectrometry (MS/MS), DIMS-MS/MS has the ability to be used as an "electronic immunoassay" for biomarkers in complex biological samples. A fast separation prior to MS for the real-time analysis of aerosols formed by pyrolysis is also achievable through the use of DIMS.

ACKNOWLEDGEMENTS

First and foremost, I would like to thank Dr. Gary Glish for guidance, support and patience over the years. Thank you for the freedom you have given me in conducting my own research, allowing me to become an independent, confident scientist.

I am so blessed to have had my parents' unwavering support over the years. I truly cannot put into words how lucky I am.

Finally, I would like to thank Glish lab members, past and present, for sharing the good and bad times. I hope my giggles have made working with me more bearable.

TABLE OF CONTENTS

LIST OF TABLES

LIST OF FIGURES

LIST OF ABBREVIATIONS AND SYMBOLS

A	alanine
Å	Angstrom (10^{-10} meters)
ANP	atrial natriuretic peptide
BNP	brain natriuretic peptide
C	cysteine
CCS	collision cross-section
CG1	antigen peptide FLLPTGAEA
CID	collision-induced dissociation
cm	centimeter
CPC	condensation particle counter
CV	compensation voltage
Cys	cysteine
°C	degrees Celsuis
D	diffusion
D	aspartic acid
Da	dalton
dc	direct current
Δd	oscillation amplitude of ion in DIMS during one period of the waveform (d_h-d_l)
DFT	density functional theory
d_h	displacement of ion during high field portion of waveform
DIMS	differential ion mobility spectrometry
DIMS-MS	differential ion mobility spectrometry coupled to mass spectrometry

DIMS-MS/MS	differential ion mobility spectrometry coupled to tandem mass spectrometry
d_l	displacement of ion during low field portion of waveform
DMA	differential mobility analyzer
DTIMS	drift-tube ion mobility spectrometry
DTT	dithiothreitol
DV	dispersion voltage
E	electric field
E	glutamic acid
e	fundamental charge constant (1.602×10^{-19} coulombs/mole)
E_C	compensation field (compensation voltage divided by gap between electrodes)
E_D	dispersion field (dispersion voltage divided by gap between electrodes)
EESI	extractive electrospray ionization
E_l	low electric field (< ~10^4 V/cm)
E_h	high electric field (> ~10^4 V/cm)
EI	electron ionization
ESI	electrospray ionization
F	phenylalanine
f	frequency
F^+	fragment ion
FBS	fetal bovine serum
Fmoc	9-fluorenylmethoxycarbonyl
FTICR	Fourier transform ion cyclotron resonance (mass spectrometer)

FWHM	full-width at half-max of a Gaussian peak
G	glycine
g	gap between electrodes
G3	generation 3
G4	generation 4
GC	gas chromatography
GC-DIMS	gas chromatography coupled to differential ion mobility spectrometry
g_e	effective analytical gap (g-Δd)
GLR	antigen peptide FLSSANEHL
H	histidine
HCT	high capacity trap
He	helium
HLA	human leukocyte antigen
HPLC	high-performance liquid chromatography
Hz	Hertz
%He	percent helium
I	isoleucine
ICP	inductively coupled plasma
i.d.	inner diameter
IMS	ion mobility spectrometry
IMS-MS	ion mobility spectrometry coupled to mass spectrometry
K	ion mobility ($cm^2V^{-1}s^{-1}$)
K	Kelvin

K_0	reduced ion mobility
k_B	Boltzmann's constant (1.38×10^{-23} J/K)
kHz	kiloHertz (10^3 Hertz)
K_h	high field mobility
kJ	kilojoule
K_l	low field mobility
kV	kilovolt
L	liter
L	leucine
LC	liquid chromatography
LC-MS	liquid chromatography coupled to mass spectrometry
LIT	linear ion trap
LLE	liquid-liquid extraction
LOD	limit of detection
LTPI	low-temperature plasma ionization
M	molar
M	methionine
m	mass
μ	reduced mass $\left(\frac{m_1 m_2}{m_1+m_2}\right)$
$[M+H]^+$	protonated molecule
$[M+Na]^+$	sodiated molecule
MHz	MegaHertz (10^6 Hertz)
min	minute

mL	milliliter
µL	microliter
µM	micromolar
mm	millimeter
MS	mass spectrometry
ms	millisecond
MS/MS	tandem mass spectrometry
mTorr	milliTorr (10^{-3} Torr)
m/z	mass-to-charge ratio
N	number density of gas molecules
N	asparagine
n	number of trials
N_2	nitrogen
nESI	nano-electrospray ionizatoin
ng	nanogram
nM	nanomolar
NT-proBNP	76 residue peptide, formed from cleavage of pro-BNP
π	pi
P	pressure
P	period of waveform
P	proline
P_0	standard pressure (1 atm)
pM	picomolar

ppm	parts per million
pro-BNP	108 residue peptide, precursor to BNP and NT-proBNP
PTR	proton transfer reaction
PyEESI	pyrolysis coupled to extractive electrospray ionization
PyLTPI	pyrolysis coupled to low-temperature plasma ionization
Q	glutamine
Q-ToF	quadrupole time-of-flight
R	resolution
R	arginine
rf	radio frequency
RP	resolving power
S	serine
σ	standard deviation
sin	sine
SPE	solid-phase extraction
T	temperature
T	threonine
t	time
T_0	standard temperature (20ºC)
TBACl	tetrabutylammonium chloride
t_h	time of high-field portion of waveform
TIMS	trapped ion mobility spectrometry
t_l	time of low-field portion of waveform

TWIMS	travelling-wave ion mobility spectrometry
%T	% ion transmission
$\%T_{trans}$	% ion transmission with transparent DIMS compared to without DIMS
$\%T_{active}$	% ion transmission with active DIMS compared to without DIMS
$\bar{x}$	average
XRF	x-ray fluorescence
V	volt
V	valine
v	volume
$V_{0\text{-}P}$	voltage from 0 to peak of a waveform
$V_{P\text{-}P}$	voltage from peak-to-peak of a waveform
w	peak width
Y	tyrosine
z	charge
Ω	collision cross-section
ω	radial frequency ($2\pi f$)

CHAPTER 1: INTRODUCTION TO DIFFERENTIAL ION MOBILITY SPECTROMETRY

1.1 Separations with mass spectrometry

Mass spectrometry (MS) is a common analytical method used in a wide variety of applications because it provides high sensitivity and resolution with fast analysis times. However, issues such as low signal-to-background, isobaric/isomeric interferences, and ionization suppression can arise with complex samples. To alleviate these drawbacks, separations are frequently used in conjunction with MS. Pre-ionization separation techniques such as chromatography and electrophoresis are regularly employed to improve MS analyses. These separations can add minutes to hours to the total analysis time and often require sample preparation prior to the separation. Common sample preparation techniques including filtration, solid-phase extraction (SPE) and liquid-liquid extraction (LLE) are often labor-intensive and time-consuming.

Alternatively or in addition to pre-ionization separation techniques and sample preparation, gas-phase separations such as ion mobility can be used in conjunction with mass spectrometry. Ion mobility techniques hold potential for signal-to-background improvement as well as the elimination of isobaric interferences in complex samples.[1-3] Because ion mobility is performed post-ionization, these separations will not lessen sensitivity issues due to ionization suppression.

1.2 Introduction to ion mobility spectrometry

Ion mobility spectrometry (IMS) uses an applied electric field to separate ions traversing through a buffer gas. Size, shape, charge state and ion-molecule interactions with the buffer gas govern the mobility of an ion traveling through a collision gas under a given electric field.[1,2] Ions with smaller collision cross-sections (CCS) will undergo fewer collisions with the buffer gas and will arrive at the detector before ions with larger collision cross-sections (Figure 1.1). The buffer gas used in IMS is most commonly helium or nitrogen, but other gases can be used.

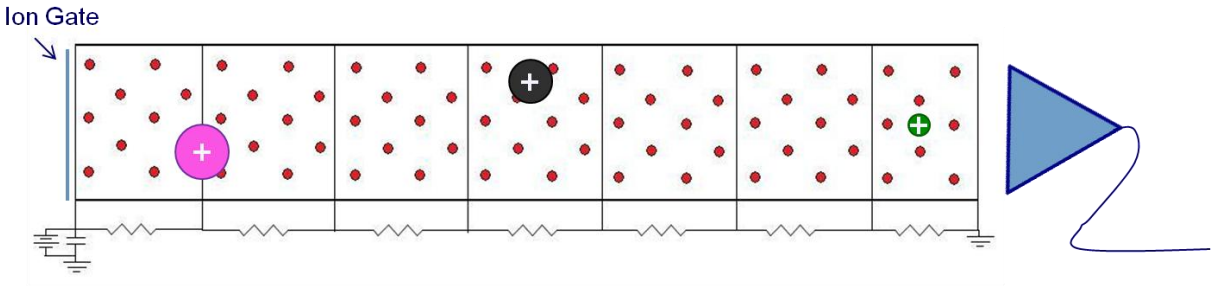

Figure 1.1 IMS drift-tube, where successive ring electrodes decrease in voltage over the length of the drift tube. Ion cross-sections: pink>black>green, such that the green ion undergoes the least number of collisions and arrives at the detector first.

In IMS, the drift time of an ion can be used to calculate reduced ion mobility and collision cross-section (Equations 1.1-1.3)[1], where t is the drift time of a given ion, d is distance or length of the IMS drift cell, K is the ion mobility, E is electric field across the drift tube, K_0 is the reduced ion mobility at standard temperature (T_0) and pressure (P_0), T is temperature, P is pressure, N is the number density of buffer gas molecules, e is the charge of the ion, μ is reduced mass, k_B is Boltzmann's constant, and Ω is the collision cross-section (CCS) of the ion.

$$t = \frac{d}{KE} \qquad \text{(Equation 1.1)}$$

$$K_0 = K\left(\frac{P}{P_0}\right)\left(\frac{T_0}{T}\right) = K\left(\frac{N}{N_0}\right) \quad \text{(Equation 1.2)}$$

$$K_0 = \frac{3e}{16N_0}\left(\frac{2\pi}{\mu k_B T}\right)^{1/2}\frac{1}{\Omega} \quad \text{(Equation 1.3)}$$

The relationship between ion mobility and CCS makes IMS useful for studying protein conformations. For example, protein misfolding diseases have been studied using IMS[6] because unfolded, partially folded, and native protein conformations are separable by their collision cross-sections in most cases. Ion mobility separations have been used to add specificity to LC-MS analyses.[7] However, sensitivity in IMS is limited by the duty cycle of the pulsed ions, which can be as low as 1%. Therefore, 99% of the ions formed by a continuous ion source are not analyzed, unless ion accumulation is implemented in the source region.[8] Also, because IMS is a pulsed technique and does not provide a continuous beam of ions, it has been a challenge to couple IMS to most mass analyzers. IMS-MS systems often employ time-of-flight mass analyzers because they are also pulsed.

Errors in CCS determined from drift-tube IMS (DTIMS) are less than 1%.[9] Resolving power (RP), which is the ratio of the peak centroid to the full-width at half-max, is typically used to compare the performance of ion mobility spectrometers. Cyclotron ion mobility spectrometers have been reported to provide RPs of greater than 1000, but sensitivity was reported as "low" and ion transmission was not reported for these high resolving powers.[10] Improvements in ion transmission through ion mobility drift cells may be possible through the use of rf ion focusing. Thus far, rf focusing in a drift cell ion mobility spectrometer has only been reported in a short drift cell with RP around 20, but ion transmission approaches 100%.[11]

In addition to DTIMS, described above, some other IMS systems have been developed, including travelling-wave IMS (TWIMS),[12,13] and trapped IMS (TIMS).[14,15]

TWIMS and TIMS do not provide direct mobility measurements, but instead use calibrants with known reduced mobilities to determine the reduced mobility of the ion(s) of interest. With appropriate calibration, CCS obtained from TWIMS are reported with less than 5% error.[16] TWIMS uses a modified stacked ring ion guide, where opposite phase rf voltages are applied to alternating electrodes, providing radial confinement of ions. A dc pulse is applied to the electrodes such that a traveling electric field is produced, pushing the ions through the ion guide. By decreasing the wave height or wave velocity produced by the dc pulse, the ion guide begins to separate ions by their mobility where low mobility ions fall behind the wave before high mobility ions (Figure 1.2).[12] The RP achievable with TWIMS is typically on the order of 30-40.[16]

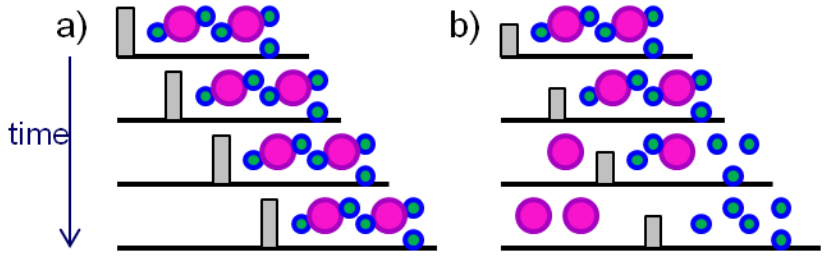

Figure 1.2 TWIMS cell operating as an ion guide in (a) and as an ion mobility spectrometer in (b). Grey rectangle represents a travelling wave pulse, blue circles represent high-mobility ions and pink circles represent low-mobility ions.

TIMS separates ions by taking advantage of a balance between drift velocity and ion mobility. The gas flow velocity through the TIMS cell determines the drift velocity of the ions, and the voltage difference ($\Delta V=V_{exit}-V_{entrance}$) between the entrance and exit lenses of the TIMS cartridge traps the ions, where for positive ions ΔV is positive to force the ions back towards the entrance. As the voltage is scanned, ions with lower mobilities elute before ions with higher mobilities (Figure 1.3).[14] In TIMS, the ions are radially confined with rf voltages, similar to TWIMS. High ion transmission approaching 100% is achievable with rf confinement, but the duty cycle is less than 50% because ions are lost during the ramp

and elution steps. As mentioned above, calibrants are used to determine the relationship between ΔV and K_0, such that K_0 can be determined for the analyte(s) of interest. With appropriate calibration, TIMS can provide CCS within about 5% error. TIMS can achieve RP up to 100-200 with ΔV ramp times on the order of 100 ms.[17]

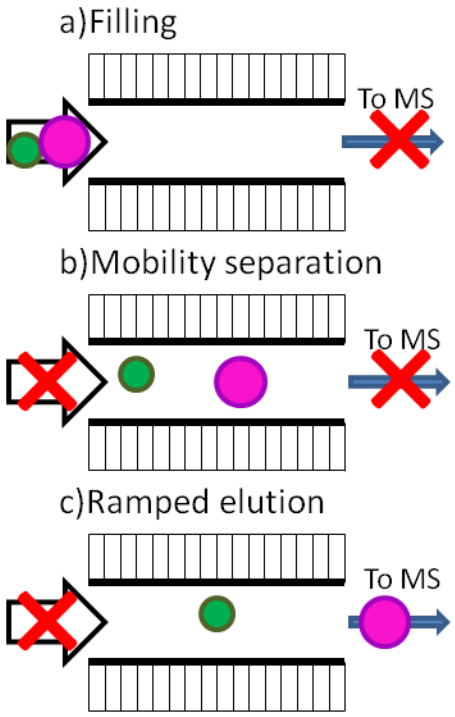

Figure 1.3 Representation of a TIMS separation, where ΔV is large enough to trap all ions to fill the cell (a), then a voltage is applied to the front-end of the instrument to direct ions formed by the source away from the TIMS cell (b), and finally ΔV is ramped to separate and elute the ions (c).

1.3 Differential ion mobility spectrometry

1.3.1 Background

At low electric fields, ion mobility is independent of electric field, but as the electric field is increased to greater than ~10^4 V/cm, ion mobility becomes dependent on the electric field.[1,2,18] Differential ion mobility spectrometry (DIMS) separates ions by exploiting the difference in the change in ion mobility with electric field. DIMS is often referred to as FAIMS (high-field asymmetric waveform ion mobility spectrometry) or DMS (differential mobility spectrometry). To illustrate the difference in low-field IMS and DIMS separations, the mobility dependence on electric field for three example ions is plotted in Figure 1.4. For example, the ion depicted by the black trace has a higher low-field mobility than the ion represented by the blue trace, so these two ions would be separable with low-field IMS, but because they have the same differential ion mobility between the low- and

high-field, they would not be separable with DIMS. Conversely, the ions represented in pink and black have the same low-field ion mobility and would not be separable with low-field IMS, but because the differential ion mobility between the low- and high-field is different, the two ions would be separable by DIMS.

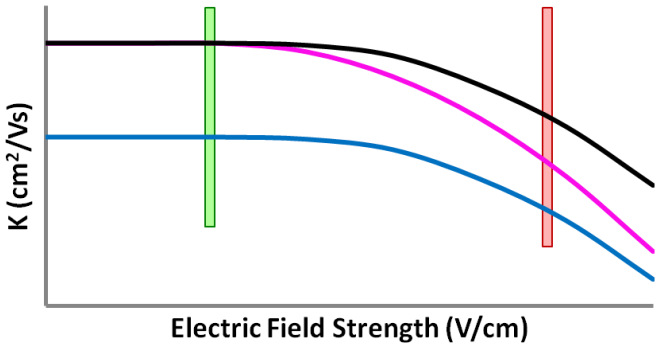

Figure 1.4 Representation of ion mobility as a function of electric field for three ions. DIMS separates ions based on their differential ion mobility between the high-field (red rectangle) and the low-field (green rectangle).

A differential ion mobility spectrometer is comprised of two parallel electrodes, with a constant gap between them. An rf voltage, alternating between high and low electric fields of opposite polarities, is applied to one or both electrodes, depending on the design. There are two basic DIMS electrode geometries: cylindrical and planar. Planar designs have two planar electrodes oriented parallel to each other with a gap in between them. Cylindrical designs use curved electrodes with one electrode having a smaller radius than the other such that the electrodes are parallel with a constant gap between them throughout the assembly (Figure 1.5a).[19] Cylindrical designs have some advantages over planar DIMS assemblies (Figure 1.5b),[20] including higher ion transmission due to improved ion focusing[21] as the dispersion field is increased. The ability to trap ions at atmospheric pressure has also been reported in cylindrical DIMS.[22] However, the ion focusing effect observed for cylindrical assemblies causes the cylindrical geometry to have lower resolving powers than those observed with planar assemblies.[20] Planar assemblies are easier to fabricate and most importantly, planar DIMS assemblies can operate in a "transparent mode" where both electrodes are held at ground potential allowing a

mass spectrum to be obtained without an IMS separation prior to mass analysis.

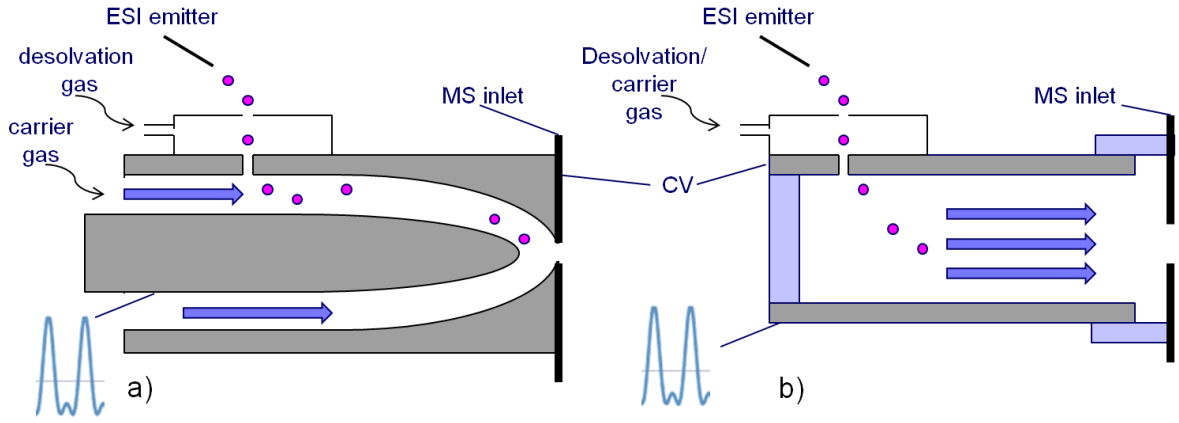

Figure 1.5 DIMS geometries with (a) cylindrical and (b) planar electrodes. Grey rectangles represent the DIMS electrodes, blue arrows represent gas flow, and pink circles represent ions.

Ions are carried through the gap between the two DIMS electrodes by a carrier gas unlike DTIMS where the voltage difference across the drift tube carries ions through the assembly. An asymmetric rf waveform is applied to the electrodes, alternating between low (E_l) and high (E_h) electric fields (Figure 1.6). During the low-field portion of the waveform (t_l) ions are displaced toward one electrode a distance proportional to the low field mobility (K_l) of the ion. Ions are displaced toward the other electrode a distance proportional to the high field mobility (K_h) of the ion during the high field portion of the waveform (t_h) (equations 1.4 and 1.5).[4]

$$d_l = K_l E_l t_l \qquad \text{(Equation 1.4)}$$

$$d_h = K_h E_h t_h \qquad \text{(Equation 1.5)}$$

The DIMS waveform is tuned such that $E_l t_l = E_h t_h$ and thus the net displacement (d_h-d_l) of an ion is directly proportional to its difference in mobilities (K_h-K_l). During the transit time through the DIMS assembly, ions are separated by differences in their net displacement (d_h-d_l) towards one of the electrodes. With $E_l t_l = E_h t_h$, an ion with K_h=K_l would have no net

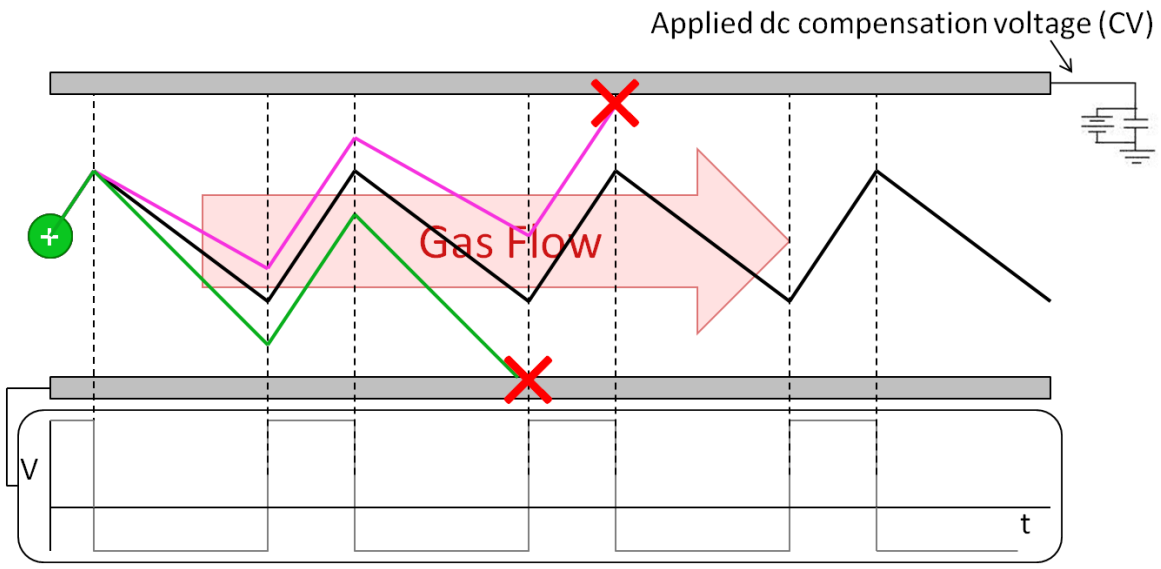

Figure 1.6 Representation of DIMS operating in filter mode, where the black trace represents the path of the ion selected by the applied CV, and the pink and green traces represent the paths of ions with differing differential ion mobilities than the selected ion. The large red arrow represents the carrier gas flow.

displacement, while ions with $K_h \neq K_l$ would be neutralized on the electrodes. A dc offset, or compensation voltage (*CV*), can be applied to one of the electrodes to counterbalance the displacement of the ion, allowing only ions with the selected K_h-K_l to pass through the assembly. The *CV* is often expressed as a compensation field (E_C) by dividing the *CV* by the gap between the electrodes (g). The E_C can be held constant during an experiment, using DIMS in filter mode (Figure 1.6) to select for a beam of ions with a given K_h-K_l. Alternatively, DIMS can be used in scanning mode, where the E_C is scanned in incrementally. Scanning mode is used for the separation of complex mixtures or to determine the peak E_C of a known analyte to be used in filter mode.

DIMS separations are affected by the separation time, dispersion field, and carrier gas parameters. Because DIMS is a dispersive technique, where ions are separated in space, longer separation times provide improved resolution.[23] However, there is no voltage confining the ions parallel to the electrodes, so lateral diffusion causes an increase in ion losses as the separation time is increased. The dispersion field (E_D which is equivalent to E_h),

which is defined as $V_{0\text{-}P}$ (DV) of the DIMS waveform divided by the gap between the electrodes (DV/g), can also be increased to improve DIMS resolution.[24] Finally, carrier gas composition and parameters such as temperature can affect separations. For example, helium can be added to the conventional nitrogen carrier gas to improve resolution for peptide and protein ions.[25-26] Additionally, organic dopants such as isopropyl alcohol have been shown to improve resolution for some analytes.[26]

At low electric fields used with DTIMS, TWIMS and TIMS, ions with smaller collision cross-sections will undergo fewer collisions with the counter-current gas and have higher mobilities than ions with larger collision cross-sections (Equation 1.3). High field mobility is not as well understood as low field mobility because the direct proportionality between ion mobility and collision cross-section no longer holds true.[1,2,18] DIMS is more orthogonal to MS than conventional IMS, but it is not currently possible to predict the E_C of an ion under a given set of conditions, even if the collision cross-section is known.

Because DIMS separates ions in space rather than in time, a continuous beam of ions is produced by DIMS, whether it is operated in filter or scanning mode. This makes DIMS straightforward to couple to any ion source and mass analyzer. DIMS is especially useful for ion trapping mass analyzers which have a finite charge capacity, where if too many ions are in the trap, space-charge effects begin to arise. For example, with DIMS in filter mode, only the ion of interest is allowed to pass through the assembly to the ion trap. Thus, the finite charge capacity of the trap is not wasted on background ions that are not of interest.

1.3.2 Current uses

Although DIMS does not provide a cross-section like low-field IMS, DIMS has proven a useful tool for the separation of protein conformations and as a separation tool for complex samples when coupled to LC. When used with LC, DIMS provides an increase in specificity and improved peak capacity[27] and has been shown to increase peptide and protein identifications in a proteomics workflow as compared to LC-MS alone.[28,29] Several conformations of model proteins, including ubiquitin[30] and cytochrome C,[31] have been separated using DIMS. DIMS has also been coupled to low-field IMS to separate more conformations of both ubiquitin and cytochrome C than were separable with DIMS or low-field IMS alone.[32]

DIMS has also been used without mass spectrometry. For example, on the international space station, DIMS is coupled to a gas chromatograph (GC-DIMS) and is used for air monitoring.[33] DIMS provides improved specificity over GC alone and is used to differentiate co-eluting contaminants. GC-DIMS replaced a GC-IMS system which employed a drift tube with much larger size requirements than the GC-DIMS.

1.3.3 Issues/drawbacks of DIMS

While DIMS has proven to be a powerful separation technique, there are some issues and room for improvement with the currently available commercial devices. As previously mentioned, cylindrical-type DIMS assemblies exhibit high ion transmission, but achieve low resolving powers due to ion focusing effects from the curved electrodes. Planar assemblies can provide higher resolving powers, but often at the cost of ion transmission. Ion transmission has a direct effect on the sensitivity of the MS method, and DIMS parameters

must be carefully tuned to maximize ion transmission while maintaining sufficient separation of analytes.

It is important to reiterate that ion mobility techniques, including both low field-IMS and DIMS, can help to improve sensitivity by reducing chemical background but cannot alleviate issues due to ionization suppression. Ionization suppression occurs within the ion source prior to the ion mobility separation. This is one of the reasons why LC and/or sample preparation techniques are still needed for most biological samples, even with ion mobility separations.

As high-field mobility is not yet well-understood, it is difficult to predict analyte behavior in DIMS. Thus, DIMS is currently well-suited to applications with a known targeted analyte. In these applications, the pure known analyte must be analyzed to determine the optimum DIMS parameters prior to running a real world sample. However, when coupled to LC, DIMS has been shown to improve non-targeted analyses as well. If the resolving power and peak capacity of DIMS were improved, it could be used for non-targeted analyses. Additionally, DIMS coupled to low-field IMS techniques could provide improved results for non-targeted and targeted approaches, providing a multidimensional gas-phase ion separation prior to mass spectrometry.[34]

1.4 Summary

The goal of this introduction chapter has been to introduce differential ion mobility spectrometry separations. The need for ion mobility separations with mass spectrometry is discussed and background is included for ion mobility separations. Several ion mobility techniques are briefly introduced. DIMS background, including how DIMS works and how

resolution is improved, is covered. Finally, current uses and drawbacks of DIMS separations are discussed.

Chapter 2 is intended to provide experimental methods for the subsequent chapters. This chapter includes solvents and other materials used. Additionally, ionization methods and mass spectrometers used are described. DIMS and TIMS devices are both described, and for DIMS, two different generations are presented. Data analysis methods are also included.

Chapter 3 includes fundamental experiments focused on the optimization of DIMS separations. Ion transmission and resolving power are investigated with varying parameters including the electrode dimensions, carrier gas temperature and composition. The improvement of DIMS separations with the addition of helium as compared to elevated dispersion fields in pure nitrogen is investigated using isobaric peptides. The chapter closes with the separation of a mixture of three isobaric peptides using the highest dispersion field achievable with pure nitrogen as the carrier gas.

Chapter 4 begins with a discussion of ion transfer optics for mass spectrometry and the ion reactions that can occur in the transfer optics. A discussion of how these ion reactions can convolute DIMS results is presented with examples. Additionally, the use of DIMS for the monitoring of ion reactions that are occurring in the transfer optics is discussed. The chapter closes with a discussion of the charge-reduction of peptides and experimental evidence that a charge-reduction can occur in the glass transfer capillary.

Chapter 5 presents the prospective for DIMS to be used as an "electronic immunoassay". A discussion of the current advantages and pitfalls of biomarker detection with immunoassays as well as MS analyses is presented. A biomarker for congestive heart failure, brain natruiretic peptide (BNP), is used as the model peptide to investigate the utility

of DIMS for biomarker detection. DIMS separations of BNP in fetal bovine serum and human plasma are included. Additionally, the importance of analyte structure in DIMS separations is discussed. Finally, the use of DIMS for the identification of leukemia antigens is presented.

Chapter 6 presents DIMS as a separation method for the analysis of aerosols formed via pyrolysis. DIMS is successful at the separation of several isomers/isobars in the pyrolysates, producing multiple unique MS/MS spectra for parent ions with the same mass-to-charge ratio. The chapter closes with a comparison of experimentally determined cross-sections from TIMS to theoretical cross-sections of proposed structures. Finally, **Chapter 7** summarizes the results of each chapter and discusses future directions related to this work.

1.5 REFERENCES

1. Mason, E. A.; McDaniel, E. W. *Transport Properties of Ions in Gases*. John Wiley & Sons Inc.: New York, 1988

2. Eiceman, G.; Karpas, Z. *Ion Mobility Spectrometry*. CRC Press: Boca Raton, 2005

3. Kolakowski, B. M.; Mester, Z. Review of Applications of High-Field Asymmetric Waveform Ion Mobility Spectrometry (FAIMS) and Differential Ion Mobility Spectrometry (DMS). *Analyst.* **132**, 842-864 (2007)

4. Xia, Y.; Wu, S. T.; Jemal, M. LC-FAIMS-MS/MS for Quantification of a Peptide in Plasma and Evaluation of FAIMS Global Selectivity from Plasma Components. *Anal. Chem.* **80**, 7137-7143 (2008)

5. Hatsis, P.; Valaskovic, G.; Wu, J. Online Nanoelectrospray/High-Field Asymmetric Waveform Ion Mobility Spectrometry as a Potential Tool for Discovery Pharmaceutical Bioanalysis. *Rapid Commun. Mass Spectrom.* **23**, 3736-3742 (2009)

6. Williams, D.M.; Pukala, T.L.: Novel insights into protein misfolding diseases revealed by ion mobility-mass spectrometry. *Mass Spectrom. Rev.* **32**, 169-187 (2013)

7. Baker, E.S.; Livesay, E.A.; Orton, D.J.; Moore, R.J.; Danielson III, W.F.; Prior, D.C.; Ibrahim, Y.M.; LaMarche, B.L.; Mayampurath, A.M.; Schepmoes, A.A.; Hopkins, D.F.; Tang, K.; Smith, R.D.; Belov, M.E.: An LC-IMS-MS platform providing increased dynamic range for high-throughput proteomic studies. *J. Proteome Res.* **9**, 997-1006 (2010)

8. Hoaglund, C. S.; Valentine, S. J.; Clemmer, D. E. An ion trap interface for ESI ion mobility experiments. *Anal. Chem.* **69**, 4156-4161 (1997)

9. Dugourd, Ph.; Hudgins, R.R.; Clemmer, D.E.; Jarrold, M.F.: High-resolution ion mobility measurements. *Rev. Sci. Intrum.*, **68**, 1122-1129 (1997)

10. Glaskin, R.S.; Ewing, M.A.; Clemmer, D.E.: Ion trapping for ion mobility spectrometry measurements in a cyclical drift tube. *Anal. Chem.* **85**, 7003-7008 (2013)

11. Bush, M.F.; Hall, Z.; Giles, K.; Hoyes, J.; Robinson, C.V.; Ruotolo, B.T.: Collision cross sections of proteins and their complexes: A calibration framework and database for gas-phase structural biology. *Anal. Chem.*, **82**, 9557-9565 (2010)

12. Giles, K.; Pringle, S.D.; Worthington, K.R.; Little, D.; Wildgoose, J.L.; Bateman, R.H.: Applications of a travelling wave-based radio-frequency-only stacked ring ion guide. *Rapid Commun. Mass Spectrom.* **18**, 2401-2414 (2004)

13. Shvartsburg, A.A.; Smith, R.D.: Fundamentals of traveling wave ion mobility spectrometry. *Anal.Chem.* **80**, 9689-9699 (2008)

14. Fernandez-Lima, F.; Kaplan, D.A.; Suetering, J.; Park, M.A.: Gas-phase separation using a trapped ion mobility spectrometer. *Int. J. Ion Mobil. Spec.* **14**, 93-98 (2011)

15. Fernandez-Lima, F.; Kaplan, D.A.; Park, M.A.: Note: Integration of trapped ion mobility spectrometry with mass spectrometry. *Rev. Sci. Instrum.* **82**, 126106 (2011)

16. Giles, K.; Williams, J.P.; Capuzano, I.: Enhancements in travelling wave ion mobility resolution. *Rapid Commun. Mass Spectrom.* **25**, 1559-1566 (2011)

17. Hernandez, D.R.; DeBord, J.D.; Ridgeway, M.E.; Kaplan, D.A.; Park, M.A.; Fernandez-Lima, F.: Ion dynamics in a trapped ion mobility spectrometer. *Analyst*, **139**, 1913-1921 (2014)

18. Purves, R. W.; Guevremont, R.; Day, S.; Pipich, C. W.; Matyjaszcyk, M. S. Mass spectrometric characterization of a high-field asymmetric waveform ion mobility spectrometer. *Rev. Sci. Instrum.* **69**, 4094-4105 (1998)

19. Barnett, D.A.; Ells, B.; Guevremont, R.; Purves, R.W.; Viehland, L.A.: Evaluation of carrier gases for use in high-field asymmetric waveform ion mobility spectrometry. *J. Am. Soc. Mass Spectrom.***11**, 1125-1133 (2000)

20. Shvartsburg, A. A.; Li, F. M.; Tang, K. Q.; Smith, R. D. High-resolution field asymmetric waveform ion mobility spectrometry using new planar geometry analyzers. *Anal. Chem.* **78**, 3706-3714 (2006)

21. Guevremont, R.; Purves, R.W. Atmospheric pressure ion focusing in a high-field asymmetric waveform ion mobility spectrometer. *Rev. Sci Instrum.***70**, 1370-1383 (1999)

22. Guevremont, R.; Ding, L. Y.; Ellis, B.; Barnett, D. A.; Purves, R. W. Atmospheric pressure ion trapping in a tandem FAIMS-FAIMS coupled to a TOFMS: Studies with electrospray generated gramicidin S ions. *J. Am. Soc. Mass Spectrom.* **12**, 1320-1330 (2001)

23. Shvartsburg, A. A.; Smith, R.D.: Ultrahigh-resolution differential ion mobility spectrometry using extended separation times. *Anal. Chem.* **83**, 23-29 (2011)

24. Shvartsburg, A. A.; Prior, D. C.; Tang, K.; Smith, R. D. High-resolution differential ion mobility separations using planar analyzers at elevated dispersion fields. *Anal. Chem.* **82**, 7649-7655 (2010)

25. Shvartsburg, A. A,; Danielson, W. F.; Smith, R. D. High-resolution differential ion mobility separations using helium-rich gases. *Anal. Chem.* **82**, 2456-2462 (2010)

26. Schneider, B.B.; Covey, T.R.; Coy, S.L.; Krylov, E.V.; Nazarov, E.G.: Chemical effects in the separation process of a differential mobility/mass spectrometer system. *Anal. Chem.* **82**, 1867-1880 (2010)

27. Varesio, E.; Le Blanc, J.C.Y.; Hopfgartner, G.: Real-time 2D separation by LC x differential ion mobility hyphenated to mass spectrometry. *Anal. Bioanal. Chem.* **402**, 2555-2564 (2012)

28. Swearingen, K.E.; Moritz, R.L.: High-field asymmetric waveform ion mobility spectrometry for mass spectrometry-based proteomics. *Expert Rev. Proteomic.* **9**, 505-517 (2012)

29. Creese, A.J.; Shimwell, N.J.; Larkins, K.P.B.; Heath, J.K.; Cooper, H.J.: Probing the complementarity of FAIMS and strong cation exchange chromatography in shotgun proteomics. *J. Am. Soc. Mass Spectrom.* **24**, 431-443 (2013)

30. Purves, R.W.; Barnett, D.A.; Ells, B.; Guevremont, R.: Elongated conformers of charge states +11 to +15 of bovine ubiquitin studies using ESI-FAIMS-MS. *J. Am. Soc. Mass Spectrom.* **12**, 894-901 (2001)

31. Purves, R.W.; Guevremont, R.: Electrospray ionization high-field asymmetric waveform ion mobility spectrometry-mass spectrometry. *Anal. Chem.* **71**, 2346-2357 (1999)

32. Shvartsburg, A.A.; Li, F.; Tang, K.; Smith, R.D.: Characterizing the structures and folding of free proteins using 2-D gas-phase separations: observation of multiple unfolded conformers. *Anal. Chem.* **78**, 3304-3315 (2006)

33. Limero, T.; Reese, E.; Wallace, W.T.; Cheng, P.; Trowbridge, J.: Results from the air quality monitor (gas chromatograph-differential mobility spectrometer) experiment on board the international space station. *Int. J. Ion Mobil. Spectrom.* **15**, 189-198 (2012)

34. Tang, K.; Fumin, L.; Shvartsburg, A.A.; Strittmatter, E.F.; Smith, R.D.: Two-dimensional gas-phase separations coupled to mass spectrometry for analysis of complex mixtures. *Anal. Chem.* **77**, 6381-6388 (2005)

CHAPTER 2: EXPERIMENTAL

2.1 Materials

Methanol (HPLC grade), acetonitrile (HPLC grade), water (HPLC grade), and acetic acid (ACS plus) were purchased from Fisher Scientific (Fairlawn, NJ). Natriuretic peptides and bradykinin were purchased from the American Peptide Company (Sunnyvale, CA). Bovine ubiquitin and equine myoglobin were purchased from Sigma-Aldrich (St. Louis, MO). Model antigenic peptides were purchased from New England Peptide (Gardner, MA). Other peptides were synthesized in-house where synthesized with a CS Bio model CS036 solid phase peptide synthesizer with Fmoc (9-fluorenylmethoxycarbonyl) protected amino acids and a 2-chlorotrityl resin.[1] Fmoc-derivatized amino acids and 2-chlorotrityl chloride resin were obtained from CS Bio Co. (Menlo Park, CA). Human plasma was donated from Laboratory Corporation of America (LabCorp). Agilent ESI tuning mix (Agilent technologies, Santa Clara, CA) was used after a 20x dilution with a final solution composition of 95/5 acetonitrile/water. Chemical formulae for tune mix components are given in Table 2.1. All compounds were used without further purification.

2.2 Mass spectrometry

Samples were ionized by electrospray ionization (ESI) and were directly infused at a flow rate of 2 μL/min. Solutions were composed of 49.5/49.5/1 (v/v/v)

Table 2.1 Chemical formulae for components in Agilent ESI tuning mix.

m/z $[M+H]^+$	Chemical Formula
322	$P_3N_3(OCH_3)_6$
622	$P_3N_3(OCH_3CF_2)_6$
922	$P_3N_3(OCH_3CF_2CF_2)_6$
1222	$P_3N_3(OCH_3C_2F_4CF_2)_6$
1522	$P_3N_3(OCH_3C_3F_6CF_2)_6$
1822	$P_3N_3(OCH_3C_4F_8CF_2)_6$
2122	$P_3N_3(OCH_3C_5F_{10}CF_2)_6$
2422	$P_3N_3(OCH_3C_6F_{12}CF_2)_6$
2722	$P_3N_3(OCH_3C_7F_{14}CF_2)_6$

methanol/water/acetic acid unless otherwise specified. An ESI voltage of 4.25 kV was used, where -4.25 kV was applied to the transfer capillary with the ESI emitter held at ground potential or +4.25 kV was applied to the ESI emitter with the transfer capillary held at ground potential.

A Bruker Esquire 3000 ion trap mass spectrometer (MS) was used or a Bruker HCT (high capacity trap) MS was used, as specified. Tandem mass spectrometry experiments were performed using collision-induced dissociation (CID) of isolated ions in approximately 1 mTorr helium bath gas in an ion trap. CID in a quadrupole ion trap has been previously described.[2] Trapped ion mobility spectrometry (TIMS) experiments were performed with a modified Bruker maXis quadrupole time-of-flight (Q-ToF) mass spectrometer.

Peptide ion fragmentation nomenclature is represented in Figure 2.1.[3,4] When the charge is retained on the N-terminal fragment, the product ions are called *a*, *b*, or *c* ions. The product ions are referred to as *x*, *y*, or *z* ions when the charge is retained on the C-terminal fragment. The bond that is broken dictates which type of ion is formed: *a* or *x* ions are formed when the C_α-C bond is broken, *b* and *y* when the peptide bond is broken, and *c* and *z* when the N-C_α bond is broken. With CID, *b*, *y* and *a* ions are expected.

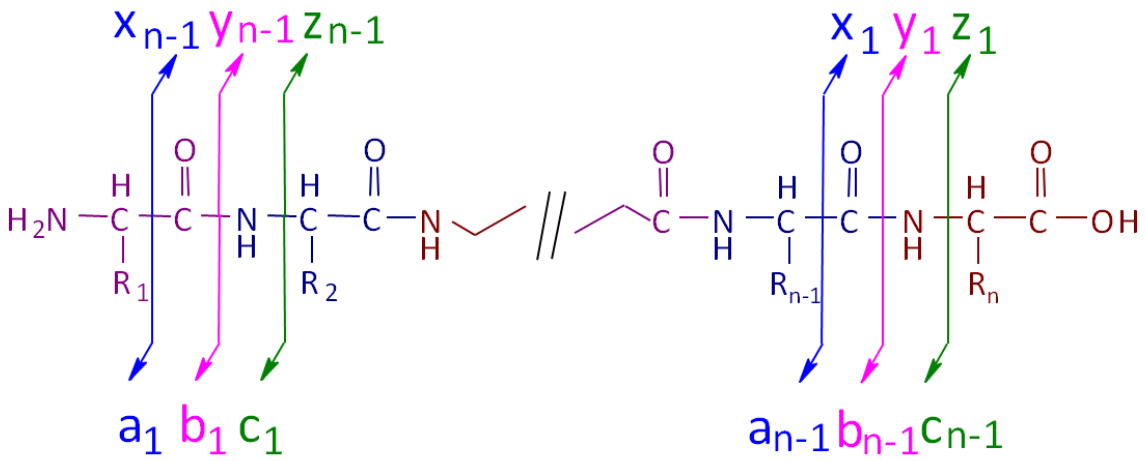

Figure 2.1 Nomenclature used for peptide product ions: *a*, *b*, and *c* ions retain the charge on the N-terminal fragment; *x*, *y*, and *z* ions retain the charge on the C-terminal fragment.

2.3 Ion Mobility Spectrometry

2.3.1 Differential Ion Mobility Spectrometry

A planar DIMS assembly (Figure 2.2) was used for these experiments. Electrode dimensions for the various generations of the DIMS assembly used throughout this dissertation are given in Table 2.2. The third generation (G3, Figure 2.2a-c) was designed so that the electrodes can be changed to vary the dimensions (G3a-d) and was used with a Bruker Esquire 3000 ion trap MS. The fourth generation (G4) was used on a Bruker HCT MS and was designed with smaller electrodes whose dimensions are not easily varied. Both G3 and G4 (Figure 2.2d-e) DIMS assemblies are designed so that the spray shield on the mass spectrometer inlet can be removed, and the DIMS assembly can be installed

Table 2.2. Dimensions of DIMS electrodes.

DIMS	Gap (mm)	Width (mm)	Length (mm)
G3a	0.3	6	25
G3b	0.5	6	25
G3c	0.5	6	50
G3d	1.0	6	50
G4	0.3	4	10

in its place. G3 is used on the Bruker Esquire 3000 ion trap MS, and G4 is used on the Bruker HCT ion trap MS. In both generations, the desolvation gas, which is already implemented in the source region of the mass spectrometer for desolvation of ions formed by ESI, is redirected through the housing of the assembly. The desolvation gas, typically 100% N_2, serves as the carrier gas through the DIMS assembly as well as for desolvation when coupled to ESI. For experiments with helium added to the carrier gas, the ratio of helium to nitrogen in the carrier gas was varied using two MKS model 1179 mass flow controllers regulated by a LabVIEW program.

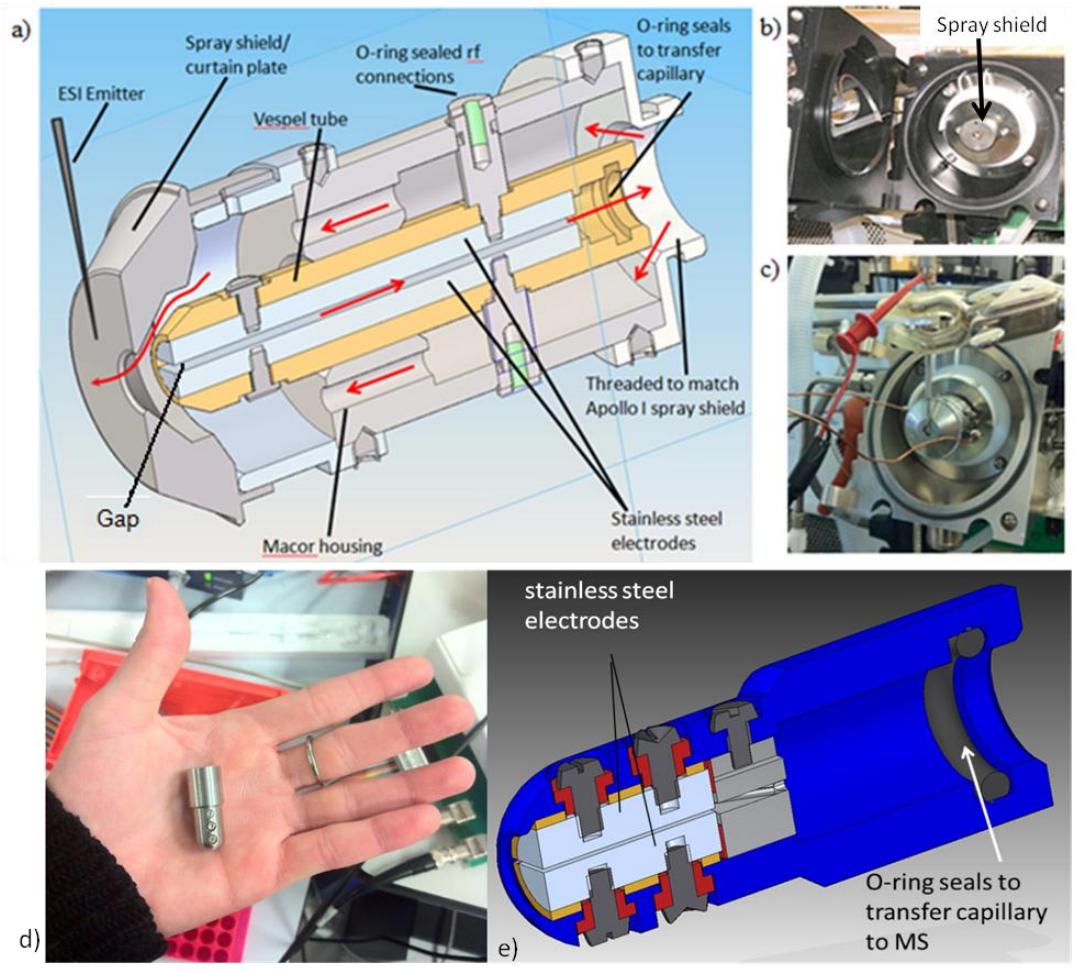

Figure 2.2 DIMS assemblies a) AutoCAD drawing of G3 design b) source with spray shield c) picture of source with spray shield removed and DIMS assembly in its place d) G4 without housing, and e) AutoCAD drawing of G4 design.

With G3, the standard glass transfer capillary of the source was replaced with a custom flared glass transfer capillary[5] to improve ion transmission through the DIMS assembly as compared to the standard capillaries. With G4, a planar flare (Figure 2.2e) was implemented after the electrodes to allow the coupling to a standard transfer capillary while maintaining greater than 80% ion transmission through the assembly in "transparent mode" where both electrodes are held at the same potential. A custom-built power supply[6] was used for experiments with G3 DIMS. Ideally, a rectangular waveform should be used for DIMS, alternating between low and high electric fields of opposing polarity. However, because of the power requirements of high voltage, high frequency rectangle waves, most DIMS waveforms are bisinusoidal, approximating a square wave.[7] In this design, one sinusoidal voltage at a given frequency and amplitude is applied to one of the electrodes, and a phase-shifted sinusoidal voltage at twice the frequency and approximately one-half the amplitude is applied to the other electrode, producing an electric field equivalent to the sum of the two individual sinusoidal waveforms (Figure 2.3). The dispersion voltage (*DV*) is defined by the maximum voltage ($V_{0\text{-}P}$) of the bisinusoidal waveform. The dispersion field (E_D) is defined as the *DV* divided by the gap (*g*) between the DIMS electrodes. The bisinusoidal DIMS

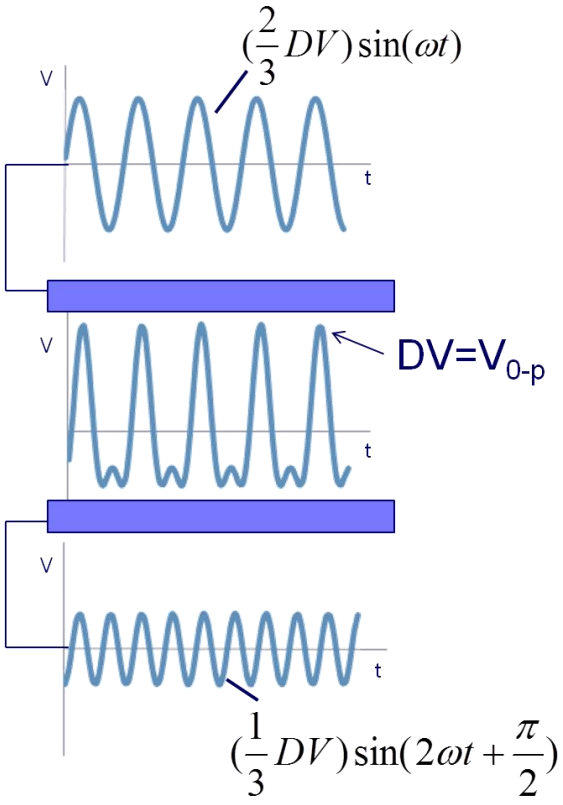

Figure 2.3 Simplified representation of the addition of two sinusoidal waves to create the bisinusoidal waveform.

waveform was tuned to a frequency of 1.7 MHz with G3 and 2 MHz with G4. For example, with G4 the addition of a sinusoidal wave at 2 MHz and a lower amplitude sinusoidal wave at 4 MHz is used to form the bisinusoidal DIMS waveform at frequency of 2 MHz. A LabVIEW program linked to the instrument control software is used to control the range of compensation voltages or to define a static value. In "scanning mode", the compensation field, E_C, is stepped over a range specified in a LabVIEW program. A static voltage can be selected to operate DIMS in "filter mode".

To use ESI with DIMS, a voltage difference of 4.25 kV between the emitter and the DIMS electrodes is applied. The DIMS electrodes are at the same potential as the transfer capillary, to which the ESI voltage is applied without DIMS. With G3, the ESI voltage must be applied to the ESI emitter rather than the DIMS electrodes because the DIMS waveform cannot be superimposed upon a high voltage with G3. A second custom power supply was designed for G4 so that the DIMS waveform can be centered about the ESI voltage and operated with the ESI emitter at ground potential. The same basic design for the application of the bisinusoidal waveform was used, but modifications were made to the power supply as well as the DIMS assembly itself to prevent arcing and to prevent drift in the applied E_C.

2.3.2 Trapped Ion Mobility Spectrometry

Trapped ion mobility spectrometry (TIMS) was used as a low-field ion mobility separation, when specified. TIMS uses a modified ion funnel, with a 4.6 cm analyzer section between an entrance and exit ion funnel (Figure 2.4).[8,9] The analyzer section has an inner diameter of 8 mm and the pressure difference between the inlet and the outlet of the analyzer creates a gas flow pushing ions through to the exit funnel. An rf voltage at 950 kHz and 200-400 V_{p-p} is

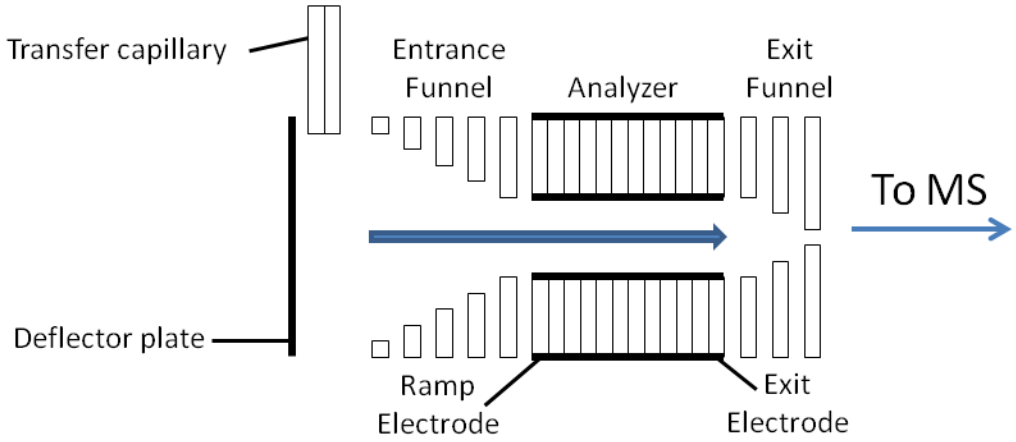

Figure 2.4 TIMS assembly with entrance funnel, analyzer region, and exit funnel. Gas flow indicated by blue arrows.

used to focus ions within the analyzer region. The temperature in the analyzer for all TIMS experiments was 304 K. The fill time for the analyzer is typically a few milliseconds, (10 ms for the experiments in this dissertation) followed by a trapping period to allow ions to separate based on low-field ion mobility, which is proportional to the collision cross-section of ions. Finally, the ions are ramped out of the analyzer section from low to high mobility (large to small cross-sections) by decreasing the voltage difference between the 1st (ramp electrode) and last electrode (exit

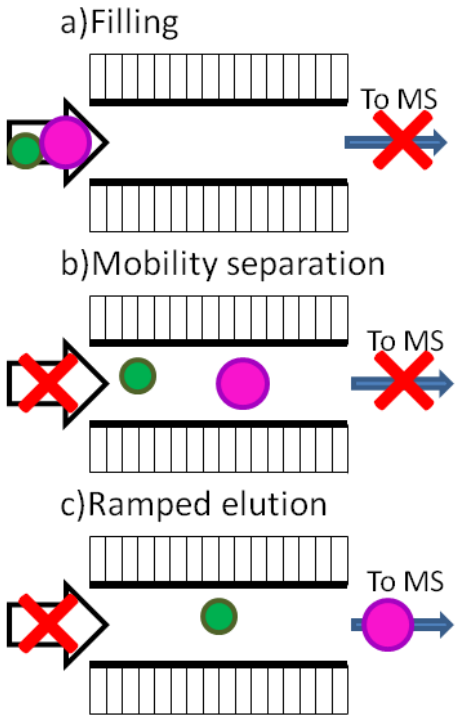

Figure 2.5 Simplified representation of TIMS separations; a) filling, b) ion mobility separation, and c) ramped elution of ions from low to high mobility. Gas flow indicated by arrows.

electrode) in the analyzer section. The three steps for the TIMS separation are depicted in Figure 2.5.

With TIMS there is no direct way to determine ion mobility from the TIMS scan so calibrants must be used to determine ion mobility and collision cross-section. Agilent ESI tuning mix (section 2.1.1) was used for the calibrant, for which the ion mobility in nitrogen gas was determined in a drift-tube ion mobility spectrometer (Table 2.3).[8] The same tuning mix (*m/z* 322, 622, 922, 1222, 1522, and 1822) was analyzed with TIMS to create a calibration plot (Figure 2.6) of K_0 versus inverse voltage, where voltage is the voltage difference between the first and last electrodes of the analyzer section. The collision cross-section (CCS) of analyte ions was determined using the calibration plot to convert inverse voltage to K_0, followed by the use of Equation 2.1,[10,11] where K_0 is the reduced ion mobility at standard temperature (T_0) and pressure (P_0), T is temperature, N_0 is the number density at standard temperature and pressure, e is the charge of the ion, μ is reduced mass, k_B is Boltzmann's constant, and Ω is the collision cross-section of the ion.

$$K_0 = \frac{3e}{16N_0}\left(\frac{2\pi}{\mu k_B T}\right)^{1/2}\frac{1}{\Omega} \qquad \text{(Equation 2.1)}$$

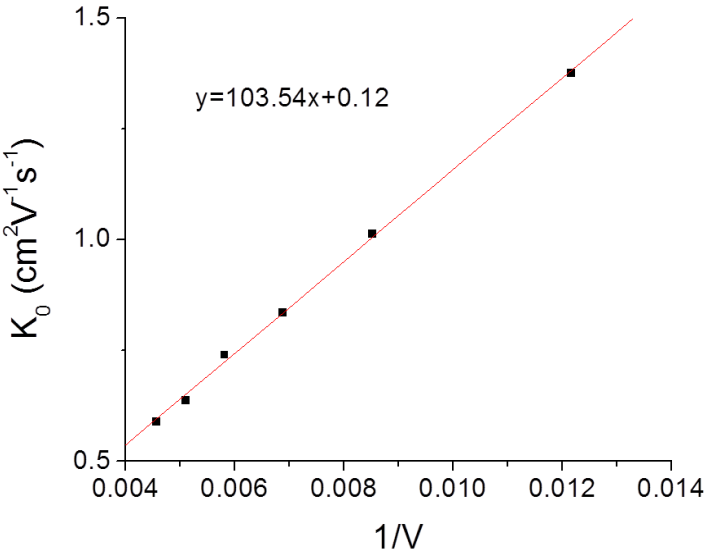

Figure 2.6 Calibration plot used for TIMS experiments correlating reduced ion mobility to inverse voltage.

2.4 Data analysis

DIMS spectra were constructed by plotting the extracted ion current or total ion current from the Bruker Data Analysis 4.1 software as a function of analysis time. Several time-to-voltage points were recorded during each DIMS scan to be used to convert the time axis of the chromatogram to voltage in Excel. Each time point in the exported ion current is an average of ten mass spectra, and each time point is equivalent to one CV step, where the step size is specified in the LabVIEW program.

Table 2.3 Reduced ion mobility and collision cross-sections in nitrogen for components in Agilent ESI tuning mix used for TIMS calibration.[8]

m/z $[M+H]^+$	K_0 ($cm^2V^{-1}s^{-1}$)	CCS ($Å^2$)
322	1.376	151.9
622	1.013	202.4
922	0.835	243.8
1222	0.740	274.1
1522	0.638	317.2
1822	0.590	342.5

The conversion is applied by using one time-to-voltage point and then the voltage step size is used to determine the voltage at each previous and subsequent time point. The other time-to-voltage points are used to confirm that there is no error in using the step size throughout the time-to-voltage conversion in the DIMS scan. The determined compensation voltage for each time point is then divided by the gap size of the DIMS device to convert to compensation field for the x-axis of the DIMS spectra. The peak width (*w*), full-width at half-max (*FWHM*), and centroid E_C for DIMS peaks were determined using the Fit Gaussian function in Origin 6.0. The following three equations are used throughout this dissertation to evaluate DIMS separations: resolving power (*RP*), resolution (*R*), and percent ion transmission (*%T*):

$$RP = \frac{CV}{FWHM(V)} = \frac{E_C}{FWHM\,(\frac{V}{cm})} \qquad \text{(Equation 2.2)}$$

$$R = \frac{E_{C2} - E_{C1}}{(\frac{w_1 + w_2}{2})} = \frac{1.178(E_{C2} - E_{C1})}{(FWHM_1 + FWHM_2)} \qquad \text{(Equation 2.3)}$$

$$\%T = \frac{signal\ with\ DIMS}{signal\ without\ DIMS} \times 100\% \qquad \text{(Equation 2.4)}$$

2.5 REFERENCES

1. Fmoc solid phase peptide synthesis : a practical approach; Oxford University Press: Oxford; New York, 2000.

2. Louris, J.N.; Cooks, R.G.; Syka, J.E.P.; Kelley, P.E.; Stafford, G.C.; Todd, J.F.J.: Instrumentation, applications, and energy deposition in quadrupole ion-trap mass spectrometry. *Anal. Chem.*, **59**, 1677-1685 (1987)

3. Roepstorff, P.; Fohlman, J.: Proposal for a common nomenclature for sequence ions in mass spectra of peptides. *Biomedical Mass Spectrometry* **11**, 601 (1984)

4. Biemann, K.: Contributions of mass spectrometry to peptide and protein structure. *Biomedical and Environmental Mass Spectrometry* **16**, 99-111 (1988)

5. Bushey, J.M.; Kaplan, D.A.; Danell, R.M.; Glish, G.L.: Pulsed Nano-Electrospray Ionization: Characterization of Temporal Response and Implementation with a Flared Inlet Capillary. *Instrum. Sci. Technol*. **37**, 257-273 (2009)

6. Ridgeway, M. E.; Glish, G. L. In preparation

7. Purves, R. W.; Guevremont, R.; Day, S.; Pipich, C. W.; Matyjaszcyk, M. S. Mass spectrometric characterization of a high-field asymmetric waveform ion mobility spectrometer. *Rev. Sci. Instrum.* 69, 4094-4105 (1998)

8. Hernandez, D.R.; DeBord, J.D.; Ridgeway, M.E.; Kaplan, D.A.; Park, M.A.; Fernandez-Lima, F.: Ion dynamics in a trapped ion mobility spectrometer. *Analyst*, **139**, 1913-1921 (2014)

9. Fernandez-Lima, F.; Kaplan, D.A.; Suetering, J.; Park, M.A.: Gas-phase separation using a trapped ion mobility spectrometer. *Int. J. Ion Mobil. Spectrom.* **14**, 93-98 (2011)

10. McDaniel, E.W.; Mason, E.A.: *Mobility and diffusion of ions in gases*; John Wiley and Sons, Inc., New York, NY, 1973, p. 381.

11. Mason, E. A.; McDaniel, E. W. *Transport Properties of Ions in Gases*. John Wiley & Sons Inc.: New York, 1988 .

CHAPTER 3: OPTIMIZATION OF DIMS SEPARATIONS

3.1 Evaluation of DIMS separations

In the optimization of any analytical technique, both sensitivity and resolution must be taken into consideration. DIMS separations are often evaluated by calculating the resolving power (*RP*) of a given peak (Equation 3.1). The *RP* essentially describes how narrow a given peak is by deteriming the ratio of the peak centroid to the full-width at half-maximum. *RP* is inherently biased such that if two peaks have the same width, but one has a higher centroid *CV* than the other, then the peak with the higher centroid will have the higher *RP*. Resolution (*R*), which is commonly used for chromatographic separations, provides an evaluation for the separation of two peaks (Equation 3.2). For *R*, the centroid and width of both peaks are taken into account to determine how well they are separated, where a value of <0.5 indicates that the two peaks overlap significantly and a value of >1.5 indicates that the peaks are baseline resolved.

$$RP = \frac{CV}{FWHM} \qquad \text{(Equation 3.1)}$$

$$R = \frac{CV_2 - CV_1}{\left(\frac{w_1 + w_2}{2}\right)} = \frac{1.178(CV_2 - CV_1)}{(FWHM_1 + FWHM_2)} \qquad \text{(Equation 3.2)}$$

In addition to evaluating resolution, sensitivity must be considered, as there is generally a trade-off between resolution and sensitivity in the optimization of analytical techniques. To evaluate sensitivity, the percent ion transmission (*%T*) through the DIMS assembly can be determined. For a given experiment, *%T* is calculated by determining the ratio of the ion signal obtained with DIMS to the ion signal without the assembly attached to

the mass spectrometer and converting to a percentage (Equation 3.3). This value is generally calculated for a specific ion, where the extracted ion current for the mass-to-charge of the analyte ion is used for the signal intensity. For $\%T_{trans}$, the numerator is the signal obtained for DIMS in transparent mode, where no rf is applied to the electrodes and all ions are allowed to pass through the device without ion mobility separation. For $\%T_{active}$, the numerator is the signal obtained for a given ion at the peak E_C for that ion. With both $\%T_{trans}$ and $\%T_{active}$, the denominator is the signal obtained with the device removed from the inlet of the mass spectrometer.

$$\%T = \frac{signal\ with\ DIMS}{signal\ without\ DIMS} \times 100\% \qquad \text{(Equation 3.3)}$$

All of the above values are useful in the evaluation of DIMS separations and can be used in the optimization of various parameters. As discussed previously (1.3.1), DIMS separation power can be affected by the dispersion field,[1-3] separation time,[4,5] carrier gas temperature and pressure, and carrier gas composition.[6-8] The separation time is varied by changing the length of the DIMS electrodes. The carrier gas settings are also examined, where temperature and percent helium in nitrogen are varied.

3.2 Electrode dimensions

3.2.1 Ion transmission with DIMS transparent

Generation 3 (G3) of the planar DIMS assembly allows for the gap between the electrodes to be easily changed between 0.3, 0.5, and 1.0 mm. Additionally, two different housing sizes, one of which can hold 50 mm long electrodes and the other can hold 25 mm long electrodes, were developed. When the electrodes are lengthened, the ion transit time through the assembly is increased. With an increase in ion transit time, a greater degree of ion losses due

to diffusion is expected. When the gap between the electrodes is increased, the volume within the device is increased, and because the volumetric flow rate of the carrier gas dictates ion transit time, ion losses due to diffusion will increase. Because the DIMS electrodes are coupled to a glass capillary (length=18 cm, i.d.=0.5 mm) that transfers ions from atmospheric pressure to vacuum, a conductance limit of approximately 1.4 L/min dictates the volumetric gas flow rate through the assembly. This gas flow is what carries ions through the assembly, thus determining the ion transit time. Therefore, if the volume between the electrodes is increased, the transit time through the assembly will increase proportionally, allowing for greater ion losses due to diffusion.

Table 3.1 summarizes the $\%T_{trans}$ determined for the tetrabutyl ammonium ion (*m/z* 242), angiotensin I^{3+} (*m/z* 433), and brain natriuretic peptide $(BNP)^{5+}$ (*m/z* 649) for DIMS transparent compared to the assembly removed. A significant difference in ion transmission is observed between the four electrode dimensions used for these experiments. The trends observed are as expected for all ions investigated, where the ion transmission decreases as the volume between the electrodes is increased. The tetrabutyl ammonium ion has a similar ion transmission between the two gap sizes with the 25 mm long electrodes, with fairly large standard deviations due to the overall low signal observed with the DIMS device attached. The low ion transmission for the tetrabutyl ammonium ion is expected because it is a low-

Table 3.1. Ion transmission with DIMS transparent observed for tetrabutyl ammonium ion (*m/z* 242), angiotensin 1^{3+} (*m/z* 433) and BNP^{5+} (*m/z* 694).

Gap, length (mm)	$\%T_{trans}$		
	m/z 242	*m/z* 433	*m/z* 694
0.3, 25	8.8 ± 4.2	27.8 ± 1.7	n/a
0.5, 25	10.3 ± 1.5	22.2 ± 1.4	50.6 ± 9.2
0.5, 50	4.3 ± 0.6	5.7 ± 0.8	26.0 ± 5.7
1.0, 50	n/a	0.9 ± 0.2	n/a

mass ion compared to the others investigated and will have more diffusion losses as it passes through the DIMS assembly.

3.2.2 Ion transmission with active DIMS: generation 3

The $\%T_{trans}$ for DIMS transparent is an important piece of information, but it is also critical to evaluate the $\%T_{active}$ for active DIMS, where the signal for the ion of interest is selected with a given dispersion field (E_D) and compensation field (E_C), and is then compared to the signal obtained without the DIMS assembly attached. With DIMS active, losses due to diffusion are expected as observed with DIMS transparent because whether DIMS is active or transparent, there is no voltage applied perpendicular to the electrodes, so lateral diffusion remains. In addition to ion losses due to lateral diffusion, ions can collide with the electrodes and be neutralized.

To clarify how ion losses occur on the electrodes with DIMS active, the effective analytical gap between the electrodes must be understood. The effective analytical gap (g_e) can be thought of as the difference between the gap size (g) and the oscillation amplitude (Δd) of an ion that has been selected with its optimum E_C. The selected ion has no net drift towards either electrode at its optimum E_C. This is represented in Figure 3.1, which includes traces for several different trajectories of ions with the same differential ion mobility (K_h-K_l) entering the gap at different positions between the electrodes and at varying time points during the DIMS waveform. The blue traces represent an ion that enters the gap halfway between the two electrodes, a distance from the electrode of $g/2$. The red traces represent ions that will be neutralized on one of the electrodes. For example, the ion in Figure 3.1a enters the gap as the waveform switches from E_l to E_h. Thus, it will be displaced toward the

upper electrode a distance of Δd before the waveform returns to E_l. If an ion enters the gap at a distance of Δd or less from the upper electrode, it will be neutralized on the upper electrode during the first period of the waveform. Ions entering the gap at any other point between the electrodes will be allowed to pass through the DIMS assembly. Thus, the effective analytical gap (g_e) can be described by equation 3.4, and Δd is described by equation 3.5, where P is one period of the waveform and K is the ion mobility.[1] Ions with a given K_h-K_l can be visualized as an ion beam traversing between the electrodes, with a width equal to g_e. The effect of constraining g_e is represented in Figure 3.2.

$$g_e = g - \Delta d \qquad \text{(Equation 3.4)}$$

$$\Delta d = \frac{1}{2}\int_0^P |KE_D(t)|dt \qquad \text{(Equation 3.5)}$$

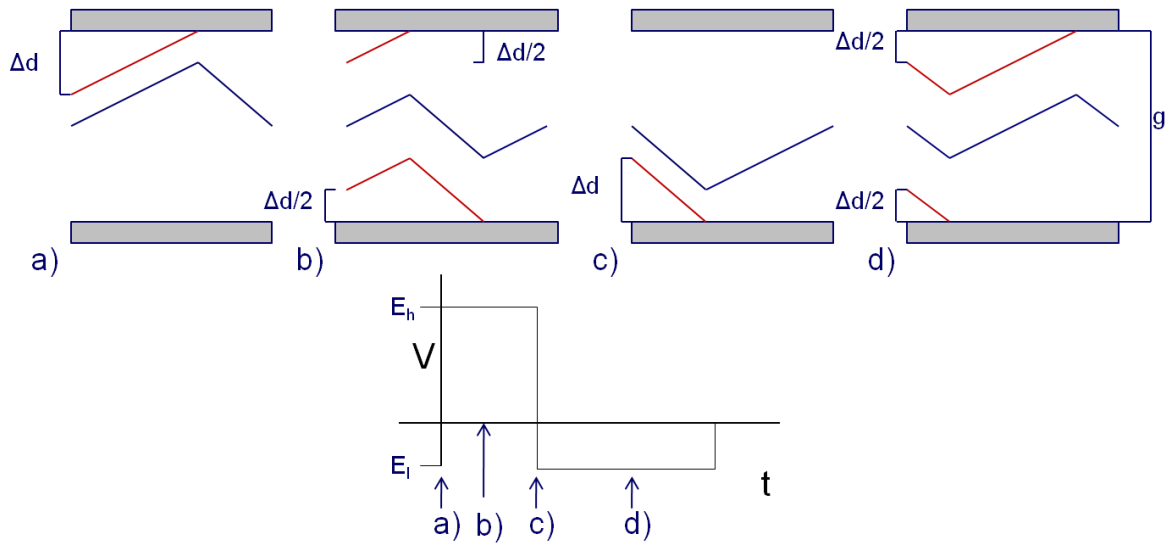

Figure 3.1 Ions entering the gap between the electrodes at various positions and time points during a cycle of the asymmetric waveform.

With DIMS active, as the physical gap between the electrodes is increased, so too is the effective analytical gap, assuming the dispersion field is constant. Therefore, a greater number of ions can be expected to pass through the assembly with the large gap size than is expected with the smaller gap size. This improvement in ion transmission is in opposition to

the expected ion losses due to lateral diffusion, where greater losses are expected for the larger transit time with the larger gap size.

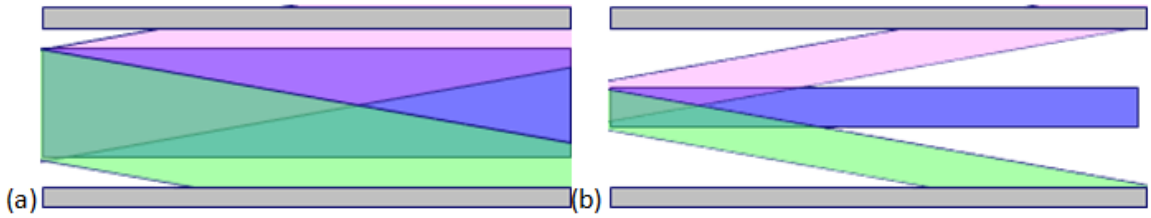

Figure 3.2. A simplified visualization of a constrained effective analytical gap, where (a) is a given separation of ion beams of varying K_h-K_l and (b) is the separation of the same set of ion beams with a constrained effective analytical gap.

The ion transmission and resolving power for active DIMS was determined using angiotensin I^{3+} with three of the different electrode sizes (Figure 3.3). From these data, it is readily apparent that the effective analytical gap plays a significant role in the observed ion transmission. Though lateral diffusion causes ion losses, the 0.5 mm gap size provides a greater $\%T_{active}$ than the 0.3 mm gap size at the electric fields used for these experiments, suggesting that ion losses on the electrodes are more significant for the smaller gap size. The ion transmission for the 50 mm long assembly was significantly lower than that observed for the shorter assembly due to diffusion losses within the assembly. At a given dispersion field, the resolving power is maximized with the long (50 mm) assembly as compared to the shorter (25 mm) assemblies. The improvement in *RP* with electrode length is expected because the *RP* is expected to increase with increased ion residence time.[5] However, the 0.5 mm gap with the 25 mm long electrodes ultimately provides the highest resolving power because a higher dispersion field can be used while still maintaining ion signal due to the

enhanced ion transmission of the shorter assembly over the longer assembly (Figure 3.3c-d).

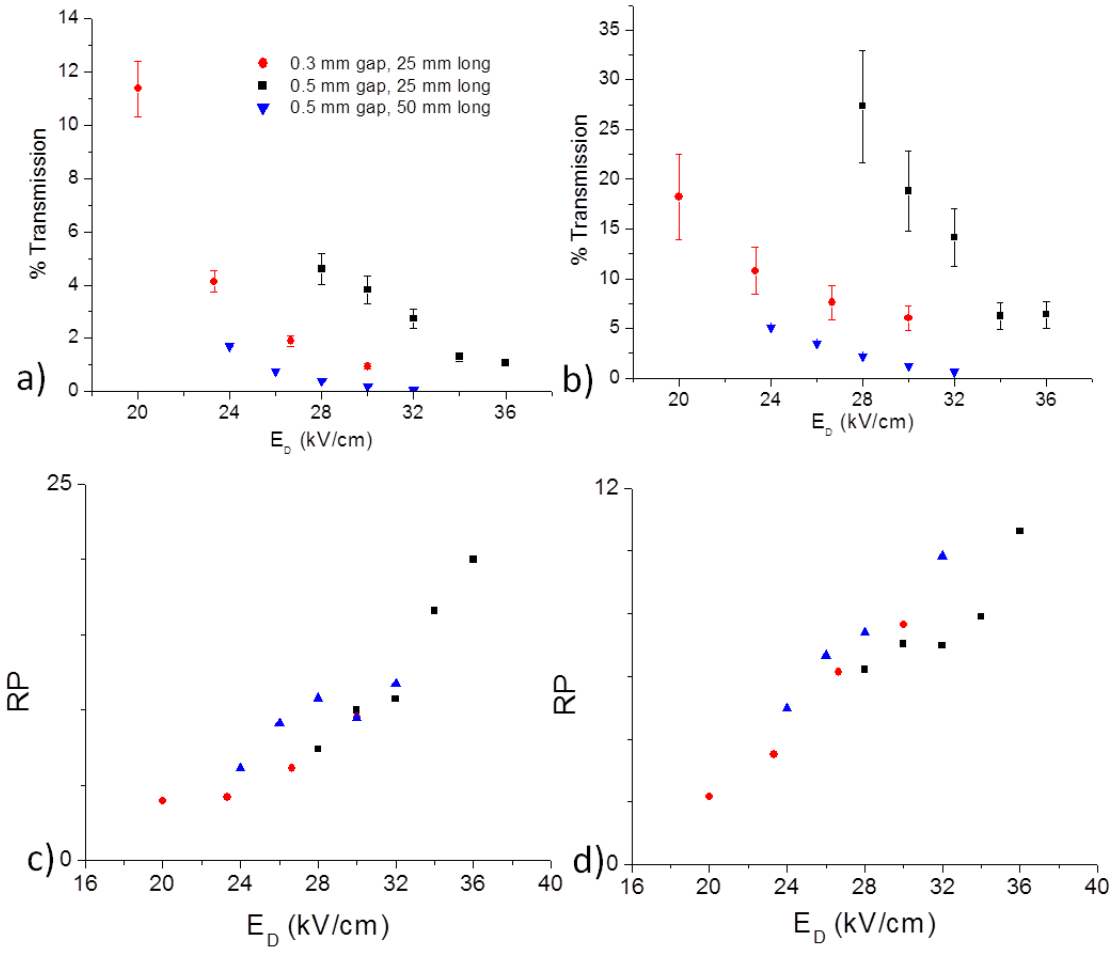

Figure 3.3. Ion transmission for DIMS active observed for angiotensin I with varying electrode dimensions: a) 3+, *m/z* 433 b) 2+, *m/z* 649 and RP with varying electrode dimensions: c) 3+, *m/z* 433 d) 2+, *m/z* 649.

The ion transmission and resolving power for active DIMS was determined using tetrabutylammonium chloride (TBACl) with three of the different electrode sizes (Figure 3.4). The $\%T_{active}$ for the singly charged tetrabutylammonium ion (*m/z* 242) with the 0.5 mm gap was greater than that observed with the 0.3 mm gap for the 25 mm long electrodes. The 50 mm long electrodes gave lower $\%T_{active}$ than the 25 mm long electrodes. As discussed for

angiotensin^{3+}, the RP is maximized by using the longer electrodes at each dispersion field, but with a lowered ion transmission.

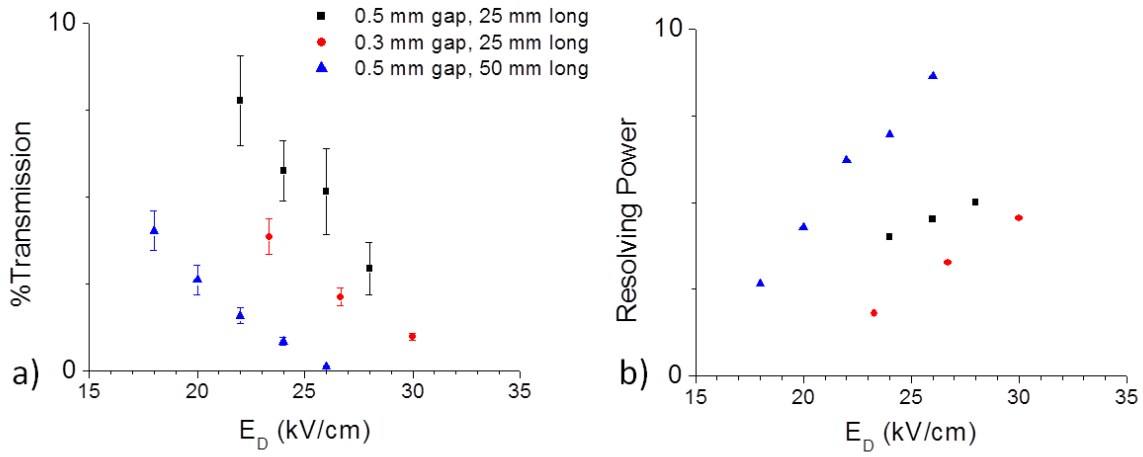

Figure 3.4. a) Ion transmission for DIMS active observed for the tetrabutyl ammonium ion (*m/z* 242) with varying electrode dimensions and b) RP with varying electrode dimensions.

The effect of changing the gap size between the electrodes was also investigated with brain natriuretic peptide (BNP), a biomarker for congestive heart failure which will be discussed further in Chapter 5. Utilizing a dispersion field of 30 kV/cm, the separation of the +5 charge state of BNP in a fetal bovine serum (FBS) extract was compared for the 0.3 (Figure 3.5a) and 0.5 mm (Figure 3.5b) gap sizes. The 0.5 mm gap provided a significant improvement in both ion transmission and resolving power over the 0.3 mm gap size, where a *RP* of 8 and *%T* of 0.11% was observed with the 0.3 mm gap, but a *RP* of 24 and a *%T* of 83% was observed with the 0.5 mm gap. Because the larger gap size has a larger volume between the electrodes, the ions will have an increased transit time through the assembly. An increase in transit time is expected to improve the separation of ions[5] and therefore can explain the improvement in resolving power.

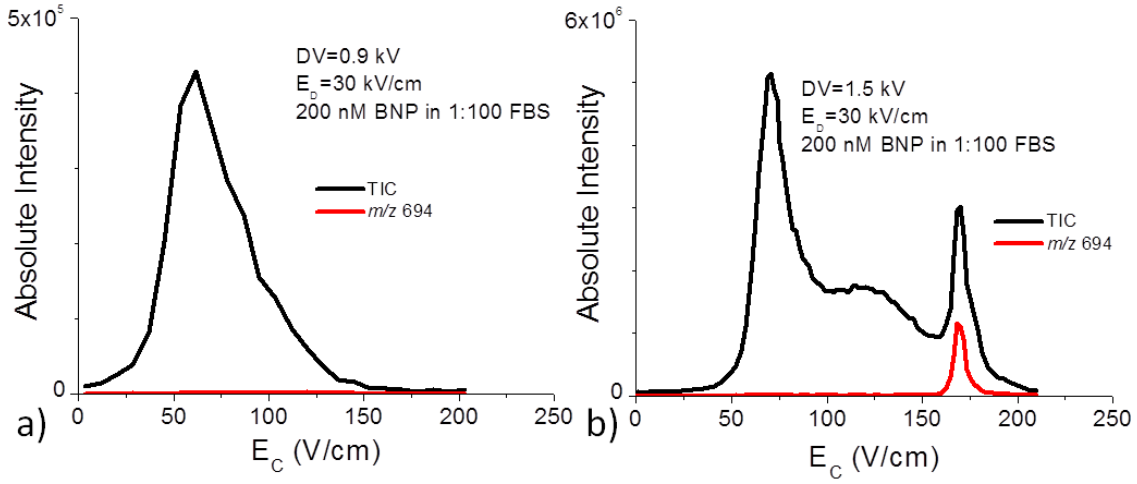

Figure 3.5. Separation of 200 nM BNP^{5+} in FBS extract with 25 mm long electrodes a) 0.3 mm gap and b) 0.5 mm gap.

3.2.3 From generation 3 to generation 4: ion transmission and resolving power

As discussed previously (2.3.1), generation 4 (G4) DIMS has smaller dimensions than G3, being 10 mm long, 4 mm wide, with a gap of 0.3 mm between the electrodes. Additionally, G4 is coupled to a transfer capillary with an i.d. of 0.6 mm, making the conductance limit 2.9 L/min, as compared to the conductance limit of 1.4 L/min for the capillary used with G3; the increased conductance limit corresponds to an increase in the gas flow between the electrodes. Due to the smaller dimensions and increased volumetric flow rate of the carrier gas, it is expected that the shorter ion transit time will cause a significant improvement in ion transmission when switching from generation 3 to generation 4. This shorter transit time is also expected to be detrimental to the observed resolving power for a given separation. BNP was used to compare the performance of G3 to G4 (Table 3.2).

Comparing G3 to G4, the primary difference is the electrode dimensions. The *RP* with G4 is lower than with G3 when compared at the same dispersion field because G4 is

shorter than G3, causing a decrease in the ion residence time. At the same dispersion field, greater than 100% ion transmission is observed with G4, whereas less than 1% is observed with G3. It should be noted that an ion transmission greater than 100% can be observed because an ion trap was used for these experiments. When background ions are filtered out by DIMS, the finite charge capacity of the ion trap is maximized with respect to the analyte ion, allowing a $\%T_{active}$ of greater than 100% to be observed (1.3.1). Because the $\%T_{active}$ was significantly increased, a higher dispersion field was able to be used, while still maintaining nearly 50% ion transmission. Thus, an increase in *RP* from 8.03 to 21.8 was observed for BNP when analyzed with generation 4.

Table 3.2. %T and RP obtained using BNP. *%T was calculated for active DIMS relative to DIMS ground rather than with the assembly removed

Electrode dimensions (mm)	E_D (kV/cm)	$\%T_{active}$* at peak E_C	RP
0.3 x 6 x 25 (G3)	33.3	0.11	8.03
0.3 x 4 x 10 (G4)	33.3	139.0	5.99
	50.0	48.8	21.8

3.3 Carrier gas parameters

3.3.1 Carrier gas temperature

As described previously (2.3.1), the housing of the DIMS assembly reroutes the desolvation gas already implemented in the source region of the mass spectrometer. This gas serves both as a desolvation gas for ESI as well as being the carrier gas through the DIMS assembly. The temperature (T) was varied from ambient to 106ºC with the protonated peptides YGGFL (*m/z* 556), AAAAA (*m/z* 374), and QQQQ (*m/z* 531). An increase in temperature is expected to increase diffusion (equation 3.6),[9] but also decrease low-field ion mobility (equation 3.7).[9]

With DIMS active, an increase in lateral diffusion is expected to decrease the ion transmission, and a decrease in ion mobility is expected to increase the ion transmission due to an increased g_e.

$$D = \frac{3}{16}\left(\frac{2\pi k_B T}{\mu}\right)^{1/2}\frac{1}{N\Omega} \qquad \text{Equation 3.6}$$

$$K = \frac{3}{16}\left(\frac{2\pi}{\mu k_B T}\right)^{1/2}\frac{ze}{N\Omega} \qquad \text{Equation 3.7}$$

In addition to investigating the ion transmission as a function of the carrier gas temperature, resolving power is an important parameter to consider. For each dispersion field, $\%T_{active}$, FWHM, peak E_C, and *RP* were determined for protonated YGGFL (*m/z* 556), AAAAA (*m/z* 374), and QQQQ (*m/z* 531) (Table 3.3). For each dispersion field used, the *RP* increased with increasing carrier gas temperature. An increase in desolvation gas temperature is expected to cause more complete desolvation of the ions formed by ESI. Bare, desolvated ions are expected to undergo more elastic, hard-sphere collisions with the carrier gas than solvated ions. The hard-sphere scattering model for ion-drift gas interactions predicts a decrease in ion mobility with increasing electric fields ($K_H < K_L$).[6] Peptide and protein ions exhibit a decrease in ion mobility with increasing electric fields in a nitrogen carrier gas, which in our assembly corresponds to a positive E_C value that increases with increasing dispersion fields.

DIMS is open to the atmosphere and therefore a change in temperature causes a change in the number density (N) of the buffer/carrier gas, where T and N are inversely proportional. Ion mobility is proportional to *E/N*,[9] increasing temperature is observed to have a similar effect on DIMS separations as increasing the dispersion field. Both desolvation effects and an increase in *E/N* are expected to shift peptide ions to higher (more

positive) E_C to be selected using DIMS. Therefore, an increase in *RP* is expected with increasing temperatures which was observed for protonated YGGFL, AAAAA, and QQQQ.

Table 3.3. $\%T_{active}$, FWHM, centroid E_C, and *RP* for protonated YGGFL (*m/z* 556), AAAAA (*m/z* 374), and QQQQ (*m/z* 531) for varying desolvation gas temperatures at E_D of 26, 30, and 34 kV/cm.

	26 kV/cm			30 kV/cm			34 kV/cm
Temp (°C)	YGGFL	AAAAA	QQQQ	YGGFL	AAAAA	QQQQ	YGGFL
$\%T_{active}$							
30	166.5	110.5	97.6	132.1	92.2	81.3	102.2
47	149.9	96.5	81	117.9	55.9	63.9	73.4
76	151.1	77.1	89.6	90.2	32.9	62.2	57.9
106	179.7	72	69.9	101.6	31.2	47.4	57.2
FWHM							
30	15.7	19	15.2	17.2	23.9	15.3	20.3
47	16.3	15	20.1	17	16.8	16.8	17.4
76	12.5	15.5	15.9	19.5	18.6	17.8	24.1
106	15.7	18	12.6	18.2	20.5	19.9	23.8
centroid EC							
30	50.6	54.6	47.5	73.8	83.2	68	114.9
47	56.4	66.2	50.7	87.1	102.6	79.2	122.4
76	65.2	83.2	62	98.4	124.5	90.9	141
106	71.8	93.6	67.7	108	137.8	102.1	151.9
RP							
30	3.3	2.9	3.1	4.2	5.6	4.5	5.9
47	3.6	4.4	2.5	5.5	6.2	4.7	6.9
76	4.7	5.4	3.9	5.2	6.6	5.1	6.1
106	4.7	4.3	5.4	5.7	6.5	5.1	6.7

3.3.2 Desolvation gas flow rate

With the DIMS design used for these experiments, the desolvation gas flow can be varied to manipulate the temperature of the carrier gas between the electrodes of the DIMS assembly. With a desolvation gas temperature setting of 300 ºC, the temperature of the electrodes is 53ºC at a flow rate of 2.5 L/min, 84ºC at 5 L/min, and 111ºC at 7.5 L/min. With an increase in the temperature, the gas number density in the analytical gap decreases because the

pressure is constant. Thus, *E/N* increases with increasing carrier gas temperature causing a shift in the observed E_C of a given ion. The default desolvation gas flow rate is 5 L/min and was used for all experiments when not specified. Using a mixture of YLFTLEPQT and LLSLLLLMPV, which are isobaric peptides with a nominal molar mass of 1111 Da, the resolution between the two peaks was determined at various desolvation gas flow rates, using 100% nitrogen and a fixed E_D of 72 kV/cm (Figure 3.6). These data confirm that for these isobaric peptides, the resolution increases from 0 to 1.26 as the desolvation gas flow rate increases from 2.5 to 7.5 L/min at a constant E_D. As with the increased electric fields, increasing the temperature within the gap causes a decrease in ion transmission through the DIMS assembly.

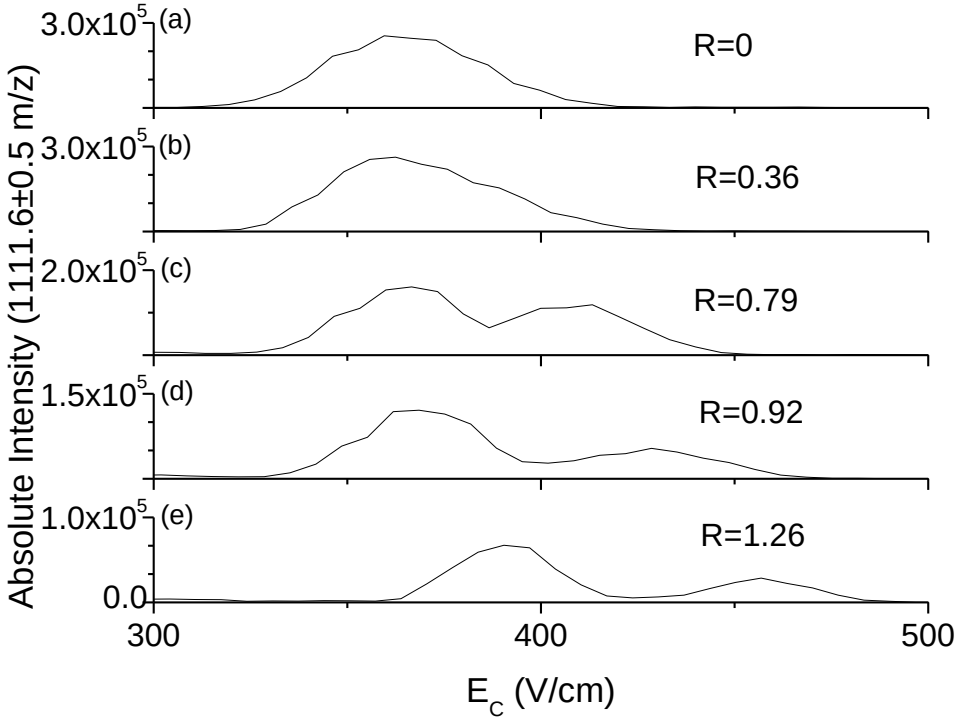

Figure 3.6 DIMS scans obtained as desolvation gas flow rate is varied at a fixed E_D of 72 kV/cm (a) 2.5 L/min, (b) 4 L/min, (c) 5 L/min, (d) 6 L/min, and (e) 7.5 L/min. Resolution was calculated at each flow rate.

In the DIMS assembly used for these experiments, varying the desolvation gas flow rate does not affect the ion residence time in DIMS. The DIMS assembly is coupled to a glass transfer capillary through which ions are drawn into the mass spectrometer. This glass capillary has a conductance limit of approximately 1.4 L/min. Because of this conductance limit, the volumetric gas flow rate through the DIMS assembly, which dictates the residence time of ions, does not change as the desolvation gas flow is varied. If the separation time is increased for a DIMS separation, the resolving power improves, but the centroid E_C of the peak of interest remains the same.[4,5] Because the centroid E_C of the peak of interest changes when the desolvation gas flow is varied, this confirms that separation time is not the reason for the observed changes in resolving power. The increase in resolving power with an increase in the desolvation gas flow rate cannot be explained by a change in separation time, but rather a change in temperature of the gas within the DIMS assembly.

3.4 Carrier gas composition: adding helium to the mix

3.4.1 Using helium to improve DIMS separations

Adding helium to the nitrogen carrier gas can improve the resolution of DIMS separations.[6,8] With all other parameters held constant, the addition of helium has a similar effect as increasing E_D, improving the separation of the mixture at the expense of signal intensity. The mobility of an ion increases with an increasing percent of helium in nitrogen because ions have a longer mean free path in helium as compared to nitrogen for a given gas number density. Therefore, it is expected that the addition of helium will cause an increase in the lateral diffusion of ions, causing a decrease in the ion transmission through the assembly relative to the ion transmission with 100% nitrogen as the carrier gas. It is also expected that

the addition of helium will increase the amplitude of ion oscillation within the gap (Δd), thereby decreasing the effective analytical gap, increasing the resolving power of DIMS separations and causing a greater percentage of ions to be neutralized on the electrodes. Helium is smaller and is less polarizable than nitrogen. Therefore, ions will undergo more elastic, "hard-sphere" collisions with helium than with nitrogen.[6] With the addition of helium to the nitrogen carrier gas, a greater differential ion mobility ($K_H << K_L$) is expected due to the increase in "hard-sphere" collisions. As discussed previously (3.3.1), an increase in hard-sphere collisions is expected to increase the E_C value required to select for a given ion. Therefore, for a given dispersion field, an increase in the helium content is expected to cause a shift to higher E_C values for DIMS scans of peptide and protein ions.

As previously discussed (3.1), a shift to higher E_C inherently leads to an increase in *RP*, even if the peak width remains the same. Therefore, to assess the separation improvement observed with helium added to the carrier gas, the resolution was determined for a mixture of two peptides with the same nominal *m/z* 1112, YLFTLEPQT and LLSLLLLMPV (Figure 3.7). At a constant dispersion field of 46.7 V/cm, the percent of helium (*%He*) in the carrier gas was increased from 20% to 50%. With the increase in helium content, the resolution of the two peaks increased from 0.39 to 0.97. These data confirm that the addition of helium to the carrier gas not only shifts the observed E_C for an analyte ion, but also improves the separation of mixtures.

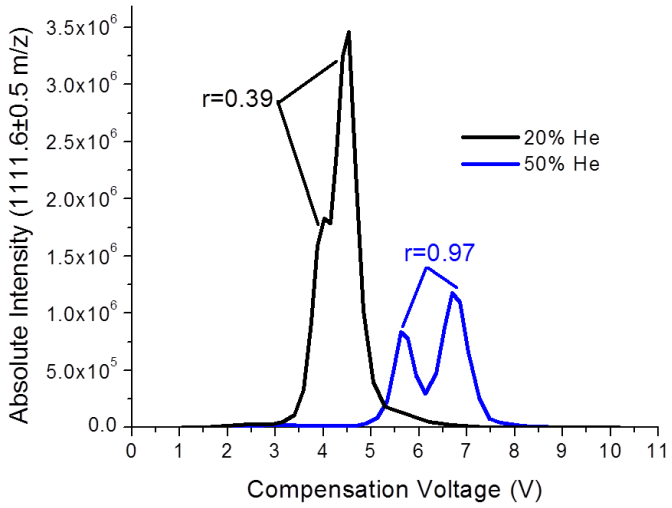

Figure 3.7 Resolution of a mixture of isobaric peptides, YLFTLEPQT and LLSLLLLMPV (*m/z* 1112) with 20% and 50% He in N_2 carrier gas.

3.4.2 Linked scanning

With the addition of helium to the carrier gas, significant losses in ion transmission are observed, especially for ions of low mass-to-charge ratios. Low mass ions have a higher diffusion rate than high mass ions, and in general exhibit more ion losses in the DIMS assembly. Additionally, low mass ions tend to have a higher ion mobility, meaning they have a smaller g_e than higher mass ions. Similarly, ions with a high charge state have a higher absolute ion mobility than ions of the same mass with a lower charge state, again leading to a difference in g_e. In an attempt to minimize ion losses while maximizing resolving power by adding helium, a linked scan, where helium content is decreased as E_C is increased was developed.

The separation of a mixture of 4 peptides, all observed as singly charged protonated ions when produced by ESI, was evaluated with 0, 20 and 40% helium, as well as for a linked scan where *%He* was decreased from 40 to 0% while the E_C was scanned. The resultant DIMS spectra were plotted in Figure 3.8 for a dispersion field of 32 kV/cm. As expected, a decrease in intensity is observed as the *%He* is increased, with the lowest mass

peptides essentially unobservable at 40% He. With the linked scan (Figure 3.8d), all four peptides are observable, and the resolving power of all four peaks is greater than that observed for any of the static *%He*. *RP* was determined for these four peptides at four different dispersion fields, and the results are tabulated in Table 3.4. For all dispersion fields, the linked scan provided the highest resolving power for all four peptides in the mixture.

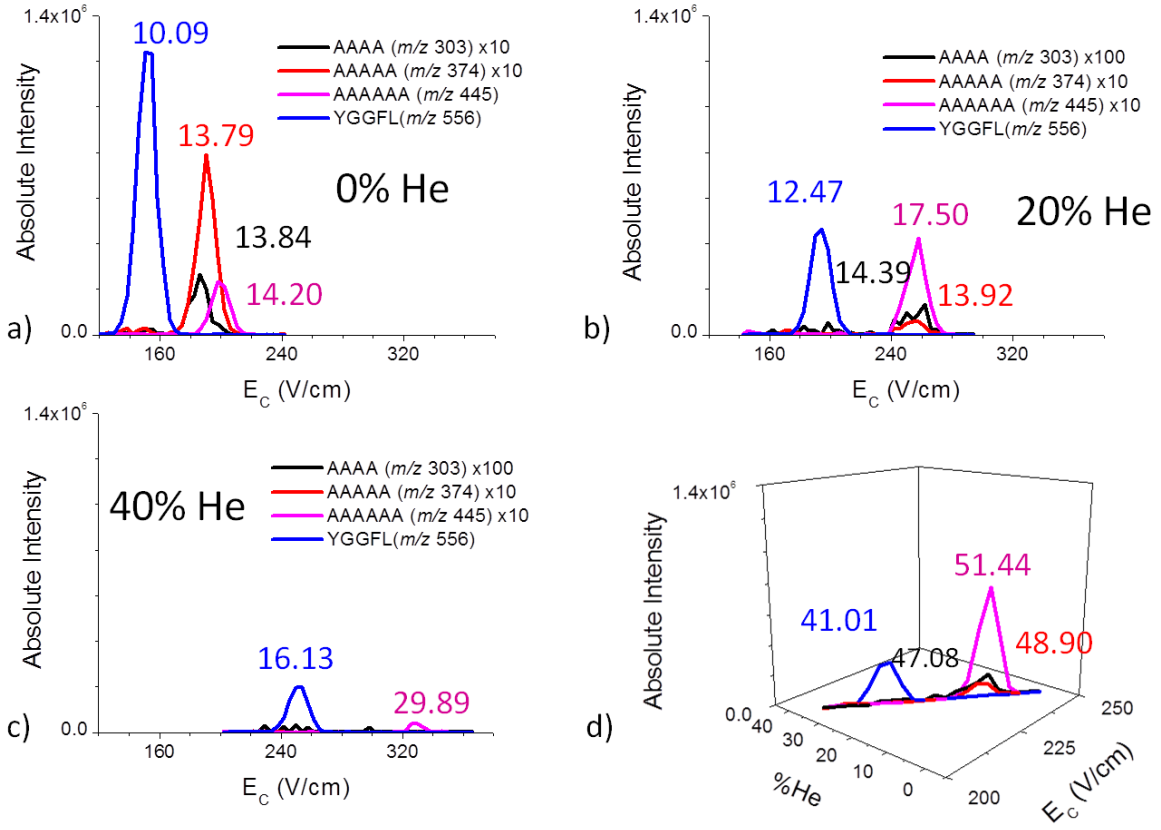

Figure 3.8. Separation of a peptide mixture with a) 0% He, b) 20% He, c) 40% He, and d) linked scan from 40 to 0% He. Resolving powers for each peak are provided above the peak.

One of the reasons that the *RP* observed for the linked scans are significantly greater than those observed for static *%He* DIMS scans is that for each observable peak, the helium content is being reduced as the E_C is increased. As previously mentioned (3.4.1), peptide and protein ions are expected to shift to higher E_C values due to a change in differential ion

Table 3.4. *RP* for each peptide in mixture of AAAA (*m/z* 303), AAAAA (*m/z* 374), AAAAAA (*m/z* 445) and YGGFL (*m/z* 556) at 0, 20 and 40% He and for the linked scan.

E_D (kV/cm)		0 % He	20% He	40% He	Linked (40-0%)
26	*m/z* 303	8.89	9.43	12.12	17.55
	m/z 374	7.25	9.27	13.57	19.21
	m/z 445	7.93	10.65	13.96	17.58
	m/z 556	4.98	7.41	11.75	13.36
28	*m/z* 303	9.34	12.38	n/a	31.00
	m/z 374	9.36	12.35	14.04	25.92
	m/z 445	10.60	13.55	15.26	28.01
	m/z 556	6.17	9.70	12.61	21.56
30	*m/z* 303	9.56	13.73	n/a	47.42
	m/z 374	9.92	13.6	17.42	40.94
	m/z 445	11.29	14.57	20.03	40.79
	m/z 556	7.40	11.06	13.33	34.58
32	*m/z* 303	13.84	14.39	n/a	47.08
	m/z 374	13.79	13.92	n/a	48.90
	m/z 445	14.20	17.50	29.89	51.44
	m/z 556	10.09	12.47	16.13	41.01

mobility as helium content is increased. Thus, when the helium content is decreased as the compensation field is increased, the range of compensation fields that allow for a given ion to be selected is effectively narrowed. This effect can be observed in Figure 3.9, where the peak observed for protonated YGGFL (m/z 556) at a dispersion field of 32 kV/cm is plotted for each fixed *%He* as well as for the linked scan. As the helium content is increased, the peak is shifted to higher compensation fields as expected, but the FWHM is near 15 V/cm for all *%He*. When a linked scan is used, the FWHM is only 5 V/cm. For this linked scan, the helium content from 210 V/cm to 225 V/cm decreases from 33% He to 20% He. The centroid E_C for the observed peak is where it would be expected for a DIMS scan with approximately 27% He, but the peak width is narrowed compared to what would be expected for a scan with a fixed *%He* because the helium content is decreased across the peak.

Considering the above discussion with respect to the observed peak width in a linked scan, the slope of the linked scan ($\%He/E_C$) is expected to have an effect on the resolving

power. It is expected that a higher slope will provide a more narrow peak than a lower slope because there will be a greater change in helium content across a given peak. For all of the linked scans within this dissertation, the slope was maximized by decreasing the helium content where peaks were observed from the sample, rather than linking the helium scan to a broad CV range. More systematic experiments are needed to determine the importance of the slope with respect to the resolving power of the DIMS scan.

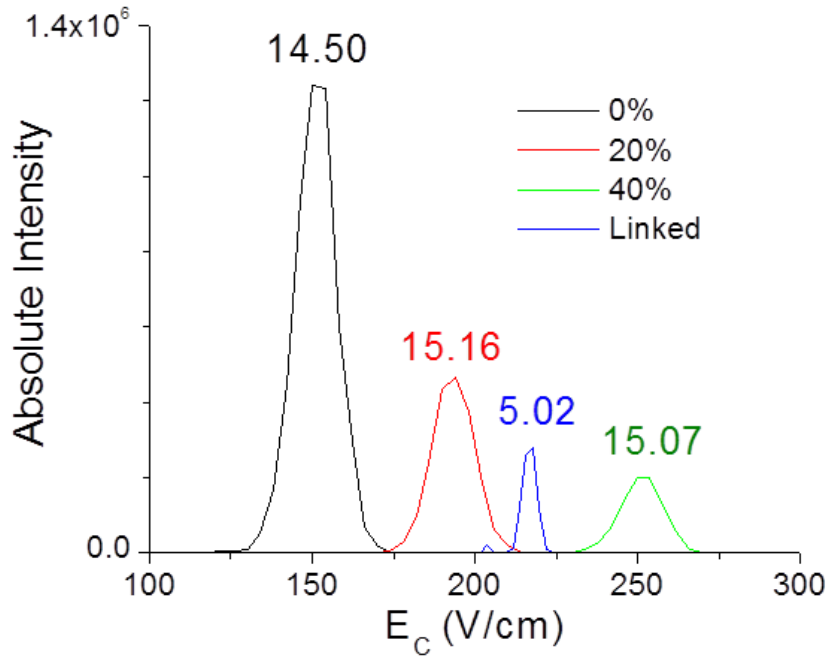

Figure 3.9. Peak observed for protonated YGGFL (*m/z* 556) for varying *%He* and for linked scan. FWHM listed above each peak.

A similar set of experiments was carried out with the protein ubiquitin to determine the effect on resolving power with the linked scan as compared to a static *%He*. The resolving powers observed for the 7+ (*m/z* 1225), 8+ (*m/z* 1072), and 9+ (*m/z* 953) charge states of ubiquitin for each condition can be found in Table 3.5. As expected, the RP observed for the linked scans was significantly higher than that observed for the fixed *%He*

DIMS scans for the same dispersion field . Additionally, the highest charge state investigated (9+, *m/z* 953) was unobservable with 40% helium at dispersion fields greater than 32 kV/cm, but when a linked scan was used, the 9+ charge state was observable at all of the investigated dispersion fields.

Table 2.5. *RP* for 7+ (1225), 8+ (*m/z* 1072), and 9+ (*m/z* 953) charge states of ubiquitin at 0, 20 and 40% He and for the linked scan.

E_D (kV/cm)		0 % He	20% He	40% He	Linked (40-0%)
26	*m/z* 953	10.28	15.72	20.08	23.08
	m/z 1072	9.74	13.48	19.07	32.53
	m/z 1225	5.34	7.57	11.83	16.29
28	*m/z* 953	20.40	22.51	28.73	40.39
	m/z 1072	16.80	17.06	24.03	34.60
	m/z 1225	10.41	10.85	14.31	20.43
30	*m/z* 953	22.13	26.88	29.68	42.45
	m/z 1072	22.57	20.98	26.99	45.84
	m/z 1225	9.47	12.44	14.02	23.97
32	*m/z* 953	20.87	32.89	n/a	43.07
	m/z 1072	26.16	25.84	26.32	40.29
	m/z 1225	13.85	9.63	26.92	22.69
34	*m/z* 953	25.83	44.71	n/a	69.86
	m/z 1072	23.27	30.39	33.06	53.10
	m/z 1225	13.27	15.13	20.22	32.28

3.4.3 Maximum E_D for varying %He

While helium improves the separation power of DIMS at a given E_D, there are a few drawbacks to the use of helium in the carrier gas, including the fact that helium has a lower pumping efficiency than nitrogen, causing elevated pressures in the fore region of the mass spectrometer. Many commercial instruments have a failsafe that will automatically shut down the instrument if the pressure rises above a given threshold. The addition of helium to the carrier gas also causes a decrease in the breakdown voltage in the gap[10] between the electrodes compared to nitrogen. Therefore, higher dispersion fields are accessible with pure nitrogen as the carrier gas than with helium added.

At a given percentage of helium in nitrogen, the highest resolving power achievable will be under conditions with the highest E_D possible. To determine which condition is optimal, the DIMS waveform was tuned up to the maximum E_D accessible for 0, 16, and 32 percent helium in nitrogen (Table 3.6). The $\%T_{active}$ was determined for YLFTLEPQT (a), LLSLLLLMPV (b), AMNGVIFLV (c), and SVSIYTPVV (d). The *RP* was determined with individual solutions of AMNGVIFLV (c) and SVSIYTPVV (d) to compare the performance of the DIMS assembly under each condition. Additionally, the *R* of a mixture of two peptides with the same nominal molar mass, YLFTLEPQT (a) and LLSLLLLMPV (b), was determined under each condition. The ion transmission was also calculated for all four of the peptides under each condition.

Table 3.6. Ion transmission, resolving power and resolution for each % helium (n=3). Peptides are designated as follows: (a) YLFTLEPQT, (b) LLSLLLLMPV, (c) AMNGVIFLV, and (d) SVSIYTPVV.

% He	Maximum E_D (kV/cm)	%T				RP		R
		a	b	e	g	e	g	(a&b)
0	74	0.93 ±0.13	1.70 ±0.21	0.87 ±0.11	0.75 ±0.12	14.01 ±0.57	12.52 ±0.97	0.73 ±0.12
16	68	1.85 ±0.20	5.66 ±0.61	1.81 ±0.21	0.84 ±0.26	14.19 ±1.12	12.83 ±3.33	0.63 ±0.12
32	57	2.04 ±0.24	7.63 ±0.76	5.31 ±0.46	1.43 ±0.27	12.01 ±1.51	9.27 ±1.23	0.50 ±0.08

The resolving power did not show a clear trend favoring a higher dispersion field or a higher percentage of helium in the carrier gas. A decrease in E_D is expected to reduce the resolving power of DIMS, but because the amount of helium can be increased as the E_D is decreased the net effect on resolving power is statistically insignificant. While a calculated resolving power is helpful in describing the performance of the DIMS assembly, it does not provide information about the separation of two peaks. For the separation of YLFTLEPQT and LLSLLLLMPV, the average resolution (n=3) was maximized with a E_D of 74 kV/cm and

0% helium added to the nitrogen carrier gas. These data show a trend in ion transmission across the three different conditions, where the highest percentage of helium investigated for these peptides did exhibit a reduction in resolution, but an increase in ion transmission was observed for all of the peptide ions because the E_D was lowered.

3.5 Separation of 3 isobaric peptides

A group of three of the peptides (YLFTLEPQT, LLSLLLLMPV and ILSFVFIMAA) that have the same nominal molar mass (1111 Da) was selected to determine if DIMS would provide the resolution necessary to separate peptides of similar mass and polarity. Due to their similarity in mass, conventional tandem mass spectrometry techniques cannot isolate one peptide from the others to produce distinct MS/MS spectra when they are ionized as a mixture. These peptides are primarily composed of hydrophobic residues, making them difficult to separate by polarity using chromatographic methods. DIMS separates ions based on K_h-K_l and is complementary to MS, so it has potential for the use as a separation method for these peptides prior to mass spectrometry.

Utilizing the enhanced resolution with decreased carrier gas pressure and the high dispersion field (72 kV/cm) achievable with 100% nitrogen as the carrier gas, the mixture of three peptides was separable (Figure 3.10). The three peptides were not separable with helium added to the carrier gas. Each individual peptide can be selected for in the mixture by applying the optimal E_C: 460 V/cm for YLFTLEPQT, 397 V/cm for LLSLLLLMPV, and 430 V/cm for ILSFVFIMAA. Collision-induced dissociation (CID) was used to produce tandem mass spectra (MS/MS) at each E_C (Figures 3.11d, f, and h). Each MS/MS spectrum was compared to the MS/MS spectrum of a pure solution of the respective peptide without

DIMS (Figures 3.11c, e, and g). Additionally, MS and MS/MS spectra of the mixture were collected without DIMS to show the convolution of product ions from the three different isobaric parent ions (Figures 3.11a and b).

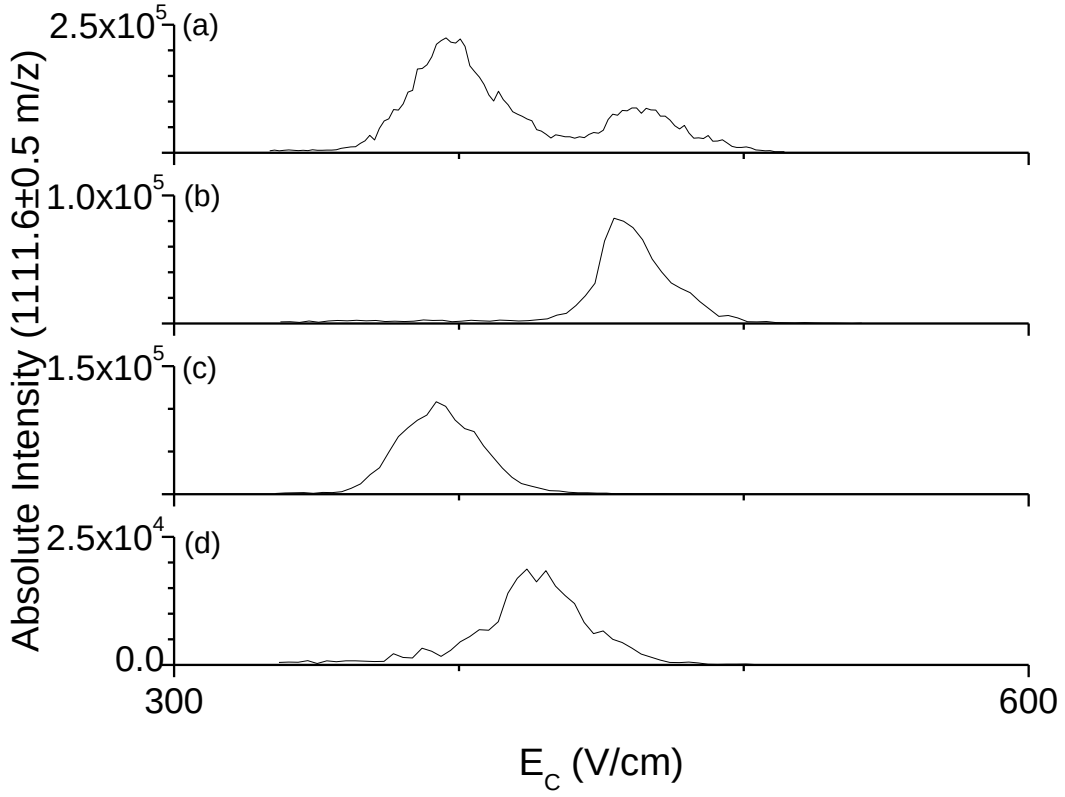

Figure 3.10. DIMS scans of isobaric peptides. (a) Mixture of 5 µM YLFTLEPQT, 5 µM LLSLLLLMPV, and 10 µM ILSFVFIMAA (b) Pure 5 µM YLFTLEPQT, (c) Pure 5 µM LLSLLLLMPV, (d) Pure 10 µM ILSFVFIMAA.

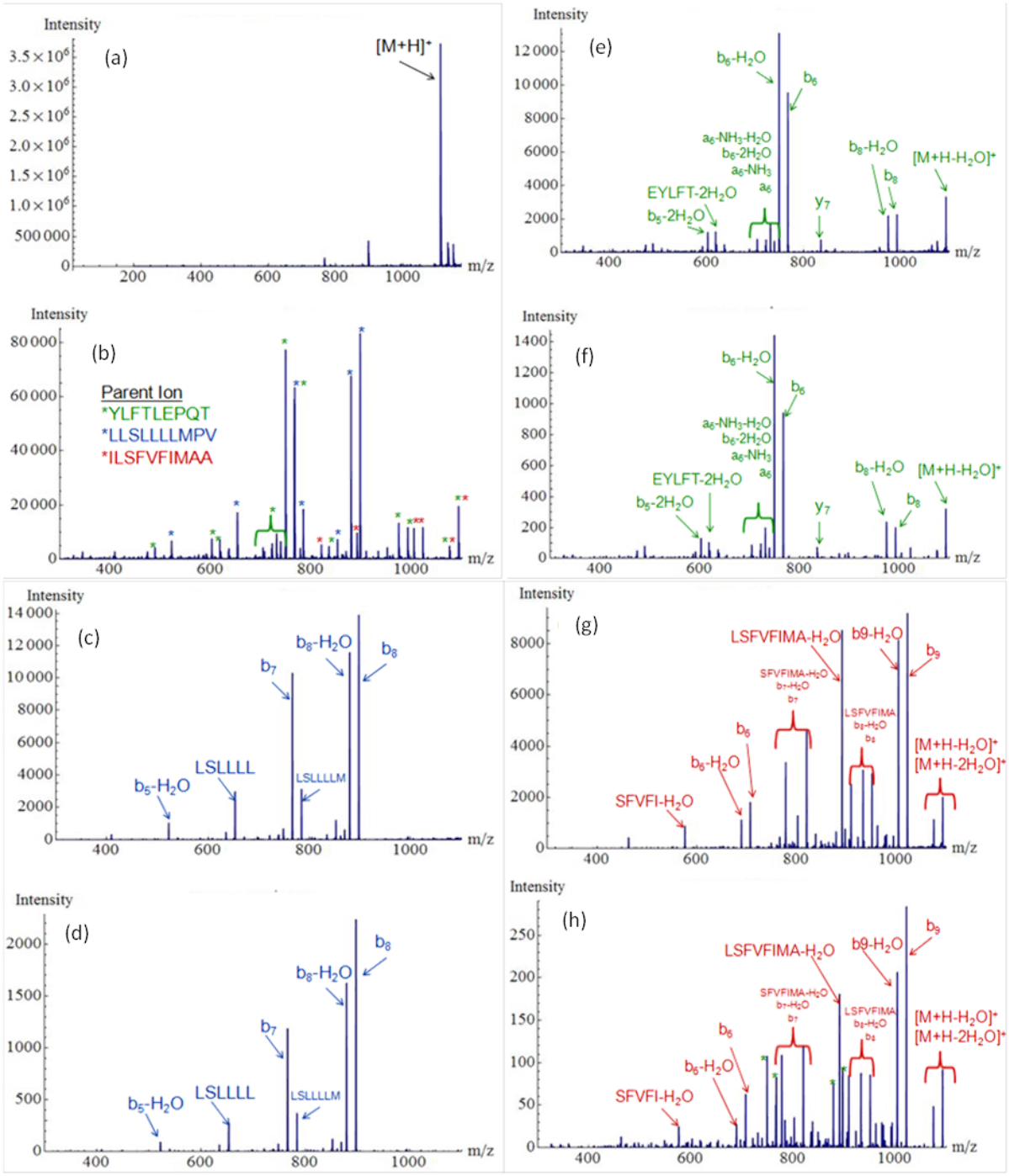

Figure 3.11. MS/MS spectra of a mixture of nominally isobaric peptides. (a) MS of mixture without DIMS, (b) MS/MS of mixture without DIMS, (c) MS/MS of pure 5 µM LLSLLLLLMPV without DIMS, (d) MS/MS of mixture at fixed E_C of 397 V/cm, (e) MS/MS of pure 5 µM YLFTLEPQT without DIMS, (f) MS/MS of mixture at fixed E_C of 460 V/cm, (g) MS/MS of pure 10 µM ILSFVFIMAA, (h) MS/MS of mixture at fixed E_C of 430 V/cm; green stars correspond to residual fragments from YLFTLEPQT, which can be reduced by applying a slightly higher E_C.

3.6 Summary and conclusions

The effects of electrode dimensions, carrier gas temperature and pressure, and carrier gas composition were investigated in the optimization of separations using DIMS. It was determined that for active DIMS, both losses due to diffusion and the effective analytical gap can affect ion transmission. This requires careful consideration of the electrode dimensions for the assembly. The length of the assembly will directly affect the transit time of ions through the assembly, which affects both ion transmission and resolving power. The gap between the electrodes will also change the transit time through the assembly and can cause losses of ions on the electrodes if the gap is too small. The effective gap is smallest for ions with a high mobility, so the gap size is critical when working with ions of low mass, high charge, or when adding helium to the carrier gas.

It was determined that temperature within the DIMS assembly can affect the separations. Both ion transmission and resolving power were increased as the carrier gas temperature was increased, due to improved desolvation prior to entering the DIMS as well as an increase in *E/N*. By increasing the desolvation gas flow rate to increase the temperature, the resolving power for the separation of peptides was increased, but the ion transmission decreased.

With helium added to the nitrogen carrier gas improvements in resolution are observed, along with decreases in ion transmission. A linked scan, where helium content is decreased as the compensation field is increased, was developed as an attempt to improve the ion transmission of high-mobility ions when helium was used. Not only does the ion transmission of high-mobility ions improve with the linked scan, but the resolving power significantly increases when a linked scan is used instead of a static *%He* DIMS scan for all

analyte ions studied. This is due to a narrowing of the peak observed when helium is decreased as the compensation field is increased.

Finally, we take into account the fact that the addition of helium to the carrier gas will reduce the maximum dispersion field achievable by comparing separations utilizing the greatest field accessible for each carrier gas composition investigated. The small gap size (0.3 mm) of the DIMS assembly allows for the maximum electric field achievable with nitrogen to be reached, with an applied DV of only 2.2 kV. For the peptides investigated in this study, it was determined that the resolution and resolving power were maximized with 100% nitrogen as the carrier gas, where an electric field of 74 kV/cm is achievable. Ion transmission, on the other hand, was maximized by increasing the percent helium in the carrier gas, and in turn lowering the maximum electric field . For a constant electric field, the addition of helium causes a decrease in ion transmission. However, when comparing the data obtained with maximized electric fields for each condition, the ion transmission is greatest when helium is added because the maximum electric field is lowered with helium as compared to pure nitrogen.

To separate a mixture of three isobaric peptides, pure nitrogen had to be used as the carrier gas. Additionally, the flow rate of the desolvation gas was elevated to lower the gas pressure in the DIMS assembly. The conditions needed to achieve the best resolution also caused the greatest decrease in ion transmission through the assembly. These data highlight the fact that for DIMS separations, as is common for most analytical techniques, it is necessary to consider the trade-off between sensitivity and resolution when optimizing conditions for a given application.

3.7 REFERENCES

1. Buryakov, I.A. Mathematical analysis of ion motion in a gas subjected to an alternating-sign periodic asymmetric-waveform electric field. *Tech. Phys*. **51**, 16-21 (2006)

2. Shvartsburg, A. A.; Prior, D. C.; Tang, K.; Smith, R. D. High-resolution differential ion mobility separations using planar analyzers at elevated dispersion fields. *Anal. Chem.* **82**, 7649-7655 (2010)

3. Barnett, D.A.;, Oullette, R.J.: Elimination of the helium requirement in high-field asymmeteric waveform ion mobility spectrometry (FAIMS): beneficial effects of decreasing the analyzer gap width on peptide analysis. *Rapid Commun. Mass Spectrom.* **25**, 1959-1971 (2011)

4. Schneider, B.B.; Covey, T.R.; Coy, S.L.; Krylov, E.V.; Nazarov, E.G.: Planar differential mobility spectrometer as a pre-filter for atmospheric pressure ionization mass spectrometry. *Int. J. Mass Spectrom.* **298**, 45-54 (2010)

5. Shvartsburg, A. A.; Smith, R.D.: Ultrahigh-resolution differential ion mobility spectrometry using extended separation times. *Anal. Chem.* **83**, 23-29 (2011)

6. Schneider, B.B.; Covey, T.R.; Coy, S.L.; Krylov, E.V.; Nazarov, E.G.: Chemical effects in the separation process of a differential mobility/mass spectrometer system. *Anal. Chem.* **82**, 1867-1880 (2010)

7. Shvartsburg, A. A.; Tang, K. Q.; Smith, R. D. Understanding and designing field asymmetric waveform ion mobility spectrometry separations in gas mixtures. *Anal. Chem.* **76**, 7366-7374 (2004)

8. Shvartsburg, A. A,; Danielson, W. F.; Smith, R. D. High-resolution differential ion mobility separations using helium-rich gases. *Anal. Chem.* 82, 2456-2462 (2010)

9. Mason, E. A.; McDaniel, E. W. *Transport properties of ions in gases*. John Wiley & Sons Inc.: New York, 1988

10. Paschen, F., Ueber die zum Funkenübergang in Luft, Wasserstoff und Kohlensäure bei verschiedenen Drucken erforderliche Potentialdifferenz. *Annalen der Physik*, **273**, 69-96 (1889)

CHAPTER 4: DIMS FOR THE INVESTIGATION OF ION REACTIONS IN TRANSFER OPTICS

4.1 Introduction to ion reactions in transfer optics

4.1.1 Ion transfer optics for ESI-MS

Electrospray ionization (ESI) was an important development in the field of mass spectrometry, but with its development came the necessity to use optics to transfer ions from atmospheric pressure to the high vacuum region of a mass spectrometer. For ESI in particular, it is important to desolvate ions prior to mass analysis. Commonly, a heated countercurrent desolvation gas is implemented on the front end of a mass spectrometer to prevent solvent droplets from entering the instrument.[1-3] In some instruments, a transfer capillary, typically composed of stainless steel or glass is used to carry ions via gas flow to the vacuum region of the mass spectrometer. Skimmers are often used in transfer optics, to which a voltage is applied to aid in breaking apart solvent clusters prior to mass analysis.

The design and settings of ion transfer optics can affect the ions that are observed in a mass spectrum. Ion reactions occurring in the transfer optics may cause fragmentation or a shift in the observed charge state distribution. These chemical reactions are often the reason that a mass spectrum for a given sample could appear different when analyzed on different mass spectrometers.

4.1.2 Ion reactions before, within, and after DIMS

As an atmospheric pressure separation method, differential ion mobility spectrometry (DIMS) can be used to separate ions at atmospheric pressure, immediately after ionization. Reactions in the ion optics will affect which ions arrive at the mass analyzer, but will not affect DIMS separations. Ions formed by a reaction in the ion source can be separated using DIMS, however reactions occurring within or after DIMS can make the results more complicated to interpret. For reference with respect to discussion of reactions in the transfer optics, a basic schematic of the instrument used for DIMS experiments is provided in Figure 4.1.

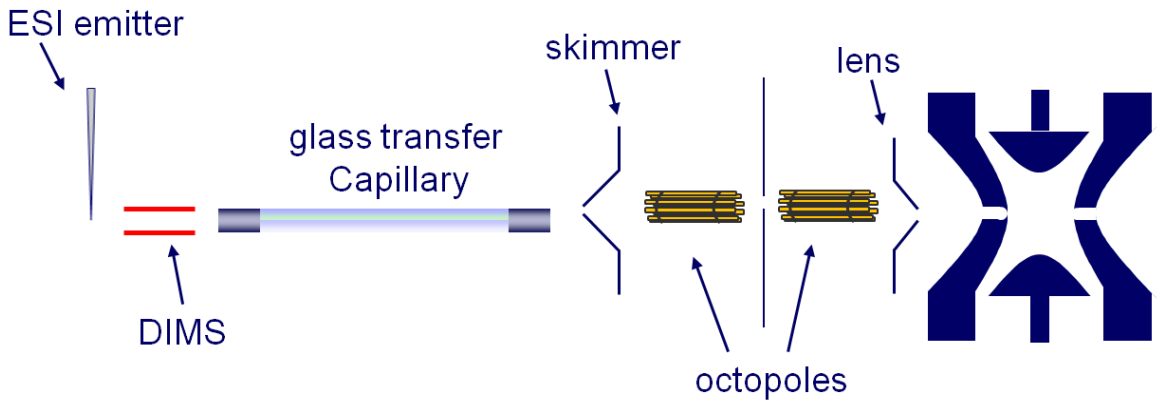

Figure 4.1. Basic schematic of ESI-DIMS-MS instrument.

A given compensation field (E_C, 1.4.3) will select for a specific differential ion mobility, where an ion with the selected differential ion mobility will have a net drift of zero and be able to pass through the device into the mass spectrometer. It is important to remember that even in scanning mode, E_C is static on the time scale of an ion passing through the device because the ion transit time is on the order of 10 ms. If the selected ion (MH^+) undergoes a reaction as it is travelling through the device, most likely the mobility of the fragment ion (F^+) formed will be different than that of the original ion that entered the

device. Therefore, F^+ will have a different trajectory, and will collide with one of the electrodes and not be detected. Some F^+ may be observed at the same compensation field as MH^+ if the reaction occurs close to the exit of the device. In general, if the reaction to form F^+ occurs within DIMS, F^+ will not be observed.

DIMS can be used determine whether the observed peaks in a mass spectrum are due to ionization or as a result of a reaction occurring in the transfer optics prior to detection at the mass analyzer. If F^+ were formed during ionization prior to DIMS, and traversed through DIMS as F^+, then it would be selected at its peak E_C value. If a reaction occurs after DIMS, in the transfer optics prior to mass analysis, F^+ will be observed in the mass spectrum at the compensation field selecting for MH^+, rather than the compensation field selecting for F^+ (Figure 4.2).

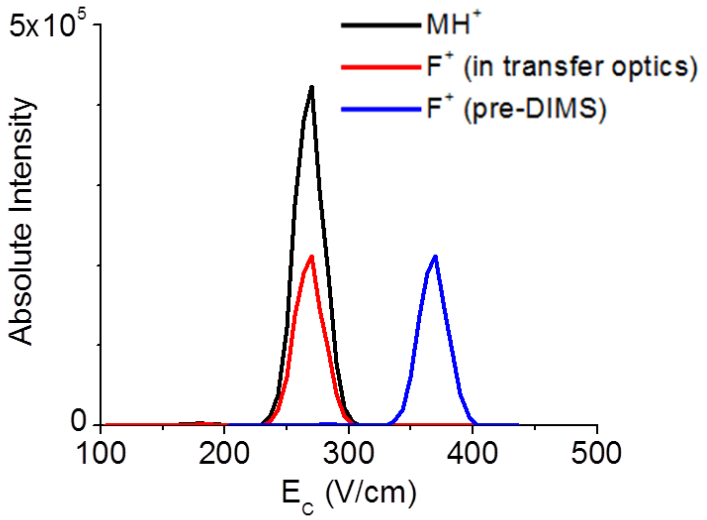

Figure 4.2. Example DIMS-MS scan of a protonated molecule (MH^+) in black and its fragment (F^+) formed in the transfer optics (red) and formed via ESI prior to DIMS (blue).

Various complexes can be formed via ESI, including proton-bound multimers and adducts.[1-3] As mentioned previously (4.1.1), ion transfer optics are designed in part to help

break apart these complexes and allow for the bare analyte ion to be analyzed. If a given analyte ion is formed via ESI and also formed via the breakdown of a complex in the transfer optics, then two peaks will be observed for that ion in the DIMS-MS scan (Figure 4.2).

4.2 Fragmentation in ion transfer optics: potential pitfalls and uses with DIMS

4.2.1 Ion reactions after DIMS can convolute results

Peptides have multiple possible protonation sites, and it is possible that the structures with different protonation sites could be separated based on their ion mobility. From spectroscopy experiments, it has been proposed that protonated GGG (*m/z* 190) formed via ESI exists in two different structures, dependent upon protonation site.[4] To investigate protonated GGG formed via ESI, DIMS-MS was used. If there are in fact two distinct protonation sites, (assuming the resolution is good enough to separate the two structures) then two peaks should be observed in the DIMS-MS scan, one for each structure present.

Two peaks are observed in the DIMS scan of protonated GGG at an E_D of 26 kV/cm (Figure 4.3a), suggesting that two distinct structures are formed via ESI. The b_2 fragment ion of GGG (*m/z* 115) is also observed. Relative to the protonated peptide, the b_2 fragment ion is much more intense at the low E_C peak than it is at the high E_C peak. This suggests that there was a fragmentation of protonated GGG prior to mass analysis. The presence of two peaks also suggested the presence of two different structures: one of which easily fragmented to the b_2 fragment ion, and the other of which was more stable. The transfer optics were retuned in an effort to minimize fragmentation prior to mass analysis. To eliminate the fragment ion, the offset voltage between the exit of the transfer capillary and the skimmer was set to 0 V. The offset between the two octopole ion guides was also set to 0 V. After tuning the transfer

optics, the DIMS-MS scan was repeated and only one peak was observed for the protonated peptide (Figure 4.3b). The default ion optics parameters used for Figure 4.3a used an offset voltage between the exit of the transfer capillary and the skimmer of 63 V and an offset between the two octopole ion guides of 10.3 V.

To further investigate the origin of the second peak observed for protonated GGG, the E_C was set to a static value of 65 V/cm. No significant peak was observed in the mass spectrum until the trap drive was increased. In Bruker ion traps, the trap drive varies the rf amplitude as ions are being gated into the trap. This value changes how effectively ions of different mass-to-charge ratios are gated into the ion trap. In essence, setting the trap drive to a higher value allows higher mass-to-charge ions to be trapped efficiently, and setting the trap drive to a lower value allows lower mass-to-charge ions to be trapped efficiently. When the trap drive was increased, with an E_C of 65 V/cm, a peak was observed at *m/z* 412 (Figure 4.3c). When this ion was dissociated in the trap via CID, product ions were observed at *m/z* 190 and *m/z* 115 (Figure 4.3d). This fragmentation indicates that the ion observed at *m/z* 412 is actually a proton-bound heterodimer, made up of protonated GGG and a species with the mass 222 Da. An ion at *m/z* 223 was observed in the mass spectrum, and was identified as protonated diethtyl phthalate. Phthalates are commonly used plasticizers and are often seen as contaminants in ESI-MS.[5]

The fragmentation in the ion transfer optics resulted in the fragmentation of a proton-bound heterodimer to protonated GGG as well as the fragmentation of protonated GGG to the b_2 fragment ion prior to mass analysis. At an E_C of approximately 5 V/cm, protonated GGG formed via ESI is selected, and is largely fragmented to the b_2 fragment ion due to harsh transfer optics. At an E_C of 65 V/cm, the heterodimer is selected, and due to harsh

transfer optics, it is fragmented to protonated GGG, and only a small amount of the b_2 fragment ion is observed. The two peaks observed initially lead to false preliminary conclusions regarding the protonation sites of GGG. Though there still may be multiple structures of GGG formed by ESI, they are not readily separated under the DIMS parameters used for these experiments.

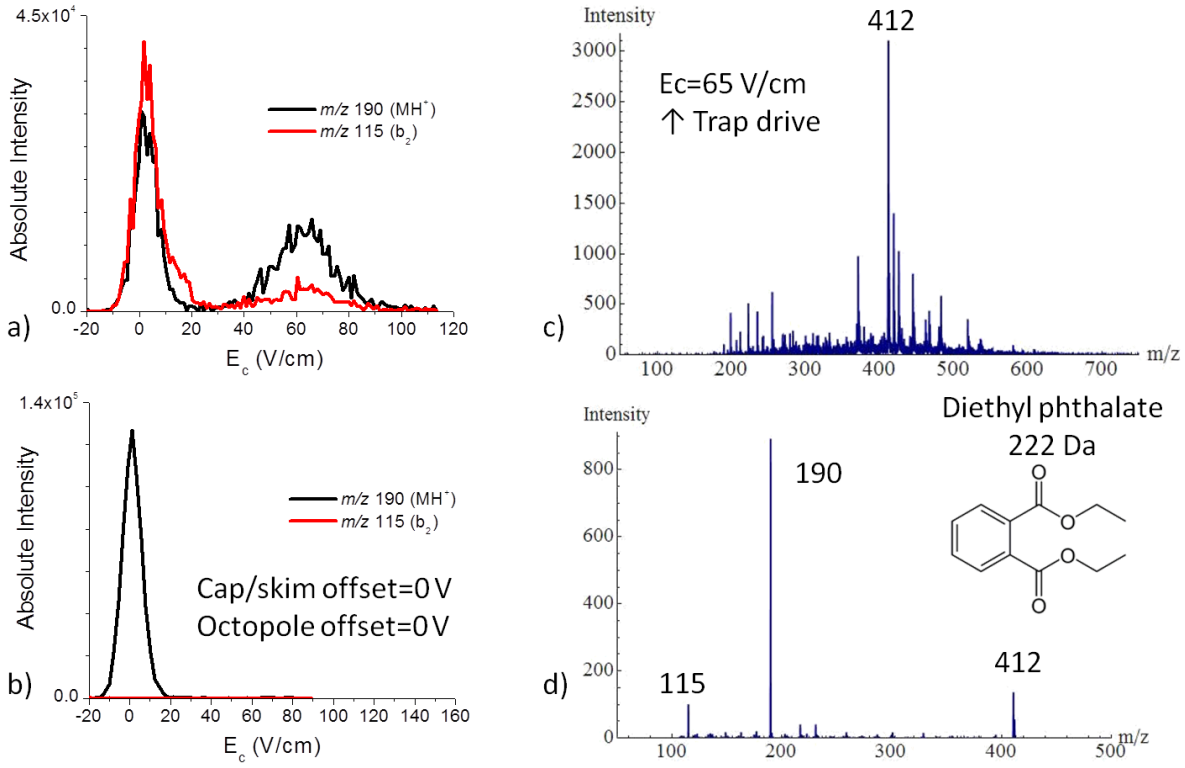

Figure 4.3. DIMS analysis of protonated GGG, E_D=26 kV/cm: (a) DIMS scan of protonated GGG (*m/z* 190) and its b_2 fragment ion (*m/z* 115) using default instrumental conditions, (b) DIMS scan with lowered capillary/skimmer and octopole offset voltages, (c) MS observed at E_C of 65 V/cm with lowered offset voltages and increased trap drive, and (d) MS/MS of the ion at *m/z* 412 observed in (c).

When attempting monosaccharide separations with DIMS, the sodiated monomer of methyl-α-glucopyranoside (*m/z* 217) exhibited multiple peaks in the DIMS scan (Figure 4.4a), which was unexpected. These peaks were investigated, much like the protonated GGG

experiments above. Again, the ion transfer optics were adjusted to prevent fragmentation prior to mass analysis and only one peak was observed in the DIMS scan for *m/z* 217 (Figure 4.4b). With a static E_C of 80 V/cm, and an increased trap drive, an intense ion at *m/z* 411 was observed. CID of *m/z* 411 in the ion trap produced a product ion at *m/z* 217, indicating that the ion of *m/z* 411 was a sodiated dimer, $(2M+Na)^+$ (Figure 4.4c). The other smaller peaks in the DIMS spectra were identified as various adducts to the sodiated monomer.

Once the origin of the multiple peaks was determined, the monosaccharides methyl-α-glucopyranoside, methyl-β-glucopyranoside, and methyl-α-mannopyranoside were analyzed using DIMS-MS with the goal of separating the three isomers in a mixture. By utilizing gentle ion transfer optics settings, a single Gaussian peak was observed for each sodiated monosaccharide isomer, and each of the three isomers was separable in a mixture of the three using DIMS (Figure 4.4d). Although the isomers are not baseline resolved relative to each other, each isomer can be individually selected with minimal overlap.

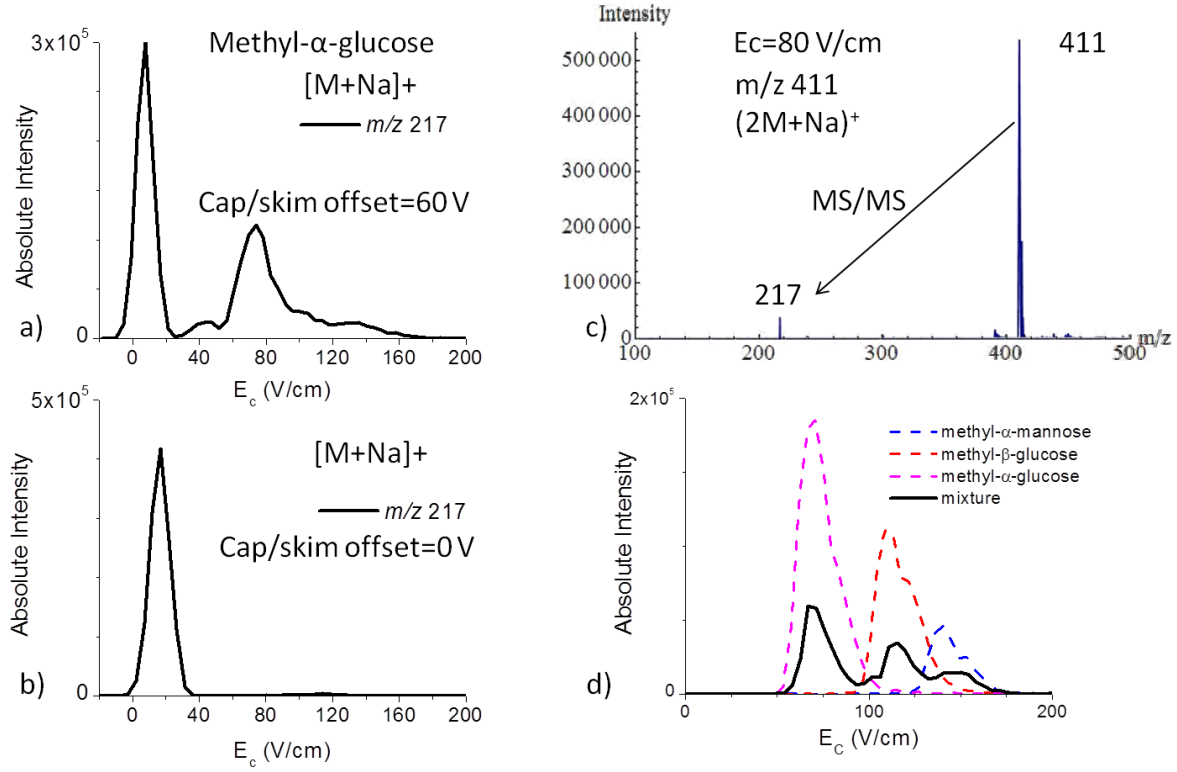

Figure 4.4. DIMS analysis of monosaccharides: (a) DIMS scan (E_D=30 kV/cm) of sodiated methyl-α-glucose (*m/z* 217), (b) DIMS scan (E_D=30 kV/cm) with lowered capillary/skimmer and octopole offset voltages, (c) MS observed at EC of 80 V/cm with increased trap drive, and (d) DIMS separation of sodiated monosaccharide isomers at E_D=40 kV/cm.

4.2.2 Optimization of DIMS-MS analyses for fragile analytes

High electric fields are known to cause an increase in the effective ion temperature,[6] which raises some concern that DIMS separations are very harsh and may induce undesired fragmentation of ions prior to mass analysis. To determine if fragmentation would occur upon exposure to the high electric fields used in a typical DIMS separation, a fragile ion that is easily dissociated should be used. Holomyoglobin has a non-covalently bound heme group that is readily lost to form apomyoglobin, making it a good candidate for the study of the harshness of DIMS.

Holomyoglobin is known to readily lose a heme group with conventional electrospray solvents employing organic components, so 100% water was used for the spray solvent. Peaks corresponding to apomyoglobin as well as a peak corresponding to a protonated heme group (*m/z* 616) were observed in the mass spectrum (Figure 4.5). These data were acquired with the standard instrument tuning, wherein the expected analyte mass-to-charge ratio is used to select the ion optics voltages. A DIMS spectrum was prepared for the protonated heme group (*m/z* 616) with 50/49/1 methanol/water/acetic acid (Figure 4.6a) to compare to the DIMS spectrum obtained with 100% water as the ESI solvent (Figure 4.6b). Although the mass spectra obtained without DIMS look similar for the two ESI solvent conditions, the heme group was observed at different E_C values in the DIMS spectra depending on the solvent used. When a typical electrospray solvent containing organic solvent is used, the protonated heme group is observed in the DIMS spectrum at a E_C of 100 V/cm (E_D=30 kV/cm) (Figure 4.6a). When 100% water is used as the ESI solvent, the ion at m/z 616 is observed an E_C of 165 V/cm (Figure 4.6b).

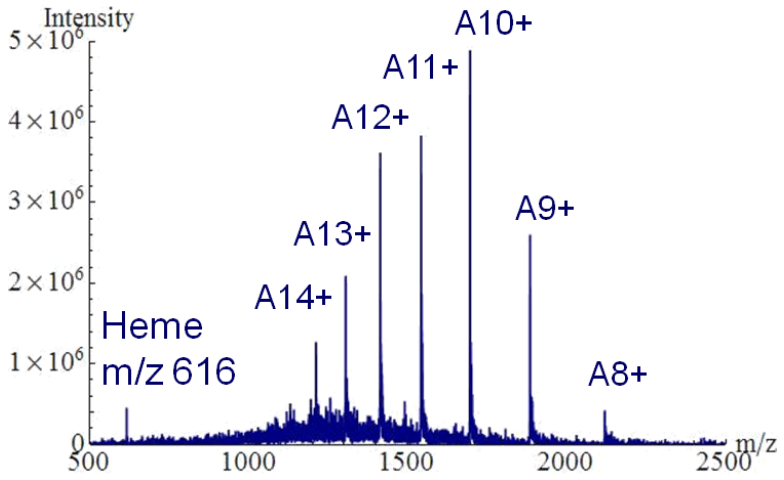

Figure 4.5. MS of myoglobin observed using default ion optics settings and 100% water as the ESI solvent.

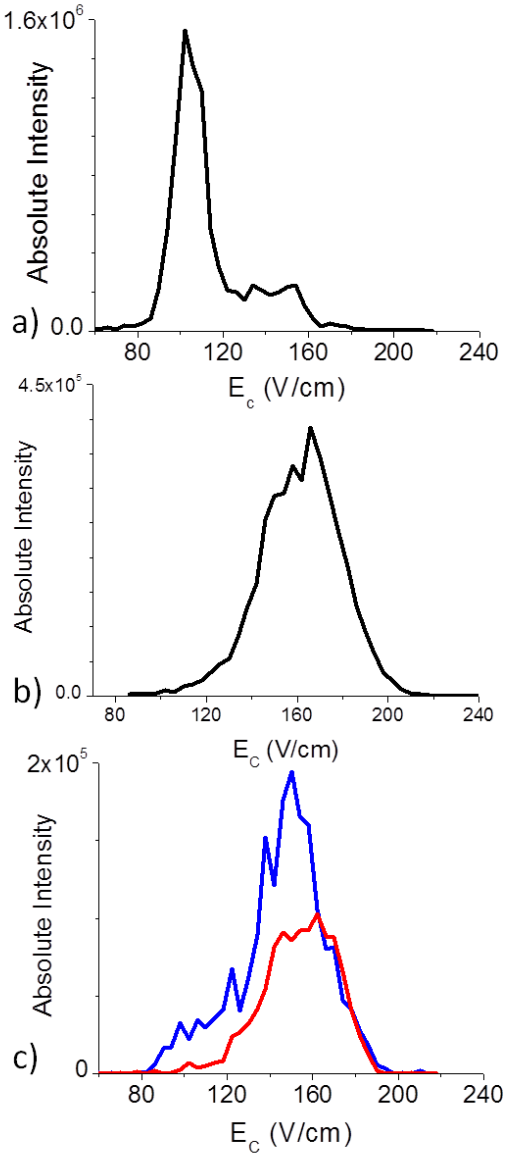

Figure 4.6. DIMS scans (E_D=30 kV/cm) of myoglobin where *m/z* 616 is plotted in black, *m/z* 1758 (10+) is red and *m/z* 1598 (11+) is blue. (a) 50/49/1 methanol/water/acetic acid used for ESI solvent and 65 V for capillary-to-skimmer offset, (b) pure water used for ESI solvent and 150 V for capillary-to-skimmer offset, (c) pure water used for ESI solvent and 65 V for capillary-to-skimmer offset.

The results obtained with varying ESI solvents suggest that only one of the DIMS spectra was observed due to the protonated heme group being separated in DIMS, and the other was due to a reaction occurring after DIMS. Using pure water as the spray solvent, but a lowered capillary-to-skimmer offset of 65 V, peaks corresponding to the 10+ and 11+ charge states of holomyoglobin are observed, centered at approximately 165 V/cm (Figure 4.6c). By lowering the capillary-to-skimmer offset, the loss of the heme group after DIMS but before mass analysis was minimized, allowing holomyoglobin to be observed in the mass spectrum. The different charge states observed for holomyoglobin are not well-separated by DIMS, so a single gaussian peak, centered at 165 V/cm, is observed for the protonated heme group when it is lost via capillary-to-skimmer fragmentation after DIMS (Figure 4.6b).

By manually adjusting the transfer optics settings to reduce fragmentation prior to mass analysis, peaks corresponding to the 9-12$^+$ charge states of holomyoglobin were

observed in the mass spectrum without DIMS (Figure 4.7a). Lower intensity peaks corresponding to the 10-20^{+} charge states of apomyoglobin were also observed. The same sample was analyzed with DIMS-MS, using a dispersion field of 30 kV/cm. To determine how the observed signal changed, the spectra were averaged over the entire range of scanned E_C values, ~50-220 V/cm (Figure 4.7b). Spectra obtained with DIMS active appear similar to those obtained without DIMS, suggesting that the ion optics can be more harsh than in DIMS separations.

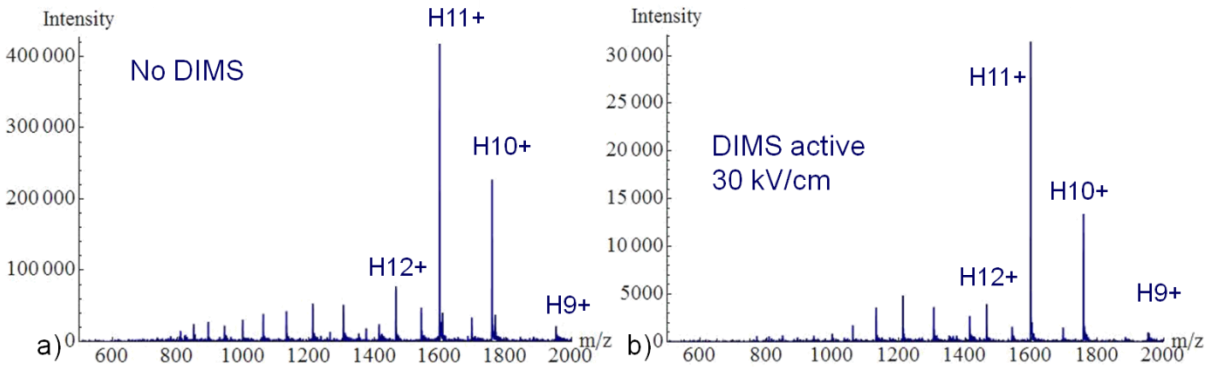

Figure 4.7. MS of myoglobin utilizing adjusted transfer optics settings to minimize fragmentation in ion optics (a) without DIMS, and (b) with DIMS active at an E_D of 30 kV/cm (signal averaged from E_C 50-220 V/cm).

DIMS is gentle enough to leave holomyoglobin intact and therefore can be used to determine whether peaks corresponding to apomyoglobin are observed as a result of the loss of the heme group due to ionization or ion optics parameters. To determine whether an observed heme group is lost due to ionization or within ion optics, a DIMS scan at an E_D of 30 kV/cm could be used to determine whether the peak at m/z 616 is selected for at a E_C of 100 V/c, or 165 V/cm. If both peaks are observed, then both the ion optics and the ionization parameters need to be adjusted. This is important because as shown in Figure 4.5, default ion optics parameters can cause undesired fragmentation of analyte ions.

4.3 Charge reduction in transfer optics elucidated by DIMS

4.3.1 Evidence of a charge reduction after DIMS

A charge reduction of some peptides and proteins after DIMS separations and prior to detection has been previously suggested as an explanation for the observation of multiple peaks in the DIMS spectra of a single charge state.[7-9] Evidence of a charge reduction after DIMS was first observed in our lab with the peptide angiotensin I (DRVYIHPFHL). Two peaks are observed for the 2+ charge state of angiotensin I (*m/z* 649) at an E_D of 26 kV/cm, one of which overlays exactly with the peak observed for the 3+ charge state of angiotensin I (*m/z* 433) in the DIMS scan (Figure 4.8a). To ensure that these peaks were exactly overlaid, the intensity was normalized to the intensity at the E_C at which both the 2+ and the 3+ charge state are observed (Figure 4.8b).

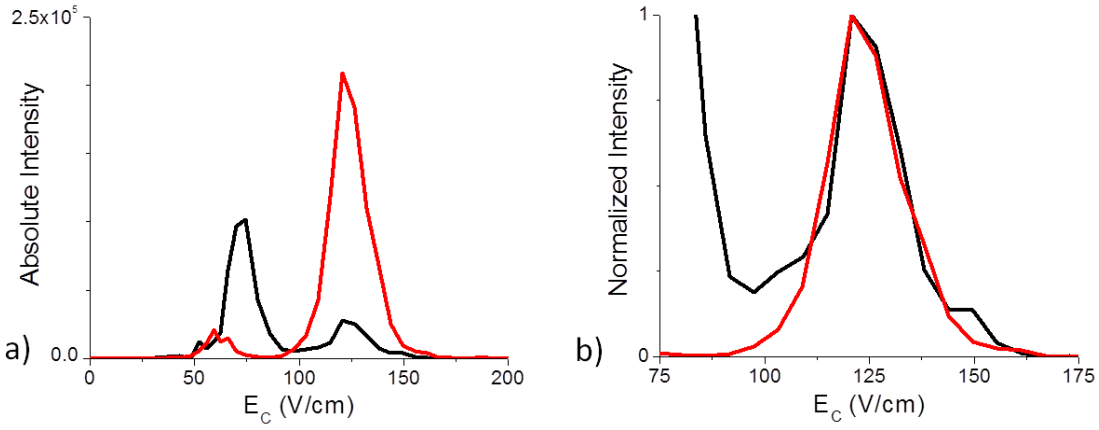

Figure 4.8. DIMS scan (E_D=26 kV/cm) of angiotensin I, where *m/z* 433 (3+) is plotted in red and *m/z* 649 (2+) is black. (a) absolute intensities are plotted, and (b) intensity is normalized to the intensity at the peak E_C of approximately 125 V/cm.

A similar effect is observed in the DIMS scan for the peptide bradykinin (RPPGFSPFR), where there is evidence of a charge reduction of the 3+ charge state to the 2+ charge state after DIMS. Again, the DIMS scan is plotted with normalized intensity to ensure that the 2+ and 3+ peaks are exactly overlaid (Figure 4.9d).

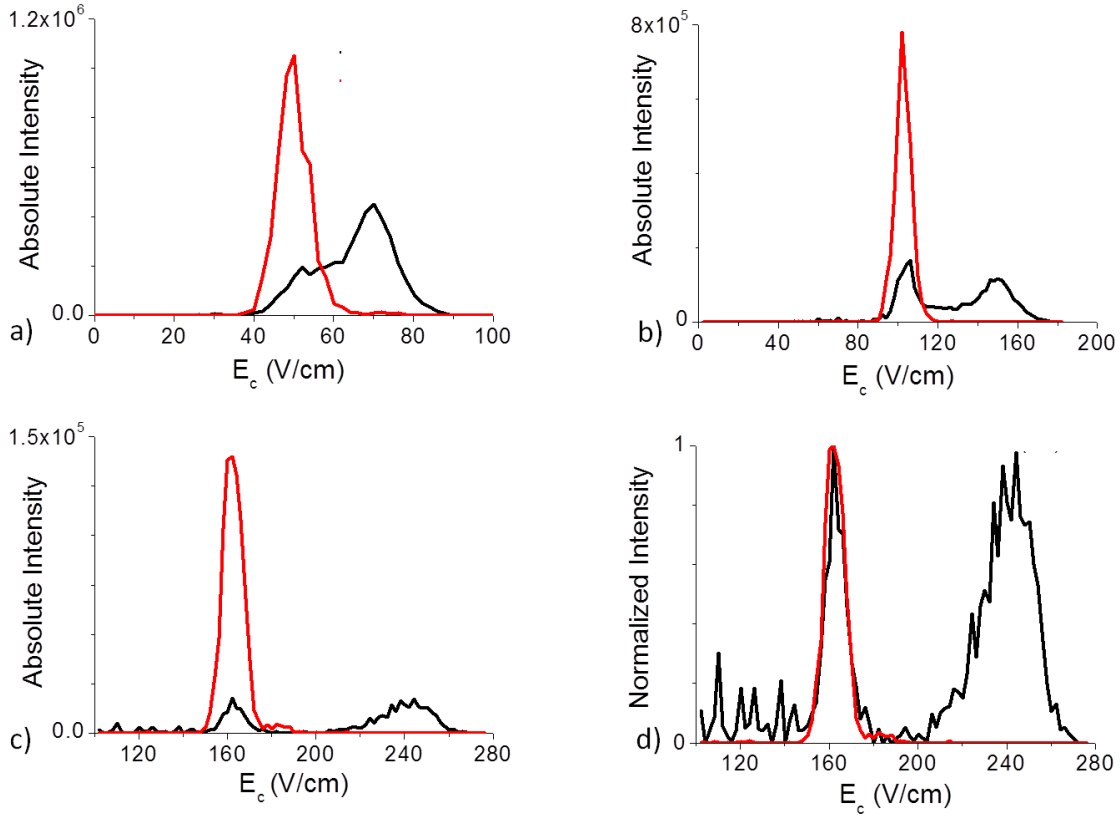

Figure 4.9. DIMS scans of bradykinin, where *m/z* 354 (3+) is plotted in red and *m/z* 531 (2+) is black. Absolute intensities are plotted for E_D of 20 (a), 26 (b), and 32 (c) kV/cm , and (d) intensity is normalized to the intensity at the peak E_C of approximately 160 V/cm at an E_D of 32 kV/cm.

4.3.2 Where does charge reduction occur?

DIMS spectra of the peptide bradykinin suggest that a population of the 3+ charge state (*m/z* 354) is reduced to a 2+ charge state (*m/z* 531) after DIMS. It has been previously suggested that a reduction in charge state could occur via a proton stripping reaction at the mass spectrometer interface between DIMS and the mass analyzer.[7] Collisions at the capillary-to-skimmer interface were first investigated as the origin of the observed charge reduction. When the capillary-to-skimmer offset was set to 0 V, both peaks for *m/z* 531 of bradykinin were observed as well as a peak for *m/z* 354 in the DIMS scan (Figure 4.10a). When the capillary-to-skimmer offset was increased to 100 V, both peaks for *m/z* 531 of bradykinin

were observed, but the peak observed for *m/z* 354 was greatly reduced in intensity (Figure 4.10b). With a static E_C of 100 V/cm, both charge states are observed in the mass spectrum with a low capillary-to-skimmer offset (Figure 4.10c). By elevating the capillary-to-skimmer offset at the same E_C value, peaks corresponding to fragment ions of both charge states were observed in the mass spectrum (Figure 4.10d). If the charge reduction were occurring as a result of harsh conditions at the capillary-to-skimmer interface, an increase in the offset voltage would be expected to decrease the amount of 3+ observed and increase the amount of 2+ observed at that E_C. Instead, collision-induced fragmentation of both charge-states was observed. The observation of fragment ions from both charge states suggests that the charge

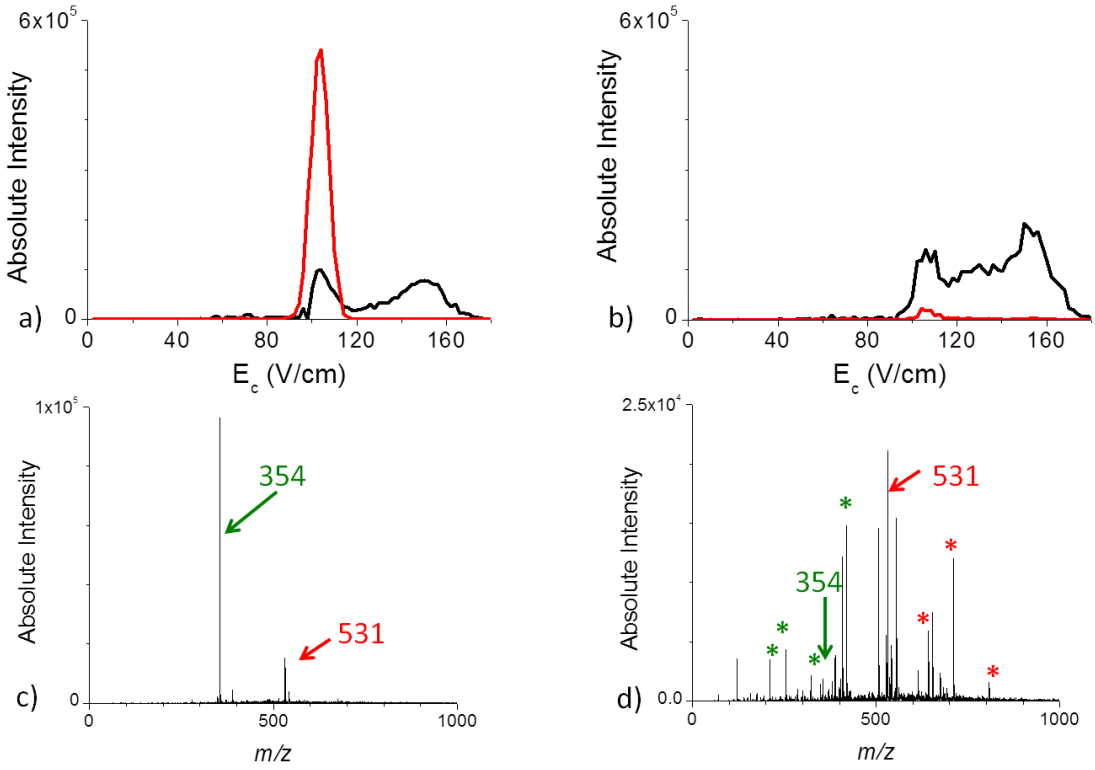

Figure 4.10. DIMS scans of bradykinin (E_D=26 kV/cm), where *m/z* 354 (3+) is plotted in red and *m/z* 531 (2+) is black. 0 V (a) and 100 V (b) capillary-to-skimmer offset, and MS at E_C 110 V/cm for 0 V (c) and 100 V (d) capillary-to-skimmer offset. Asterisks indicate fragment ions at the capillary-to-skimmer interface that were also observed as product ions formed via CID of *m/z* 531 (red) and *m/z* 354 (green) in the ion trap.

reduction occurs prior to the capillary-to-skimmer interface because fragment ions from both charge states are observed and some of the charge-reduced peak was still observed in the DIMS scan. If the charge reduction occurs after this interface, then very little charge-reduced peak would be observed because very little *m/z* 354 is leftover after the capillary-to-skimmer fragmentation.

Although the above results suggest that the charge reduction occurs prior to the capillary-to-skimmer interface, the trapping time after ion accumulation was varied to see if the charge reduction of bradykinin occurs in the ion trap. The trapping time was varied without applying isolating or activating the trapped ions, but increasing the total trapping time prior to ion ejection from the trap. If the charge-reduction of bradykinin is due to a reaction in the trap, then a significant decrease in the ratio of the 3+ charge state to the 2+ charge state would be expected. With no DIMS separation, the trapping time was increased by 40 ms and by 1000 ms, and the ratio of the 3+ charge state to the 2+ charge state of bradykinin was approximately 0.2, as was observed with 0 ms added to the trapping time.

Spray solvent composition was investigated to determine the effect on the observed charge-reduced peak. When 5% ammonium hydroxide was added to the 50/50 methanol/water spray solution instead of the usual 1% acetic acid used in the previous experiments, the 3+ charge state of bradykinin nor the charge-reduced peak are observed in the DIMS scan (Figure 4.11). This supports the theory that the lower E_C peak observed for *m/z* 531 is a result of a charge reduction after DIMS.

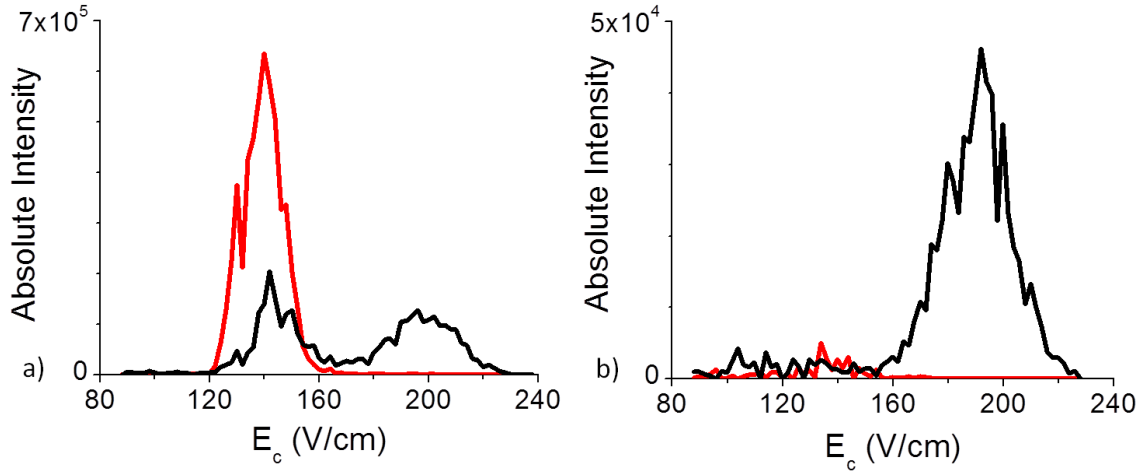

Figure 4.11. DIMS scans (E_D=30 kV/cm) of bradykinin, where *m/z* 354 (3+) is plotted in red and *m/z* 531 (2+) is black. 50/49/1 methanol/water/acetic acid as ESI solvent (a) and 50/45/5 methanol/water/ammonium hydroxide as ESI solvent (b).

It is not energetically favorable for a protonated peptide to lose a proton upon collisions with neutrals in the gas phase. Rather, it is more likely for fragmentation of the peptide to occur, as observed with the elevated capillary-to-skimmer offset voltage (Figure 4.10d). However, if there is a negative species present, a proton could be transferred from the peptide to the negative species. The surface of glass is comprised of silanol groups, some of which are deprotonated and carry a negative charge.

Typically, a glass transfer capillary 18 cm in length is used in this instrument. The instrument was modified to accept a longer 30 cm transfer capillary for comparison purposes. A E_D of 33.3 kV/cm was used with G4 DIMS, and a DIMS scan for each capillary is shown in Figure 4.12. The ratio of peak B to peak A (where peak A is the lower E_C and peak B is the higher E_C for *m/z* 531) was greater for the 18 cm capillary than for the 30 cm capillary (Table 4.1).

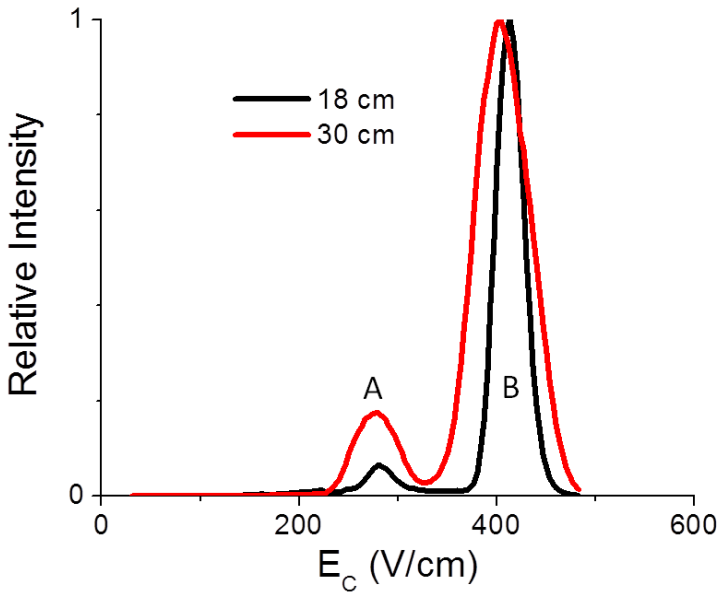

Figure 4.12. DIMS scans (E_D=33.3 kV/cm) for bradykinin^{2+} (*m/z* 531) with an 18 cm capillary (black) and a 30 cm capillary (red).

The decrease in the ratio of peak B to peak A with the increase in capillary length suggests that a greater degree of charge reduction occurs with the longer transfer capillary as compared to the shorter capillary. It should be noted that the peak widths observed in the DIMS scan were larger for the 30 cm capillary than for the 18 cm capillary. The 30 cm capillary has an i.d. of 0.7 mm, meaning the conductance limit of the 30 cm capillary is approximately 3.3 L/min, whereas that of the 18 cm capillary with a 0.6 mm i.d. is 2.9 L/min. The increased gas flow with the 30 cm capillary will cause a decrease in the transit time of ions through DIMS, which causes a widening of observed peaks.[10] The transit time through the 30 cm capillary (~2 ms) is still greater than that of the 18 cm capillary (~1 ms) even though the 30 cm capillary has a higher conductance limit than the 18 cm capillary.

Table 4.1. Average ratio of peak B to peak A for 18 cm and 30 cm long capillaries.

capillary length	peak B/peak A	
	ave	std dev
18 cm	13.23	1.34
30 cm	7.86	0.4

4.3.3 Capillary functionalization

In an attempt to neutralize the negative charge on the surface of the glass capillary, the capillary was submerged in trimethylchlorosilane for 15 minutes in an attempt to "end-cap" the silanol groups (Figure 4.13). This reaction is commonly used for chromatography particles to end-cap leftover silanol groups after functionalization.[11] When the functionalized capillary was used the ratio of peak B to peak A increased significantly, indicating that a lesser degree of charge reduction occurred with the functionalized capillary as compared to the regular unfunctionalized capillary (Figure 4.14 and Table 4.2). These experiments support the theory that a charge reduction can occur within the glass transfer capillary and suggest that the surface chemistry of glass, specifically the silanol groups, is responsible for the observed charge reduction of bradykinin.

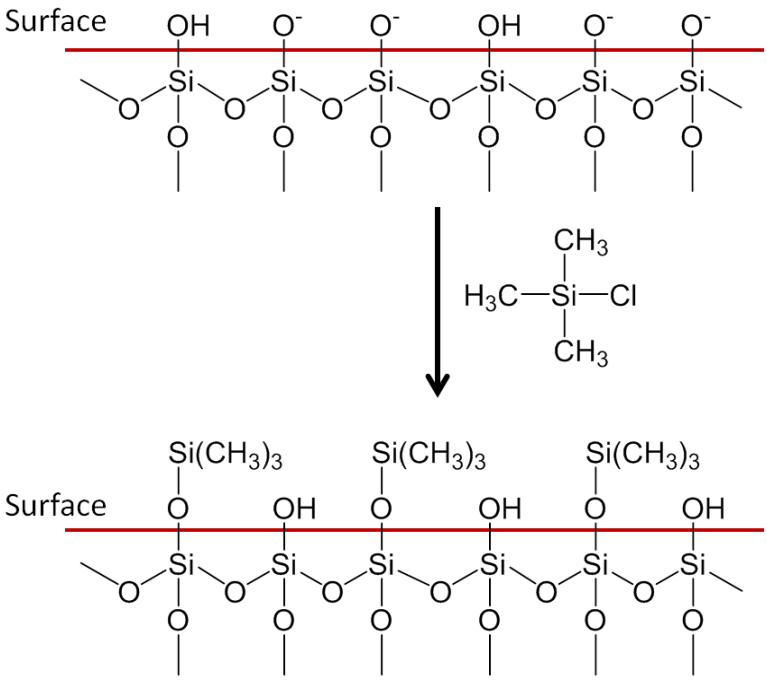

Figure 4.13. Functionalization of glass transfer capillary via reaction with trimethylchlorosilane.

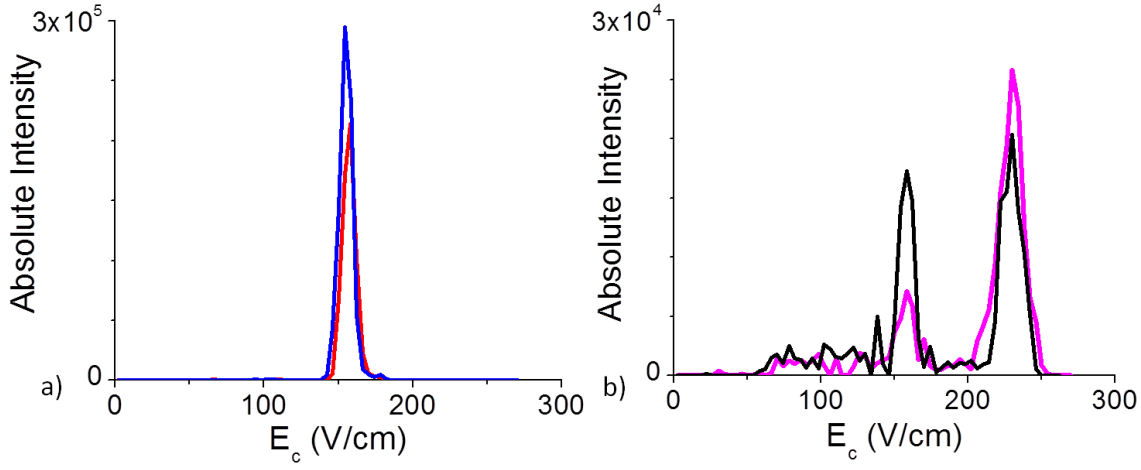

Figure 4.14. DIMS scans (E_D=30 kV/cm) of (a) bradykinin^{3+} (*m/z* 354) with regular capillary (red) and functionalized capillary (blue), and (b) bradykinin^{2+} (*m/z* 531) with regular capillary (black) and functionalized capillary (pink).

4.3.4 Collision cross-sections from TIMS

One possible explanation of the observation of two peaks the DIMS spectrum of the 2+ charge state of bradykinin is that there are two distinct conformations of bradykinin^{2+} that are separable in DIMS. Although the above experiments support the theory that one of the peaks is actually due to a charge-reduction of bradykinin^{3+} after DIMS, trapped ion mobility spectrometry (TIMS) was used to obtain collision cross-sections for bradykinin^{2+} and bradykinin^{3+} after the DIMS separation. TIMS (2.3.2) is a low-field ion mobility technique that separates ions based on their collision cross-section (CCS). If the two peaks observed in the DIMS spectrum of

Table 4.2. Ratios of peak B to peak A for regular and functionalized capillaries.

Trial	capillary	peak B/peak A
Trial 1	Regular	1.6
	Functionalized	3.5
Trial 2	Regular	1.8
	Functionalized	7.0
Average	Regular	1.7 ± 0.2
	Functionalized	5.3 ± 2.6

bradykinin^{2+} were due to the presence of two conformations, it is likely that the two species would have differing collision cross-sections.

TIMS experiments were performed with DIMS in filter mode using pure nitrogen as the carrier gas in DIMS as well as for TIMS. A E_D of 40 kV/cm was used, with a E_C of 250 V/cm to select for peak A and 380 V/cm to select for peak B. At 250 V/cm, both the 2+ and 3+ charge state of bradykinin are observed, of which the 2+ is believed to arise as a result of the charge reduction of the 3+ charge state after DIMS. The DIMS assembly is mounted on the entrance of the glass transfer capillary, and the TIMS cell is directly after the glass transfer capillary. Based on previous results, the charge-reduction occurs within the transfer capillary, and thus, the charge-reduced 2+ is expected to be present in TIMS. At 380 V/cm, only the 2+ charge state is observed. For both E_C values, the 2+ charge state is observed with the same collision cross-section (Figure 4.15), indicating that the observation of two peaks

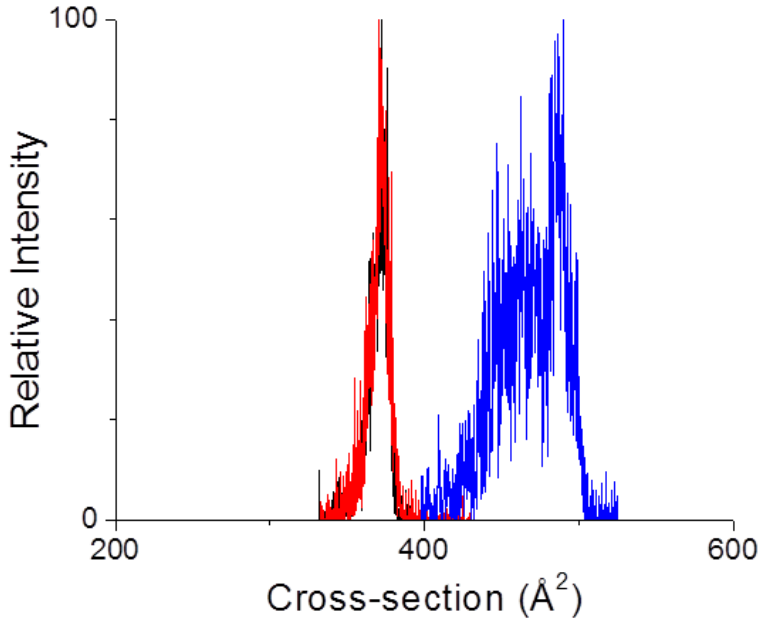

Figure 4.15. TIMS scans with DIMS in filter mode at E_D 40 kV/cm for bradykinin^{2+} (*m/z* 531) at E_C 380 (black) and 250 (red) V/cm and bradykinin^{3+} (*m/z* 354) at E_C 250 V/cm (blue).

observed in DIMS are not due to the separation of two different conformations of the 2+ charge state. The experimental cross-section in TIMS for bradykinin^{2+} is 335 Å^2 (error is ±5% for TIMS), which is comparable to the previously obtained cross-section of bradykinin^{2+} in nitrogen of 344 Å^2, from an experiment using a drift-tube ion mobility spectrometer.[12]

4.4 Summary and conclusions

Often the presence of multiple peaks for a given ion in an ion mobility experiment leads researchers to conclude that there is a presence of multiple conformers of that species. The experiments presented in this chapter demonstrate that it is of great importance to investigate the observed peaks and consider the ion reactions that could be occurring after the ion mobility separation, such as charge reduction or collision-induced fragmentation.

Ion optics parameters affect which ions arrive at the mass analyzer, but do not affect DIMS separations. DIMS provides a unique way to study ions immediately after ionization, but also requires ion optics to be carefully tuned to prevent "in-source" fragmentation. The protonated peptide GGG and sodiated methyl-α-glucopyranoside both exhibited unexpected peaks in their DIMS scans which were determined to have originated from fragmentation of multimers and adducts within the ion optics.

The fact that peaks in DIMS scans originating within ion optics can be differentiated from those originating from ionization conditions allows DIMS to be used as a diagnostic tool. For example, heme dissociation from myoglobin due to spray solvent composition can be distinguished from “in-source” fragmentation using DIMS. Also, DIMS separations allowed for the investigation of the 2+ charge state of bradykinin under various different

parameters in the ion optics as well as various ion trapping times. These experiments lead to the conclusion that there is a charge reduction of a population of the 3+ charge state in the glass transfer capillary. By functionalizing the glass transfer capillary, the peak observed due to the charge reduction was reduced, supporting the theory that the deprotonated silanol groups on the surface of the glass are responsible for the charge reduction. TIMS was used to confirm that both peaks observed in the DIMS scan for bradykinin^{2+} have the same collision cross-section, supporting the belief that the two peaks are not due to the presence of two conformations of bradykinin^{2+} but rather due to a charge-reduction of bradykinin^{3+} after DIMS.

4.5 REFERENCES

1. Whitehouse, C.M.; Dreyer, R.N.; Yamashita, M.; Fenn, J.B.: Electrospray interface for liquid chromatographs and mass spectrometers. *Anal. Chem.* **57**, 675-679 (1985)

2. Fenn, J.B.; Mann, M.; Meng, C.K.; Wong, S.F.; Whitehouse, C.M.: Electrospray ionization for mass spectrometry of large biomolecules. *Science*. **247**, 64-71 (1989)

3. Fenn, J.B.; Mann, M.; Meng, C.K.; Wong, S.F.; Whitehouse, C.M.: Electrospray ionization-principles and practice. *Mass Spectrom. Rev.* **9**, 37-70 (1990)

4. McMahon, M.; Wu, R.: Infrared multiple photon dissociation spectroscopy as structural confirmation for $GlyGlyGlyH^+$ and $AlaAlaAlaH^+$ in the gas phase. Evidence for amide oxygen as the protonation site. *J. Am. Chem. Soc.* **129**, 11312-11313 (2007)

5. Keller, B.O.; Sui, J.; Young, A.B.; Whittal, R.M.: Interferences and contaminants encountered in modern mass spectrometry. *Anal. Chim. Acta.* **627**, 71-81 (2008)

6. Mason, E. A.; McDaniel, E. W. *Transport Properties of Ions in Gases*. John Wiley & Sons Inc.: New York, 1988

7. New York, 1988.Purves, R.W.; Barnett, D.A.; Ells, B.; Guevremont, R.: Elongated conformers of charge state +11 to +15 of bovine ubiquitin studied using ESI-FAIMS-MS. *J. Am. Soc. Mass Spectrom.* **12**, 894-901 (2001)

8. Shvartsburg, A.A.; Tang, K.; Smith, R.D.: Differential ion mobility separations of peptides with resolving power exceeding 50. *Anal. Chem.* **82**, 32-35 (2010)

9. Shvartsburg, A.A.; Danielson, W.F.; Smith, R.D.: High-resolution differential ion mobility separations using helium-rich gases. *Anal. Chem.* **82**, 2456-2462 (2010)

10. Shvartsburg, A.A.; Smith, R.D.: Ultrahigh-resolution differential ion mobility spectrometry using extended separation times. *Anal. Chem.* **83**, 23-29 (2011)

11. McMurtrey, K.D.: Reaction of silica gel with trimethyl silyl donors using conditions useful for end-capping HPLC bonded phase packings. *J. Liq. Chromatogr.* **11**, 3375-3384 (1988)

12. Bush, M. F.; Hall, Z.; Giles, K.; Hoyes, J.; Robinson, C. V.; Ruotolo, B. T.: Collision Cross Sections of Proteins and their Complexes: a Calibration Framework and Database for Gas-Phase Structural Biology. *Anal. Chem.* **82**, 9557-9565 (2010)

CHAPTER 5: DIMS AS AN ELECTRONIC IMMUNOASSAY

5.1 Biomarker detection and quantification

5.1.1 Current methods

A substance indicative of a specific biological state is commonly referred to as a biomarker. In the medical field, this term generally describes a peptide, protein, or metabolite that can be monitored to track the progression of a disease. An ideal biomarker should be specific to one disease, and the concentration of a biomarker should change in measurable amounts as the disease progresses. Biomarkers not only allow for the early detection of diseases, but also allow the progression of the disease to be tracked. For example, the effect of a particular treatment can be assessed by tracking an appropriate biomarker. This can ultimately lead to a better understanding of the disease and improved treatment regimens.

Immunoassays are commonly employed in biomarker detection and quantification. Essentially, immunoassays use an antibody that selectively binds to an antigen, which is the analyte of interest. For each biomarker of interest, antigen-antibody binding studies are necessary, as well as specificity studies to ensure that the antibody will not bind to other species present in the biological sample. Immunoassays can ultimately provide a fast technique for biomarker detection, but the method development studies are time consuming and labor intensive. Although specificity studies are often performed, interferences can still pose a problem with respect to immunoassay specificity, e.g. the presence a protein fragment that still contains the epitope that binds to the antibody.

Mass spectrometry (MS) based techniques provide a higher degree of specificity than immunoassays. As previously discussed (1.1), MS-based techniques suffer from issues with the analysis of complex samples such as low signal-to-background. Therefore, electrophoretic or chromatographic separations are often needed for biological samples. These separations can add minutes to hours to the total analysis time, which is why immunoassays are often employed instead of MS. DIMS is an appealing separation technique for MS for applications requiring fast analysis times because transit time through a DIMS device is on the order of milliseconds. A DIMS-MS method must be optimized for specific analytes, but would not require the antibody-antigen binding studies necessary for immunoassay development. Additionally, DIMS-MS has the potential to test for multiple biomarkers within one method. In this sense, DIMS-MS could potentially be used as an "electronic immunoassay".

5.1.2 Brain natriuretic peptide immunoassays

Brain natriuretic peptide (BNP, Figure 5.1[1]) is a 32 residue peptide that is currently used as a biomarker for congestive heart failure.[2-6] The cleavage of a 108 residue precursor pro-BNP[7] forms BNP and NT-proBNP. NT-proBNP is considered to be biologically inactive. Immunoassays employed for congestive heart failure either test for BNP or NT-proBNP, but there is evidence of cross-reactivity of these immunoassays with the precursor proBNP as well as other related peptides.[8,9] Additionally, measured values can be

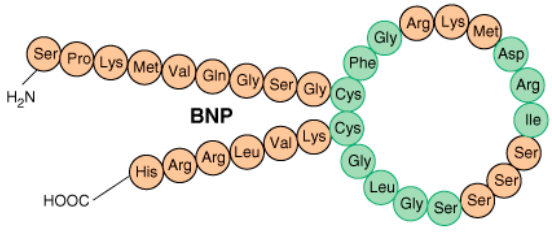

Figure 5.1 Brain natriuretic peptide (BNP).

significantly different between different commercially available immunoassays for the same sample, but the same concentration (for BNP, 100 ng/L[10]) is used for the decisional value regardless of the immunoassay used. For example, the coefficient of variance for the measured concentration of BNP was determined to be 43% in a recent study including four different commercially available BNP assays.[10] The variability in measured values can be attributed to the cross-reactivity of these assays and suggests that there is a need for improvement in the specificity of these immunoassays or a more specific analytical method.

5.2 BNP in serum

BNP was spiked into a fetal bovine serum (FBS) extract to determine how well DIMS could resolve peptides from other components in a complex biological matrix. A simple protein precipitation was performed with FBS (1:3 FBS:methanol) and the resulting supernatant was spiked with BNP prior to dilution with 50/49/1 methanol/water/acetic acid. The signal observed for BNP in a neat spray solvent was compared to varying dilution factors of the serum extract in the spray solvent (Table 5.1) to determine which dilution factor should be used to minimize ionization suppression (Equation 5.1).

Table 5.1 Dilution of FBS extract to minimize ionization suppression.

FBS extract:solvent	% Ion Suppression
1:10	84
1:50	53
1:100	1

$$\%\ Ion\ Suppression = \left(1 - \frac{signal_{extract}}{signal_{neat\ solvent}}\right) \times 100\% \qquad \text{Equation 5.1}$$

The dilution factor that minimized ionization suppression to about 1%, meaning that the signal obtained in the diluted extract is 99% of the signal observed in the neat solvent, is 1:100. Using G3 (25 mm long electrodes with a 0.5 mm gap) at a dispersion field of 30 kV/cm, the 5+ charge state of BNP (*m/z* 693.8) is well-separated from other serum

components (Figure 5.2). Considering how well BNP^{5+} is separated from serum components, the observed ion transmission of 83% at the peak E_C is impressive.

Figure 5.2. DIMS spectra of BNP^{5+} in FBS extract, where TIC is plotted in black, and EIC for BNP^{5+} (m/z 694) is plotted in red.

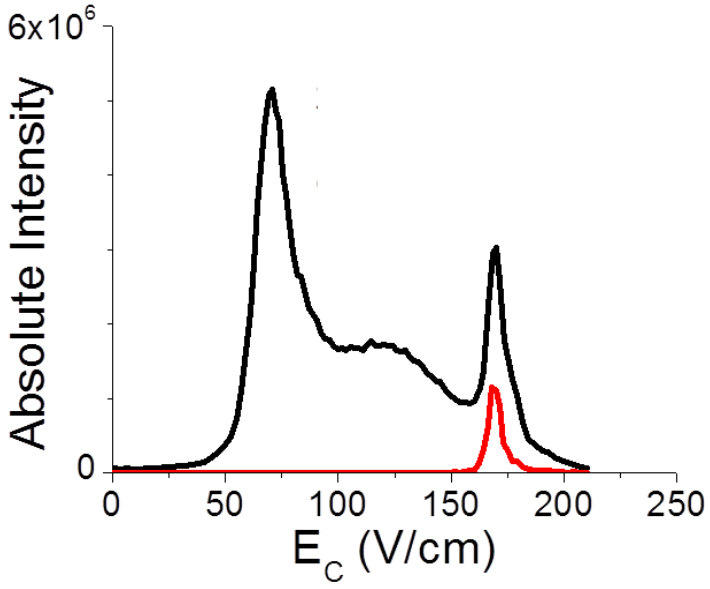

5.3 Importance of peptide structure in DIMS separations

The resolving power (RP) of the peak observed for BNP^{5+} at a E_D of 30 kV/cm is 23.8 ± 0.5 (n=4). The high ion transmission observed for BNP^{5+} (83%) under conditions that generate a RP greater than 20 was not expected. A possible explanation for the unexpected results observed for BNP is that due to its disulfide linkage between Cys9 and Cys26, BNP exists as a ring structure with two tails. To determine if the confined structure of BNP plays a role in the observed results, the disulfide bond of BNP was reduced using dithiothreitol (DTT). The DIMS separation of reduced BNP was compared to that of native BNP (Figure 5.3). The RP for the 5+ charge state of reduced BNP is only 9.2 ± 0.9 (n=4) and the ion transmission at the

peak E_C is 57%. The low resolving power of reduced BNP indicates that reduced BNP will not separate as well from the rest of the components in serum and exhibits a greater degree of structural heterogeneity compared to native BNP. A low RP corresponds to a high peak width, indicating that the total signal is spread over a wider range of compensation voltages than a peak with a high RP. These data suggest that the confined conformation of native BNP allows for the separation from serum components while maintaining excellent ion transmission.

To confirm that the change in RP and %T with DTT added to the solution was due to the reduction of the disulfide bond and not due to the presence of DTT in the spray solution,

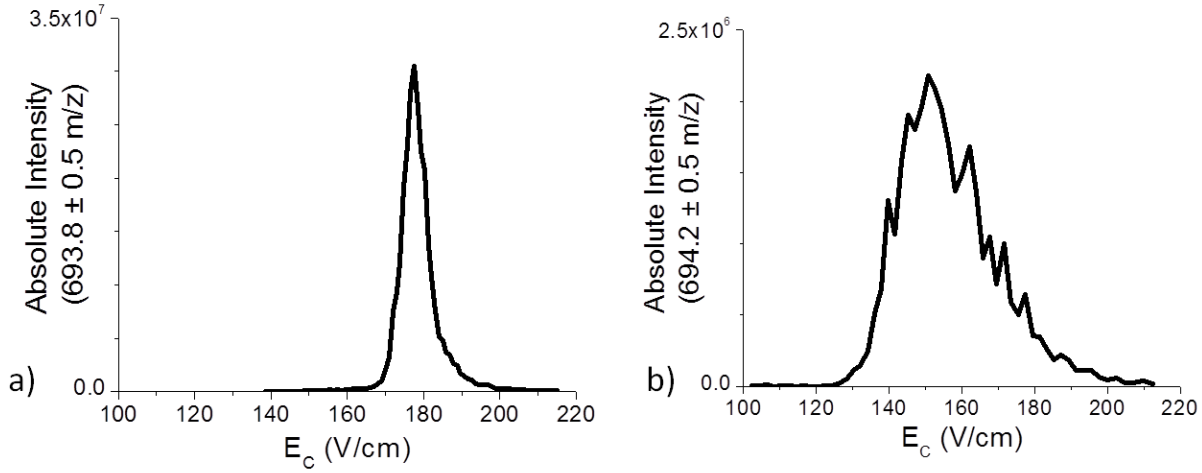

Figure 5.3. Representative DIMS scans of native (a) and reduced (b) BNP^{5+}. Average RPs in text were determined from 4 DIMS scans.

a similar experiment was performed with angiotensin I, which does not have any disulfide linkages (Table 5.2). The RP with DTT does decrease as compared to the RP obtained without DTT, but the relative change in RP for angiotensin with DTT added is less than 15%, whereas for BNP the change in RP is closer to 60%. The centroid E_C of the peak also shifts to slightly higher values for both dispersion fields used. The relative change in centroid E_C for angiotensin is less than 5%, and for BNP the change in E_C is about 15% in the opposite

direction. The %T is comparable, and actually increased with DTT added at 22 kV/cm, which is the opposite of the trend observed for BNP^{5+}. These experiments suggest that the addition of DTT to the ESI solvent does not cause a change in RP or %T, but rather that the reduction of the difsulfide bond of BNP caused the change in RP and %T.

To determine if confined peptide structure provides improved DIMS results, three other peptides were investigated: ANP (atrial natriuretic peptide), ratBNP, and Gramacidin S.

Table 5.2. Results of DIMS scans for angiotensin^{3+} with and without the addition of DTT to the electrospray solvent.

E_D (kV/cm)		E_C	FWHM	RP	%T
22	No DTT	55.4	10.6	5.2	80.3
	With DTT	57.2	12.9	4.4	105.1
26	No DTT	90.4	11.6	7.8	51.8
	With DTT	91.2	13.0	7.0	52.9

For ANP and ratBNP, the disulfide bond was reduced via the same reaction with DTT as with BNP. To investigate Gramicidin S, Cyclo (-Val-Orn-Leu-D-Phe-Pro-)$_2$, a linear analog was synthesized via Fmoc synthesis with a 2-chlorotrityl resin.[11] The linear analog used lysine in place of ornithine (a difference of one methylene on the side chain) as well as L-phenylalanine in place of D-phenylalanine. The centroid E_C, FWHM, and RP for the experiments are tabulated below (Table 5.3). Only the charge state that was observed for both native and reduced (or linear and cyclic) was tabulated.

For all of the peptides investigated, the RP decreases for the linear/reduced as compared to the native/cyclic. For ANP^{4+}, the centroid E_C increases for the reduced peptide compared to the native peptide, but the peak width increases significantly, making the RP significantly lower for the reduced peptide compared to the native peptide. For $ratBNP^{6+}$, the centroid E_C decreases, but the FWHM does not change significantly when comparing reduced to native. With Gramacidin S^{2+}, the peak width increases for the linear analog as compared to the cyclic, but the E_C is also shifted higher, so the RP is only slightly lower for

the linear analog as compared to the cyclic Gramacidin S. Although the peptides do not all give as striking differences in the DIMS scans as BNP^{5+} and ANP^{4+}, it is clear that structure plays a role in the DIMS separations. These data suggest that peptide structure is important to consider for DIMS separations, but that it is not as simple as linear versus cyclic.

Table 5.3. Results of DIMS scans for ANP^{4+} (native and reduced), $ratBNP^{6+}$ (native and reduced) and Gramacidin S^{2+} (linear and cyclic).

		E_c		FWHM		RP	
		ave	stdev	ave	stdev	ave	stdev
ANP^{4+}	native	242.3	0.2	13.3	0.4	18.2	0.6
	reduced	276.6	0.5	32.5	1.3	8.5	0.3
$ratBNP^{6+}$	native	279.7	0.2	16.1	0.5	17.3	0.6
	reduced	226.8	0.2	15.6	0.4	14.6	0.4
Gram S^{2+}	cyclic	188.8	0.1	12.6	0.2	15.0	0.3
	linear	203.7	0.1	14.6	0.2	13.9	0.2

It should be noted that the DIMS scan for ANP^{5+} (not included in Table 5.3) changed drastically when the disulfide bond was reduced, splitting into multiple peaks, where there was only one peak for the native peptide with the disulfide bond intact (Figure 5.4). This suggests that rather than adopting a less-defined structure when reduced as with BNP, ANP actually adopts at least two distinct structures. MS/MS spectra were obtained for the two large peaks observed in the DIMS spectra for reduced ANP^{5+}, and the observed product ions were not significantly different.

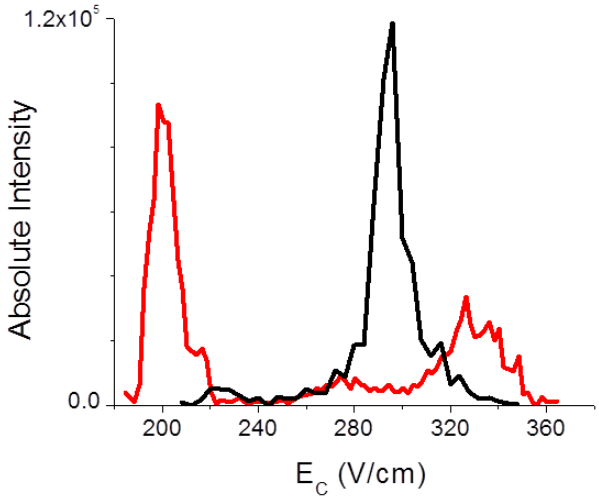

Figure 5.4. DIMS scans of ANP^{5+}, where the native peptide is plotted in black and the reduced peptide is plotted in red.

5.4 LOD of BNP in human plasma

As a proof of concept that DIMS could be used as an "electronic immunoassay", the LOD for BNP in human plasma was determined. For these experiments, known concentrations of BNP were spiked into human plasma. A simple protein precipitation was performed using 1:1 plasma:acetonitrile which provided a recovery of approximately 60%. The recovery was determined by comparing the signal obtained by spiking BNP into plasma before the protein precipitation to that obtained by spiking the BNP into the supernatant after the protein precipitation. The resulting supernatant was diluted 1:100 with 75/24/1 methanol/water/acetic acid for electrospray ionization.

Without DIMS, the MS spectrum of BNP in plasma has a high background signal, making the peak expected for BNP^{5+} indiscernible from the background. With DIMS applied with dispersion and compensation fields optimal for the selection of BNP^{5+}, much of the background signal is decreased, and a peak corresponding to BNP^{5+} is readily apparent (Figure 5.5).

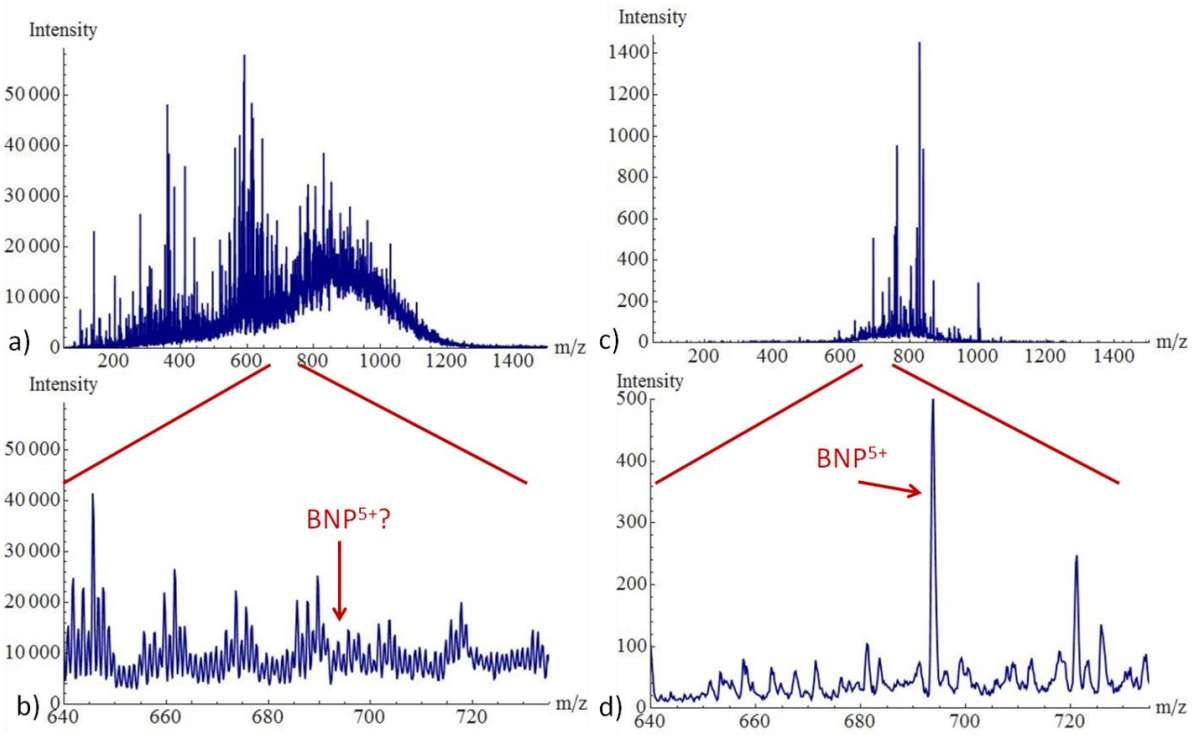

Figure 5.5. Mass spectra obtained for BNP in human plasma extract, where (a & b) were obtained without DIMS with a BNP concentration of 1 µM in plasma prior to extraction and dilution and (c & d) were obtained with DIMS, utilizing a E_D of 53.3 kV/cm and an E_C of 933 V/cm, with a BNP concentration of 400 nM in plasma.

The signal intensity of the 5+ charge state of BNP (*m/z* 693.8) was determined for concentrations ranging from 200 to 1600 nM in plasma prior to extraction and dilution (Figure 5.6). Without DIMS or MS/MS, the error bars are large, and the signal intensity does not exhibit a linear increase in intensity with increasing BNP concentration due to a high background signal. Therefore, without DIMS or MS/MS, a limit of detection (LOD, Equation 5.2) was unable to be calculated.

$$LOD = \frac{\bar{x}_{blank} + 3\sigma_{blank}}{sensitivity} \qquad \text{Equation 5.2}$$

It was unclear which E_D would provide the best LOD because as E_D increases, there is a trade-off between resolving power and sensitivity. As E_D is increased, RP increases but ion transmission decreases causing an observed decrease in sensitivity. This is readily apparent in these data (Table 5.4) as the sensitivity decreases with increasing E_D, and the signal of the

blank decreases with increasing E_D. The lowest LOD for the concentration initially in the plasma is 94 nM and is achieved at the highest E_D investigated, 53.3 kV/cm.

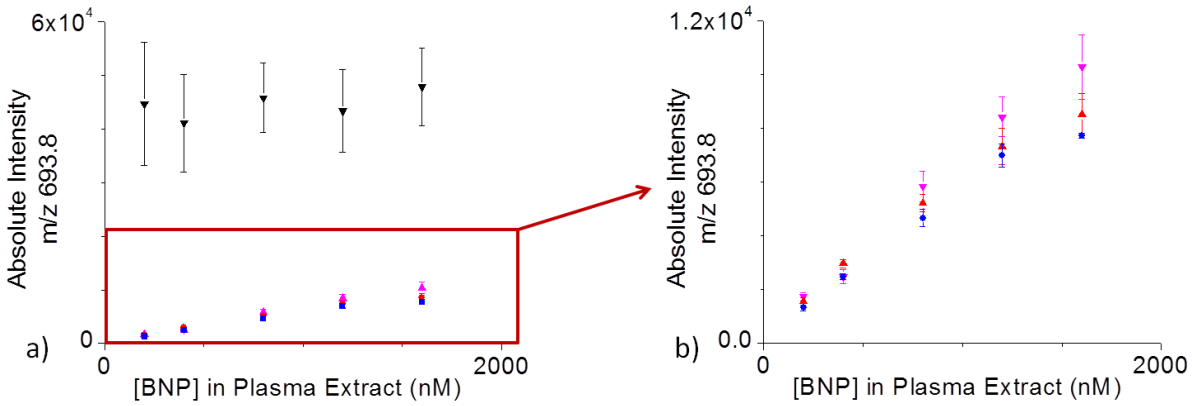

Figure 5.6. LOD curves for BNP in a human plasma extract, where black upside-down triangles are without DIMS, pink upside-down triangles are with DIMS at an E_D of 40.0 kV/cm, red triangles are with DIMS at an E_D of 46.7 kV/cm, and blue circles are with DIMS at an E_D of 53.3 kV/cm.

Detection limits were also determined from LOD curves using the same samples, but with MS/MS using collision-induced dissociation (CID). The signal intensities of the four most intense product ions observed from CID of the 5+ charge state of BNP were summed together. These product ions include *m/z* 657 (y_{30}^{5+}), 666 ($b_{31}^{5+} + H_2O$), 690 (a_{27}^{4+}), and 789 (y_{29}^{4+}). With CID, LODs were able to be determined without DIMS as well as for the three dispersion fields chosen for these experiments (Table 5.5). The LOD is improved with DIMS as compared to without DIMS. The sensitivity decreases as the dispersion field increases as was observed in the LOD experiment without MS/MS, but the signal of the blank does not have a clear trend as a function of E_D. The best LOD obtained with CID is 42 nM

Table 5.4. Results obtained from LOD curves with DIMS for BNP in human plasma.

E_D	Sensitivity (counts/nM)	$signal_{blank}$	LOD in plasma (nM)
40	6.4	813 ± 271	254
46.7	5.6	396 ± 66	105
53.3	4.5	319 ± 35	94

Table 5.5. Results obtained from LOD curves obtained with CID without and with DIMS for BNP in human plasma.

E_D	Sensitivity (counts/nM)	$signal_{blank}$	LOD in plasma (nM)
no DIMS	0.88	132 ± 17	207
40	1.2	23 ± 9	42
46.7	1.2	49 ± 13	75
53.3	0.95	22 ± 8	49

with an E_D of 40 kV/cm.

In addition to the CID experiments, a proton transfer reaction (PTR) was also investigated for the LOD of BNP with MS/MS. A proton transfer reaction effectively decreases the charge state of the ion of interest. The PTR reagent used for these experiments is generated by methane chemical ionization of fluoranthene. The multiply charged analyte ion transfers a proton to the fluoranthene anion: $C_{16}H_{11}^- + [M+nH]^{n+} \rightarrow C_{16}H_{12} + [M+(n-1)H]^{(n-1)+}$. The reason the LOD with PTR was compared to that obtained with CID is that fewer product ions are observed with PTR. Because the signal is spread out over a smaller number of product ions, PTR may provide an improved signal-to-background ratio than CID. With BNP, the 5+ charge state (m/z 693.8) was isolated, and PTR produced the 4+ and 3+ charge states of BNP, *m/z* 866.8 and 1155.0 respectively. The intensities of both the 3+ and 4+ charge stated formed via PTR were summed together for each concentration of BNP. As with CID, the LOD is improved with DIMS as compared to without, but the trend with respect to E_D is unclear (Table 5.6).

The best LOD achieved for BNP in human plasma thus far is 39 nM. The cutoff value for BNP immunoassays is 100 ng/L or 29 pM. Thus, with the current method, DIMS-MS/MS would

Table 5.6. Results obtained from LOD curves obtained with PTR without and with DIMS for BNP in human plasma.

E_D	Sensitivity (counts/nM)	$signal_{blank}$	LOD in plasma (nM)
no DIMS	0.71	104 ± 22	239
40	1.4	53 ± 15	70
46.7	1.2	49 ± 14	78
53.3	1.1	21 ± 7	39

not be able to replace the current immunoassays. However, improved sample preparation methods could remove the requirement to dilute the extract by 100 times, giving an improved LOD closer to the cutoff value used for current immunoassays. A more sensitive mass spectrometer equipped with an ion funnel[12] would improve the sensitivity by approximately an order of magnitude. Finally, nanoESI is expected to provide improved sensitivity as compared to conventional ESI. With improved sample preparation and instrumentation, DIMS-MS/MS could very well be used to reach biologically relevant LODs for BNP in human plasma.

5.5 Detection of Leukemia antigens

Another potential application for DIMS as an "electronic immunoassay" is the identification of computationally predicted cancer antigens. T-lymphocytes can kill cancer cells by binding to cancer antigens, which consist of 9-10 amino acid peptides that are presented on the cancer cell surface by human leukocyte antigen (HLA) molecules. The majority of these antigenic peptides have been confirmed using shotgun HPLC-MS approaches on complex mixtures of antigenic peptides. While these methods have proven useful for peptide discovery, they are limited due to complicated sample preparation and handling. More importantly, these methods preferentially identify the most prevalent peptides, which are not necessarily the most immunogenic. Differential ion mobility spectrometry (DIMS) can be used as a filter to select targeted analytes, making DIMS coupled to tandem mass spectrometry (DIMS-MS/MS) an appealing technique for the detection of cancer antigens predicted by computational algorithms.

As a proof of concept, a model peptide pool of 94 peptides (Appendix 1) was generated and was intended to simulate a complex mixture of very similar peptides (by molecular weight, hydrophobicity, sequence) such as would be seen in a collection of antigen peptides obtained from a biological source. The target peptide selected was GLR (amino acid sequence = FLSSANEHL, 1016 g/mol), for which the peak CV is 6.5 V at a DV of 1.2 kV using G4 DIMS. The MS/MS spectrum obtained for pure GLR was compared to that obtained for the mixture of 94 peptides (Figure 5.7a). Without GLR spiked into the mixture, none of the product ions observed from pure GLR were present (Figure 5.7b). The GLR peptide was spiked into the 94-peptide pool at concentrations ranging from 1 μM to 1 pM, where the 94 other peptides were 1 μM each. For each solution the MS/MS spectrum of the at the mass-to-charge ratio of the target protonated GLR peptide was taken with and without DIMS active. The 5 most intense product ions observed in the MS/MS spectrum of pure GLR, $[M+H-H_2O]^+$, $[M+H-NH_3]^+$, $[M+H-H_2O-NH_3]^+$, b_8, and b_8-NH_3 were used to evaluate whether GLR was detectable at each concentration. With 1 pM GLR spiked into the mixture, 2 of the 5 product ions were observable at a signal-to-background ratio greater than 3, where background is defined as the signal obtained for the mixture without GLR spiked in. However, the ratio of these product ions deviated too much from the reference spectrum to consider the peptide to be detected at this concentration. With 10 pM GLR spiked into the mixture, all 5 of the product ions were observable, with a contaminant ion present that was observed without GLR (Figure 5.7c). Without DIMS, none of the product ions observed at greater than 5% relative intensity match those observed from MS/MS of protonated GLR (Figure 5.7d).

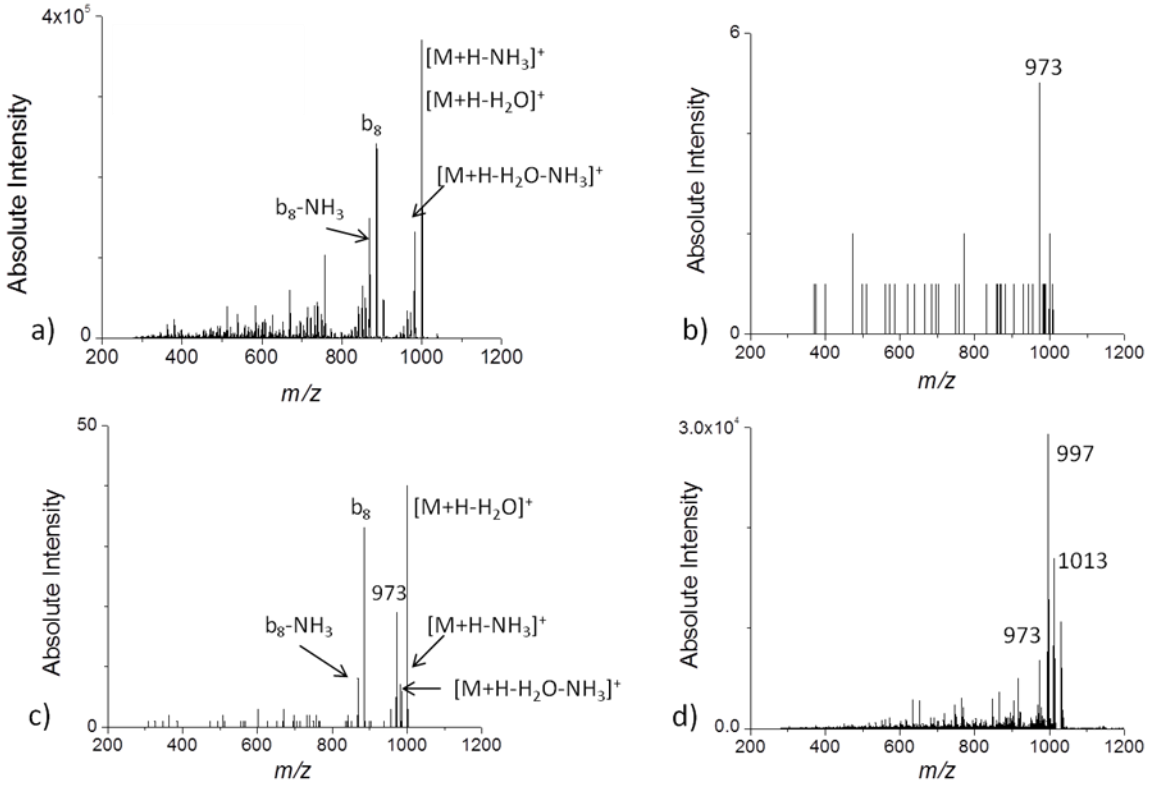

Figure 5.7. MS/MS of protonated FLSSANEHL (GLR), where (a) was obtained for 10 µM FLSSANEHL in 50/49.9/0.1 acetonitrile/water/formic acid, (b) and (c) were obtained with DIMS at a DV of 1200 V and a CV of 6.5 V, where (b) was obtained for a mixture of 94 peptides without FLSSANEHL added, (c) was obtained for the same mixture of 94 peptides, but with 10 pM FLSSANEHL in the mixture and (d) was obtained without DIMS for the mixture of 94 peptides with 10 pM FLSSANEHL.

Using the identification of 5 product ions as indicative of the detection of the target ion, a comparison of the detection of GLR in the peptide mix was made (Figure 5.8a and b), where the red line represents the signal intensity at which the signal-to-background ratio is equal to 3. In this model peptide pool, the target antigen was detected at a concentration of 10 pM in a mixture of 94 other peptides possessing similar chemical properties. Each MS/MS scan was obtained using a volume of ≈ 2 µL so the system was able to identify peptides at the low attomole level. This level of sensitivity (20 amol = 1.2×10^7 molecules) is important when considering applying this technique for use in human cancer samples. In the case of acute leukemia, most patient samples have ≈ 1×10^7 leukemia cells per mL of whole

blood with each cell possessing ≈ 10,000 HLA molecules. A routine blood draw of 10 mL would therefore be expected to yield 1×10^{12} peptides, present at various frequencies, making the application of DIMS-MS for leukemia antigen discovery feasible in most clinical samples.[13,14] In solid tumors, a 1 cm^3 sample contains ≈ 1×10^8 cells so again DIMS-MS has the potential for use in readily accessible clinical specimens.[15]

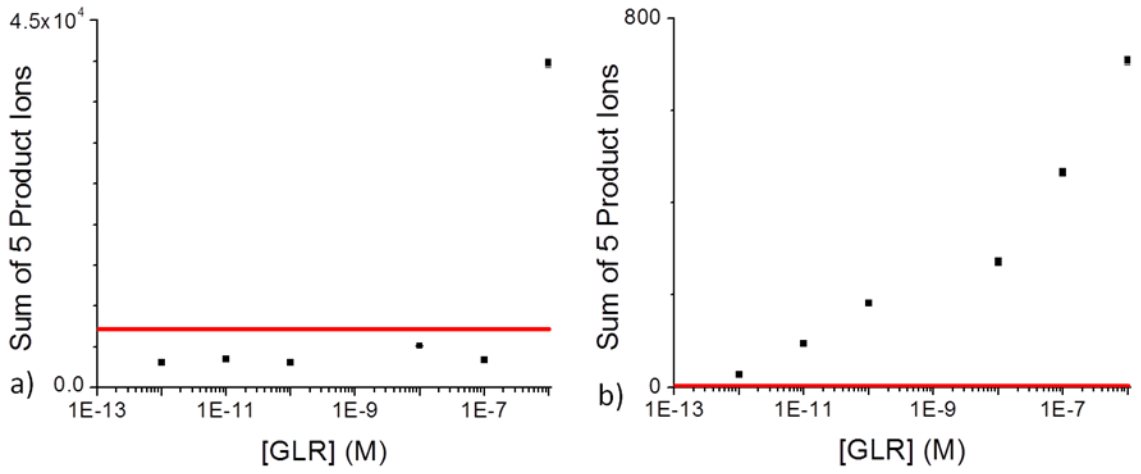

Figure 5.8. Sum of the intensities of the five most intense product ions observed from MS/MS of protonated FLSSANEHL as a function of the concentration of FLSSANEHL (GLR) in the mixture of 94 peptides, where (a) is without DIMS and (b) is with DIMS under the optimum conditions for the selection of protonated GLR. The red line indicates the signal intensity at which the signal-to-background ratio is 3, where background is defined as the signal obtained for the mixture of 94 peptides without GLR spiked in.

The optimum CV to select for sodiated CG1 (FLLPTGAEA, an antigen that had been previously identified by HPLC-MS/MS)[16] at a DV of 1200 V was determined to be 7.8 V from a DIMS scan of the pure peptide (Figure 5.9a). The MS/MS of the pure CG1 peptide is shown in Figure 5.9b. With DIMS, the peptide cell extract exhibited five product ions that matched MS/MS of the pure peptide as well as a contaminant peak (Figure 5.9c). Without DIMS, none of the product ions observed at greater than 5% relative intensity match those observed from MS/MS of sodiated CG1 (Figure 5.9d).

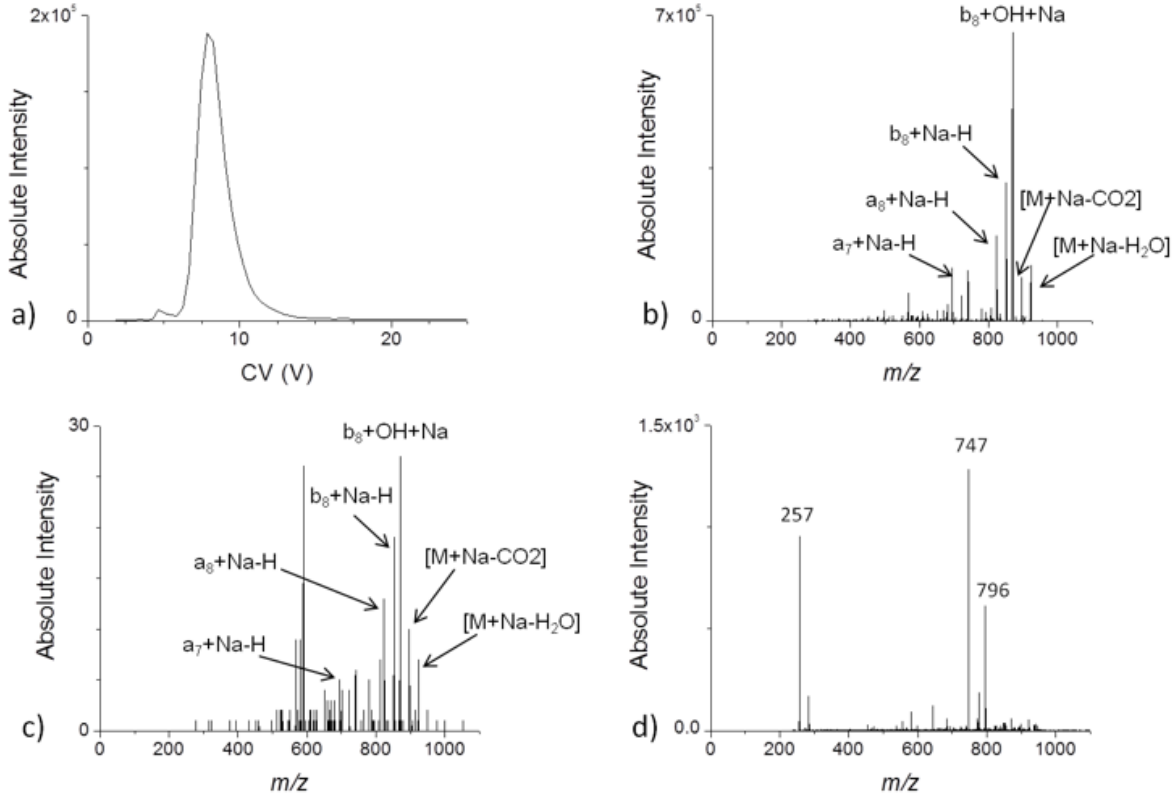

Figure 5.9. (a) DIMS scan of sodiated FLLPTGAEA (*m/z* 940.6) and MS/MS obtained for sodiated FLLPTGAEA, where (b) was obtained for 10 µM FLLPTGAEA in 50/49.9/0.1 acetonitrile/water/formic acid, (c) was obtained for the peptide cell extract with DIMS with a DV of 1200 V and a CV of 7.8 V and (d) was obtained for the peptide cell extract without DIMS.

5.6 Summary and conclusions

Immunoassays are commonly employed for the detection and quantification of biomarkers, but the specificity of these assays is often lacking. DIMS separations can provide improvements in the signal-to-background of targeted analytes when coupled to mass spectrometry. When operated in filter mode, DIMS only adds a few milliseconds to MS analysis time. For targeted biomarkers, DIMS-MS/MS may be able to provide a more specific "electronic immunoassay".

As a proof of concept that DIMS-MS/MS could potentially be used as an "electronic immunoassay", the separation of peptides in complex biological samples was investigated. BNP has an high ion transmission (83%) and resolving power (23.8) with DIMS, which can be attributed to the confined structure of BNP resulting from the disulfide linkage between Cys9 and Cys26. The utility of DIMS for the detection of BNP in human plasma was explored, and the best LOD obtained is 39 nM BNP in plasma, utilizing DIMS with PTR for MS/MS. This is three orders of magnitude higher than the decision limit used for immunoassays. However, this could be improved with the utilization of improved sample preparation methods to remove the necessity to dilute the extract by 100 times. A DIMS-MS/MS method would provide an improved degree of specificity as compared to the currently commercially available assays for BNP. If the LOD can be improved for BNP and related peptides, DIMS-MS/MS could be used to study real human plasma samples to determine which form of BNP is actually being detected by the commercially available immunoassays.

In addition to exploring the use of DIMS for the detection of BNP in plasma, the application of DIMS for the identification of leukemia antigens was investigated. In a proof of concept experiment where a target peptide was spiked into a mixture of 94 similar peptides, DIMS-MS/MS significantly outperformed MS/MS in the detection of the peptide. Additionally, a peptide that was previously identified by HPLC-MS/MS was able to be identified by DIMS-MS/MS, but not MS/MS alone.

5.7 REFERENCES

1. Katzung, B.G.; Masters, S.B.; Trevor, A.J.: *Basic & Clinical Pharmacology*. The McGraw-Hill Companies, Inc.: New York, 2009

2. Clerico, A.; Recchia, F.A.; Passino, C.; Emdin, M.: Cardiac endocrine function is an essential component of the homeostatic regulation network: physiological and clinical implications. *Am. J. Physiol. Heart Circ. Physiol.* **290**, H17-H29 (2006)

3. Clerico, A.; Emdin, M. Diagnostic accuracy and prognostic relevance of the measurement of the cardiac natruiretic peptides: a review. *Clin. Chem.* **50**, 33-50 (2004)

4. Doust, J.A.; Glasziou, P.P.; Pietrzak, E.; Dobson, A.J.: A systematic review of the diagnostic accuracy of natriuretic peptides for heart failure. *Arch. Intern. Med.* **164**, 1978-1984 (2004)

5. Clerico, A.; Fontana, M.; Zyw, L.; Passino, C.; Emdin, M.: Comparison of the diagnostic accuracy of brain natriuretic peptide (BNP) and the N-terminal part of the propeptide of BNP immunoassays in chronic and acute heart failure: a systematic review. *Clin. Chem.* **53**, 813-822 (2007)

6. Clerico. A. Pathophysiological and clinical relevance of circulating levels of cardiac natruretic hormones: are they merely markers of cardiac diseases? *Clin. Chem. Lab. Med.* **40**, 752-760 (2002)

7. Schellenberger, U.; O'Rear, J.; Guzzetta, A.; Jue, R.A.; Protter, A.A.; Pollitt, N.S.: The precursor to B-type natriuretic peptide is an O-linked glycoprotein. *Arch. Biochem. Biophys.* **451**, 160-166 (2006)

8. Luckenbill, K.N.; Christenson, R.H.; Jaffe, A.S.; Mair, J.; Ordonez-Llanos, J.; Pagani, F.; Tate, J.; Wu, A.H.B.; Ler, R.; Apple, F.S.: Cross-reactivity of BNP, NT-proBNP, and proBNP in commercial BNP and NT-proBNP assays: preliminary observations from the IFCC committee for standardization of markers and cardiac damage. *Clin. Chem.* **54**, 619-621 (2008)

9. Prontera, C.; Zaninotto, M.; Giovannini, S.; Zucchelli, G.C.; Pilo, A.; Sciacovelli, L.; Plebani, M.; Clerico, A.: Proficiency testing project for brain natriuretic peptide (BNP) and the N-terminal part of the propeptide of BNP (NT-proBNP) immunoassays: the CardioOrnoCheck study. *Clin. Chem. Lab. Med.* **47**, 762-768 (2009)

10. Clerico, A.; Zaninotto, M.; Prontera, C.; Giovannini, S.; Ndreu, R.; Franzini, M.; Zucchelli, G.C.; Plebani, M.: State of the art BNP and NT-proBNP immunoassays: The CardioOrnoCheck study. *Clin. Chem. Acta* **414**, 112-119 (2012)

11. Fmoc solid phase peptide synthesis: a practical approach; Oxford University Press: Oxford; New York, 2000.

12. Shaffer, S.A.; Tang, K.; Anderson, G.A.; Prior, D.C.; Udseth, H.R.; Smith, R.D.: A novel ion funnel for focusing ions at elevated pressure using electrospray ionization mass spectrometry. *Rapid Commun. in Mass Sp.* **11**, 1813-1817 (1998)

13. Princiotta MF, Finzi D, Qian SB, et al. Quantitating protein synthesis, degradation, and endogenous antigen processing. Immunity **18**, 343-354 (2003)

14. Yewdell JW, Reits E, Neefjes J. Making sense of mass destruction: quantitating MHC class I antigen presentation. Nature reviews Immunology **3**, 952-961 (2003)

15. Del Monte U. Does the cell number 10(9) still really fit one gram of tumor tissue? Cell Cycle **8**, 505-506 (2009)

16. Zhang M, Sukhumalchandra P, Enyenihi AA, et al. A Novel HLA-A*0201 Restricted Peptide Derived from Cathepsin G Is an Effective Immunotherapeutic Target in Acute Myeloid Leukemia. Clinical cancer research : an official journal of the American Association for Cancer Research **19**, 247-257 (2013)

CHAPTER 6: DIMS FOR THE ANALYSIS OF AEROSOLS

6.1 Introduction to the analysis of aerosols

Atmospheric aerosols can influence atmospheric chemistry[1] as well as human health.[1,2] The chemical composition, size, mass concentration, and number concentration of aerosol particles determine how these particles will affect the environment and human health.[1] Natural and anthropogenic aerosols can affect cloud formation as well as cause issues with respiratory function in humans. A better understanding of atmospheric aerosols and improved monitoring of their concentrations in the atmosphere is expected to help reduce the harm caused by atmospheric aerosols.

Currently, the majority of aerosol analysis is effected by filter collection followed by analysis of the sample directly on the filter or extraction of the sample prior to further analysis. When the filters are kept for further analysis, issues such as temperature and humidity for storage and transport conditions must be considered. Analytical methods for the chemical analysis of aerosols directly on the filter include mass measurements, X-ray fluorescence (XRF) and proton-induced X-ray emission.[3] Mass measurements provide mass concentrations of the aerosol, while other techniques are employed for elemental composition of the bulk aerosol. Methods that require extraction of the aerosols from the filter prior to analysis include ion exchange chromatography, gas chromatography-mass spectrometry (GC-MS) and inductively coupled plasma MS (ICP-MS).[3]

While the analysis of samples collected on filters can provide a some chemical information, issues such as the loss of volatile components and contamination of the filter during storage can arise. Additionally, filter collection methods do not provide information about the size or shape of the particles and they do not provide data in real time. To provide this important information, aerosol mass spectrometers have been developed for the real time analysis of aerosols.[4,5] These instruments are often equipped with a differential mobility analyzer (DMA) for size separation of aerosols and a condensation particle counter (CPC) to obtain number densities. A vacuum aerodynamic diameter is obtained by velocimetry within the mass spectrometer inlet by utilizing the time of flight of particles between chopper wheels and/or lasers. Prior to mass analysis, compounds in the aerosol particles must be desorbed and ionized. Commercially available instruments employ thermal desorption followed by electron ionization (EI) or laser ablation and photoionization.[6,7] EI and photoionization impart enough energy to compounds that fragments are often observed in the mass spectra rather than the intact compounds that made up the aerosol particle being analyzed. Therefore the empirical formulae of the molecular components cannot be determined using commercial aerosol mass spectrometers.

Our lab is interested in the development of ambient aerosol ionization techniques that do not impart large amounts of internal energy and keep the molecular components of aerosols intact upon ionization. To form the aerosol particles, pyrolysis of solids such as cellulose is performed in a chamber at 400-900°C. Ionization of the compounds in the aerosol particles is effected by extractive electrospray ionization (EESI) or low-temperature plasma ionization (LTPI). When the ionization techniques are coupled to pyrolysis, they are referred to as PyEESI and PyLTPI, respectively. Mass spectra observed from PyEESI and

PyLTPI are often complicated due to the complexity of aerosols formed by pyrolysis. Chromatographic separations are not an option for these samples because too much time would be added to the total analysis. Due to the fast analysis times, ion mobility spectrometry is a good candidate for separations coupled to the ambient ionization of compounds in aerosols formed by pyrolysis.

6.2 Experimental: pyrolysis

Aerosols were formed by the pyrolyzing cellulose (Alfa Aesar: Ward Hill, MA) or ethyl cellulose (TCI America: Philadelphia, PA), as specified. Pyrolysis for experiments performed on the Bruker Esquire3000 was carried out at approximately 600ºC utilizing a quartz crucible wrapped in a heated filament. This crucible was contained in a graphite box, through which nitrogen was passed through at 3 L/min to minimize combustion that would occur with oxygen present. Pyrolysis for experiments performed on the Bruker HCT, the Thermo LTQ-FTICR and the modified Bruker maXis Q-ToF was carried out at 650ºC using a Pyroprobe 5250 (CDS Analytical, Inc.: Oxford, PA).

The compounds in the aerosols were ionized by extractive ESI (EESI) or low temperature plasma ionization (LTPI), as specified (Figure 6.1). PyEESI was carried out by orienting the electrospray emitter over the aerosol cloud with the source region of the mass spectrometer open to the atmosphere. The electrospray solvent used was 50/49/1 methanol/water/acetic acid. PyLTPI was carried out with a custom LTP probe. Plasma is formed with helium gas by applying a high voltage sine wave at approximately 4 kHz to the inner electrode and grounding the outer sheath. In-line PyLTPI experiments were performed

with a custom mini-LTP probe. Instead of using helium, the pyrolysate in nitrogen gas was routed through the LTP probe.

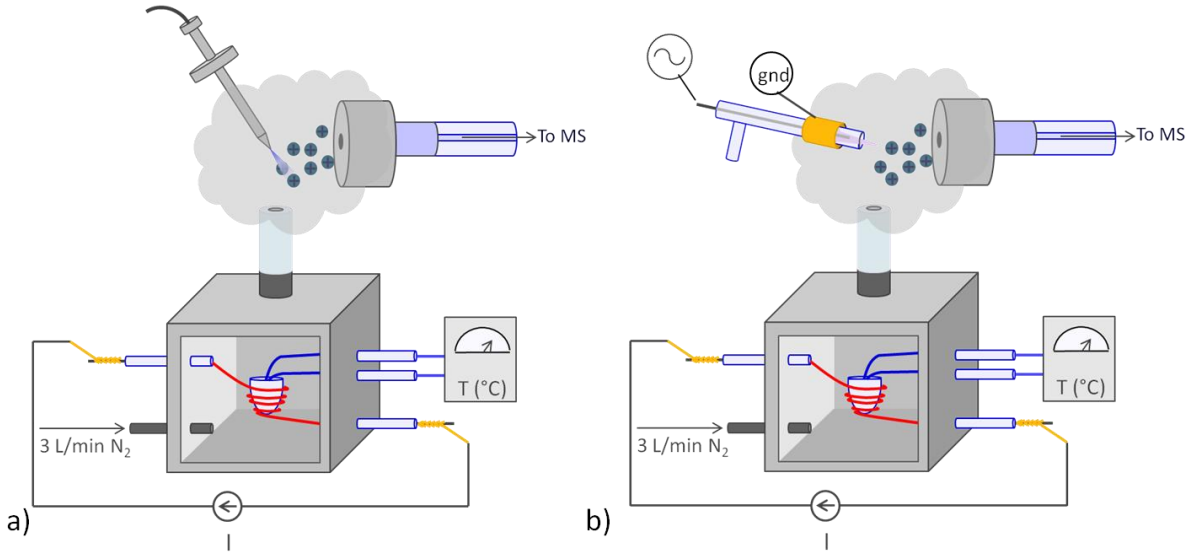

Figure 6.1 Ambient ionization techniques used for aerosol analyses: (a) PyEESI (b) PyLTPI. Figures use graphite box as representation for pyrolysis experiments, but pyroprobe was used when specified.

6.3 Ion mobility separations for aerosol analysis

6.3.1 Need for separations with aerosol analysis

Spectra obtained from the pyrolysis of natural products are often complex, even when employing an ionization source that does not cause fragmentation. A typical mass spectrum obtained by in-line PyLTPI of cellulose at 650ºC is plotted in Figure 6.2. Protonated, even electron ions are formed by both EESI and LTPI. Because cellulose does not contain any nitrogens, most of the peaks observed in the mass spectrum are odd mass-to-charge ratios. An abundance of low-mass species are observed in the spectrum, with mass-to-charge ratios less than *m/z* 400.

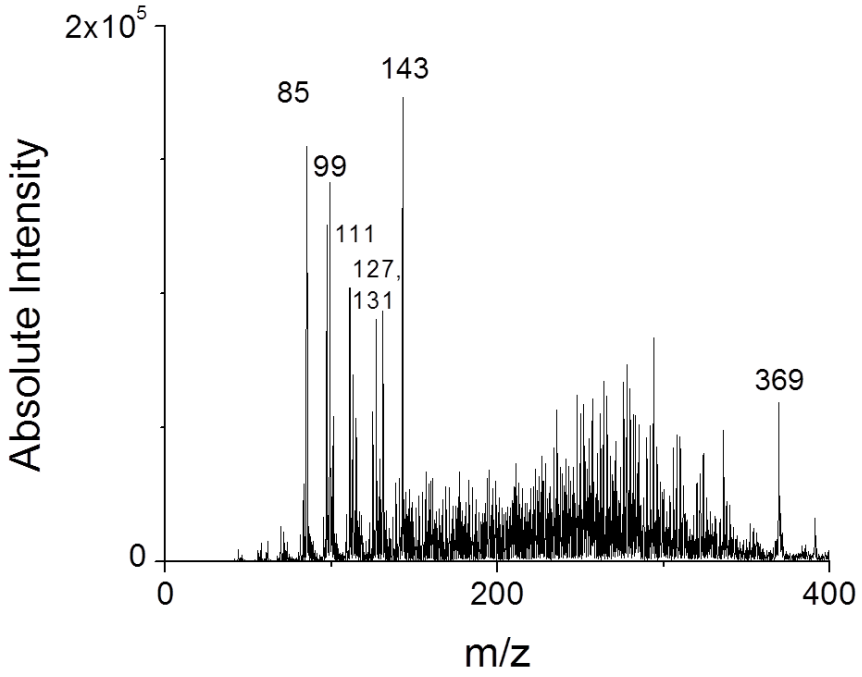

Figure 6.2 Mass spectrum obtained from in-line PyLTPI of cellulose at 650°C.

It is possible that for an observed peak in the mass spectrum, more than one species could be present at that mass-to-charge ratio. Isomers may be present in the pyrolysate, having the same chemical makeup but different structures, making them indistinguishable by mass spectrometry. Isobars may also be present in the aerosol particles, having the same nominal molar mass but differing in chemical makeup. Isobars can be distinguished by high-resolution mass spectrometers, including FTICR and high-resolution time-of-flight MS, but are not distinguishable with lower-resolution instruments such as quadrupole ion traps. Both isomers and isobars complicate MS/MS spectra because the isolation of parent ions is currently limited to about a 1 dalton window and product ions corresponding to all of the parent ions present at the isolated mass-to-charge ratio will be observed. Separations would be helpful in interpreting these complicated spectra, but to keep this as a real-time analysis,

chromatography is not an option. Due to the speed of the separations, DIMS is a good candidate for the separation of aerosols prior to mass analysis.

6.3.2 Differential ion mobility spectrometry

Representative DIMS spectra are plotted in Figure 6.3, where 6.3a is the background, 6.3b is the spectrum obtained during the pyrolysis of cellulose at 650°C, and 6.3c is the difference between the two, called the background-subtracted DIMS spectrum. In-line LTPI was used as the ionization source, and G4 DIMS was used on the Bruker HCT. The 10 most intense ions observed in the spectra were plotted as a function of the compensation field (E_C) at a dispersion field (E_D) of 33.3 kV/cm. It is readily apparent that for some of the mass-to-charge ratios plotted, multiple peaks are observed in the background-subtracted DIMS spectrum. For example, the ion observed at *m/z* 113 (plotted in pink) has two peaks in the DIMS spectrum, centered at approximately 70 V/cm and 200 V/cm respectively. Additionally, the peaks centered at approximately 200 V/cm appears to have a shoulder which may be separable from the other two peaks with improved resolving power. This suggests that isomers or isobars are present at that mass as is expected for these complex samples produced by pyrolysis.

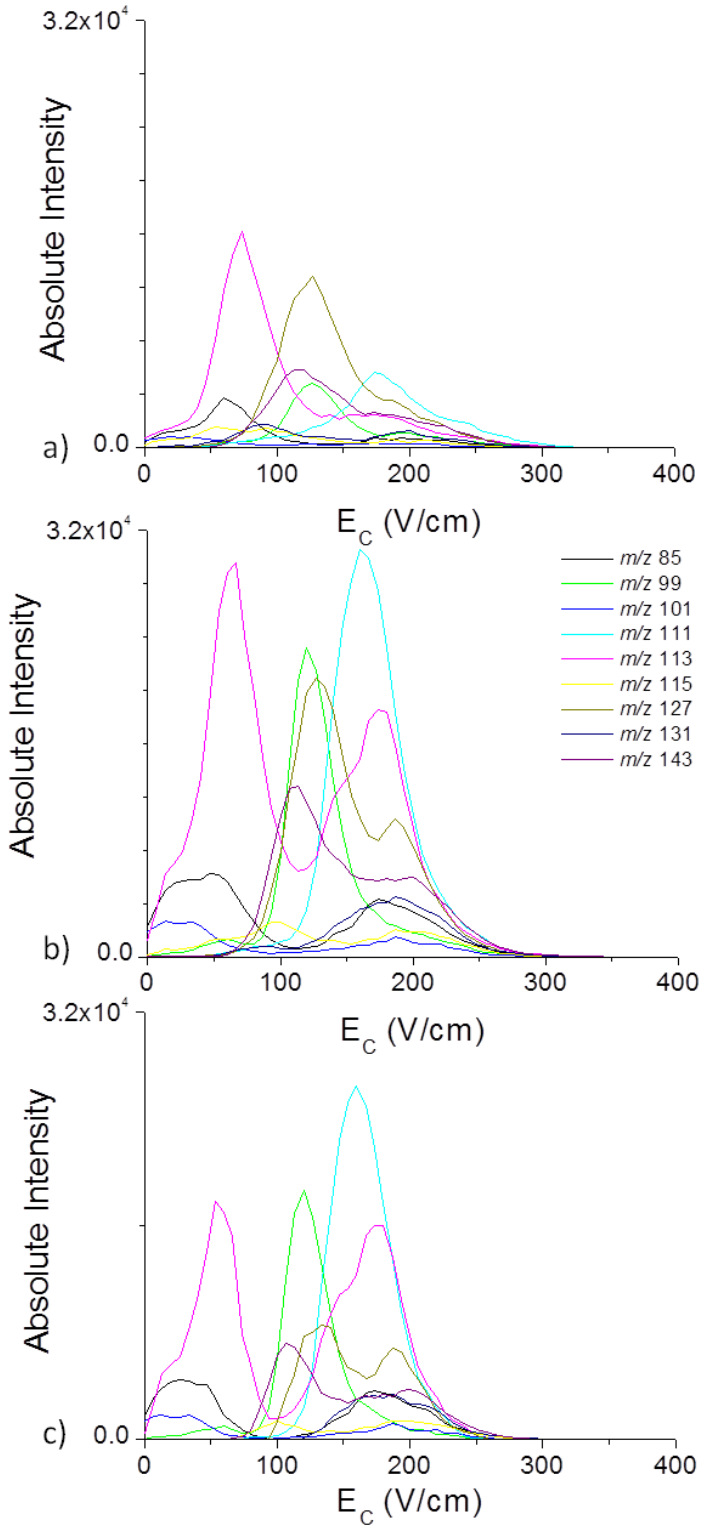

Figure 6.3 DIMS spectra obtained for in-line LTPI of (a) background: nitrogen passing through the empty pyrolysis chamber and (b) pyrolysis of cellulose at 650°C and (c) background subtracted DIMS spectrum (b-c).

High-mass accuracy MS (<10 ppm error) was performed to determine chemical formulae for the species produced from pyrolysis. Isobaric species that are unresolvable in a quadrupole ion trap MS can be differentiated in FTICR-MS instruments due to the high resolving power (>100000). Although these species can be differentiated from one another, they cannot be individually isolated for tandem mass spectrometry because isolation is performed prior to the FTICR analyzer in a quadrupole or linear ion trap as is used in the LTQ-FTICR. The difference in resolving power can be observed in Figure 6.4, where only one peak is observable at *m/z* 199 in the LIT, but three identifiable isobars are observable with the FTICR. The fourth peak, at *m/z* 199.19 was not identified because no chemical formula was able to be matched with less than 15 ppm error.

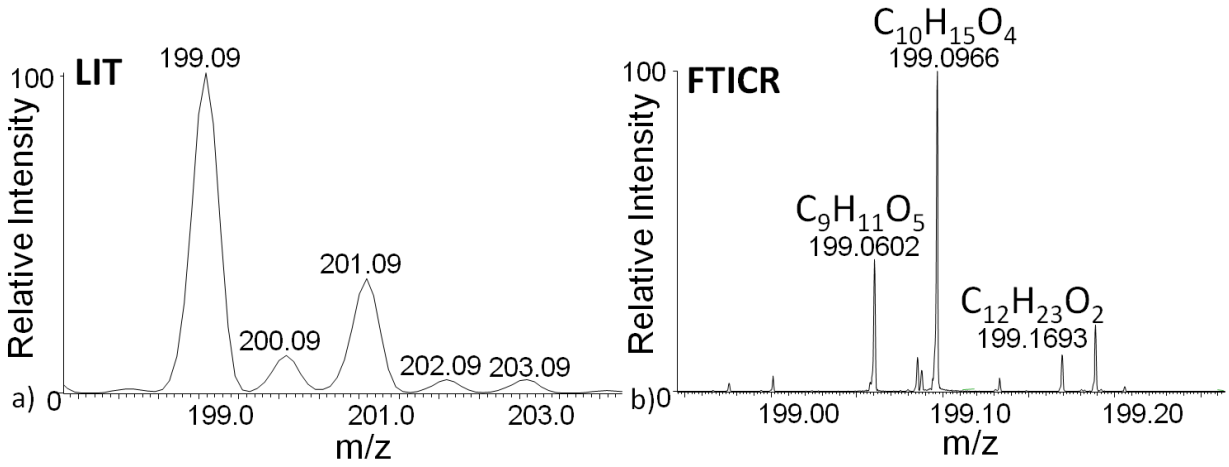

Figure 6.4 Mass spectra obtained from PyLTPI of ethyl cellulose at 650°C with (a) linear ion trap and (b) FTICR. Spectra are zoomed in on *m/z* 199 to show the difference in mass resolution.

When MS/MS was performed on the ion observed at m/z 199, the only observable product ion was at *m/z* 171 (Figure 6.5). The chemical formula of the product ion observed at *m/z* 171.0651 is $C_8H_{11}O_4$ (171.0657 Da, 3.5 ppm error). From the observed isobars in the MS spectrum, this product ion could correspond to a loss of C_2H_4 from *m/z* 199.0966

($C_{10}H_{15}O_4$, 199.0970 Da, 2 ppm error) and a loss of CO from m/z 199.0602 ($C_9H_{11}O_5$, 199.0606 Da, 2 ppm error).

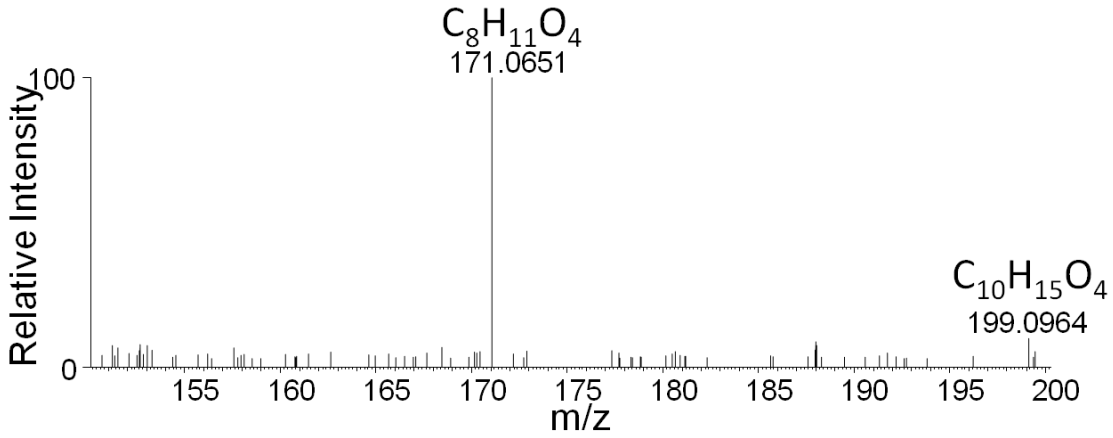

Figure 6.5 MS/MS of the ion observed at *m/z* 199 from the PyLTPI of ethyl cellulose with labeled chemical formulae.

Currently, G3 and G4 DIMS devices are not configured for the source region of the FTICR, so DIMS scans were carried out with a Bruker HCT quadrupole ion trap MS. A DIMS scan using a E_D of 40 kV/cm of the product ions observed from MS/MS of the ion at *m/z* 199 from the pyrolysis of ethyl cellulose at 650°C is plotted in Figure 6.6a. As expected a large product ion at *m/z* 171 is observed and is the biggest peak in the DIMS scan, with an optimum E_C of 350 V/cm (Figure 6.6b). If a E_C of 325 V/cm is used, an ion at *m/z* 171 is still observed, but several additional product ions are now observable as well, including *m/z* 86, 125, and 153 (Figure 6.6c). If a E_C of 275 V/cm is used, only the product ion at *m/z* 86 is observable (Figure 6.6d). The fact that multiple distinct MS/MS spectra can be observed when the compensation field is changed suggests that there are isobaric species present at *m/z* 199, as observed by FTICR-MS. The two MS/MS spectra at the lower compensation fields appear to be from trace components and are significantly lower abundance than the major ion observed at *m/z* 199. From the FTICR spectrum, it was expected that two of the isobars

would be closer in abundance relative to each other. It is possible that the two most abundant isobars were not separated by DIMS, and both dissociated to a product ion at *m/z* 171. It is also possible that at least one of the unique MS/MS spectra obtained using DIMS is due to the presence of an isomer that would not be apparent from the FTICR spectrum.

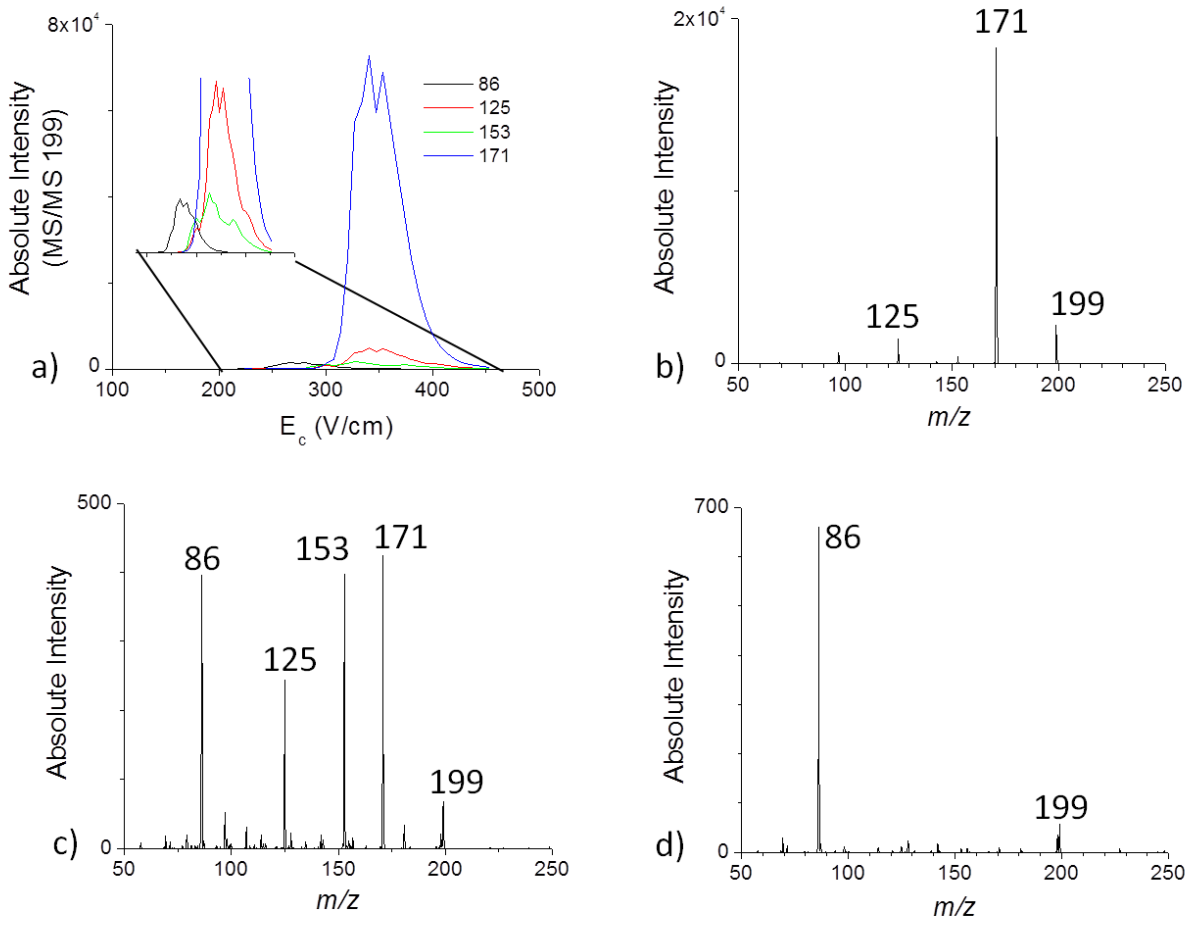

Figure 6.6 DIMS results at a E_D of 40 kV/cm for the ion observed at *m/z* 199 from the PyLTPI of ethyl cellulose: (a) DIMS scan plotting major observed product ions, MS/MS spectra obtained at a E_C of (b) 350 (c) 325, (d) 275 V/cm.

The most intense ion from PyEESI of cellulose at 600°C is observed at *m/z* 163. This cellulose sample was known to be contaminated with nicotine, for which $[M+H]^+$ is *m/z* 163. A known pyrolysis product of cellulose is levoglucosan,[8] for which $[M+H]^+$ is also *m/z* 163. The product ions observed from MS/MS of *m/z* 163 were plotted as a function of E_C at a E_D of 20 kV/cm (G3) in Figure 6.7a. At a E_C of 7 V/cm, product ions matching those observed

for a nicotine standard are observed (Figure 6.7b). At an E_C of 17 V/cm, product ions matching those observed from a levoglucosan standard are observed (Figure 6.7c). At an E_C of 32 V/cm, an MS/MS spectra is observed that does not match any of the standard compounds investigated as of yet (Figure 6.7d).

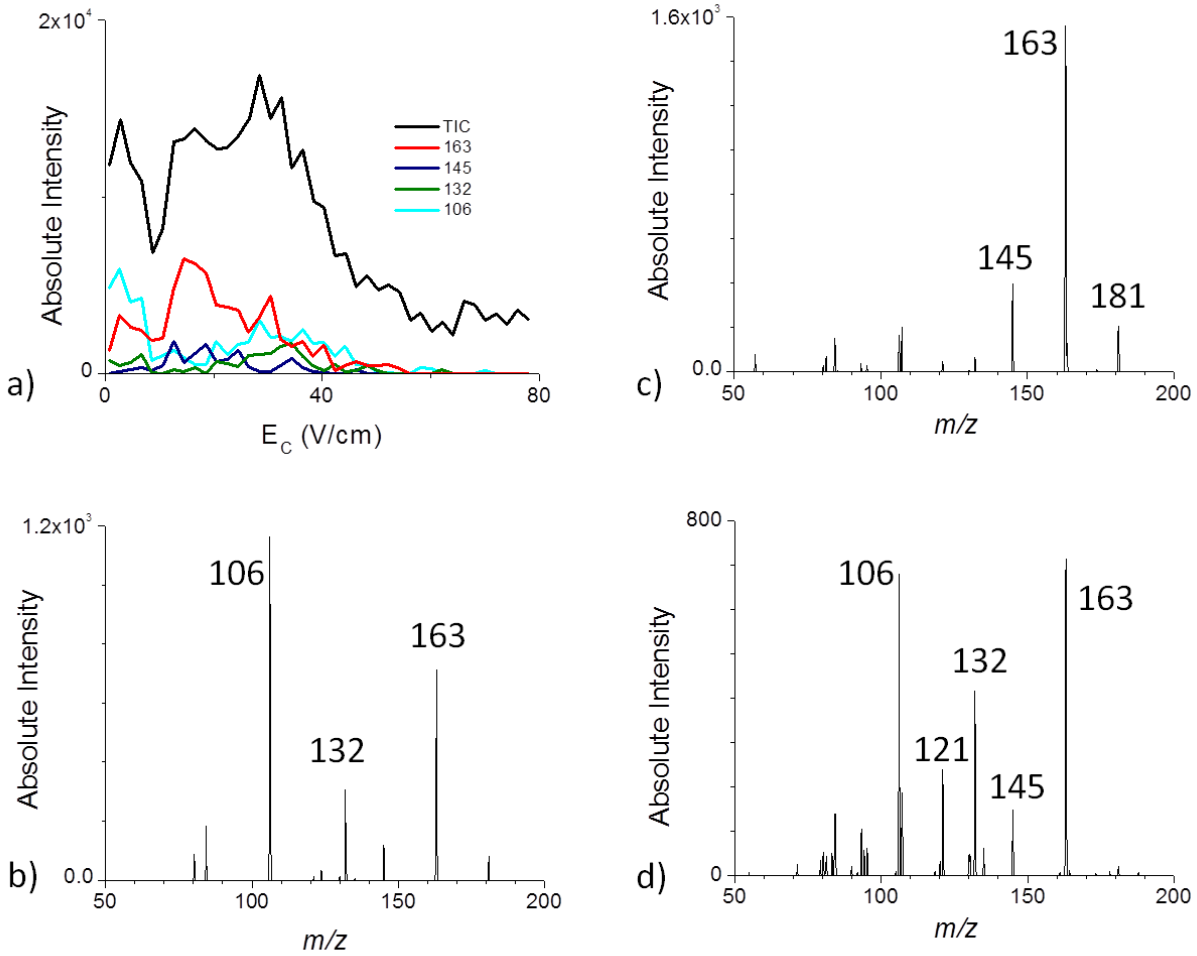

Figure 6.7 DIMS results at a E_D of 20 kV/cm for the ion observed at *m/z* 163 from the PyEESI of cellulose: (a) DIMS scan plotting major observed product ions, MS/MS spectra obtained at a E_C of (b) 7 (c) 17, (d) 32 V/cm.

One of the ions observed from PyLTPI of ethyl cellulose at 650°C is observed at *m/z* 183. Syringaldehyde has been reported to be a pyrolysis product of cellulose,[8] for which $[M+H]^+$ is *m/z* 183. Initially, it was believed that syringaldehyde was the ion observed from PyLTPI of ethyl cellulose, but the MS/MS spectrum obtained for *m/z* 183 did not match that

observed for the syringaldehyde standard, which gives a product ion at *m/z* 123. To confirm the absence of syringaldehyde in the PyLTPI spectrum of ethyl cellulose, the standard was spiked into the sample of ethyl cellulose prior to pyrolysis. Without the addition of syringaldehyde, only one peak is observed in the DIMS scan for *m/z* 183 (Figure 6.8a), but with the addition of syringaldehyde, two well-resolved peaks are apparent (Figure 6.8b). The MS/MS spectra obtained without the addition of syringaldehyde is shown in Figure 6.8c, and the MS/MS spectra obtained with DIMS active selecting for syringaldehyde is shown in Figure 6.8d.

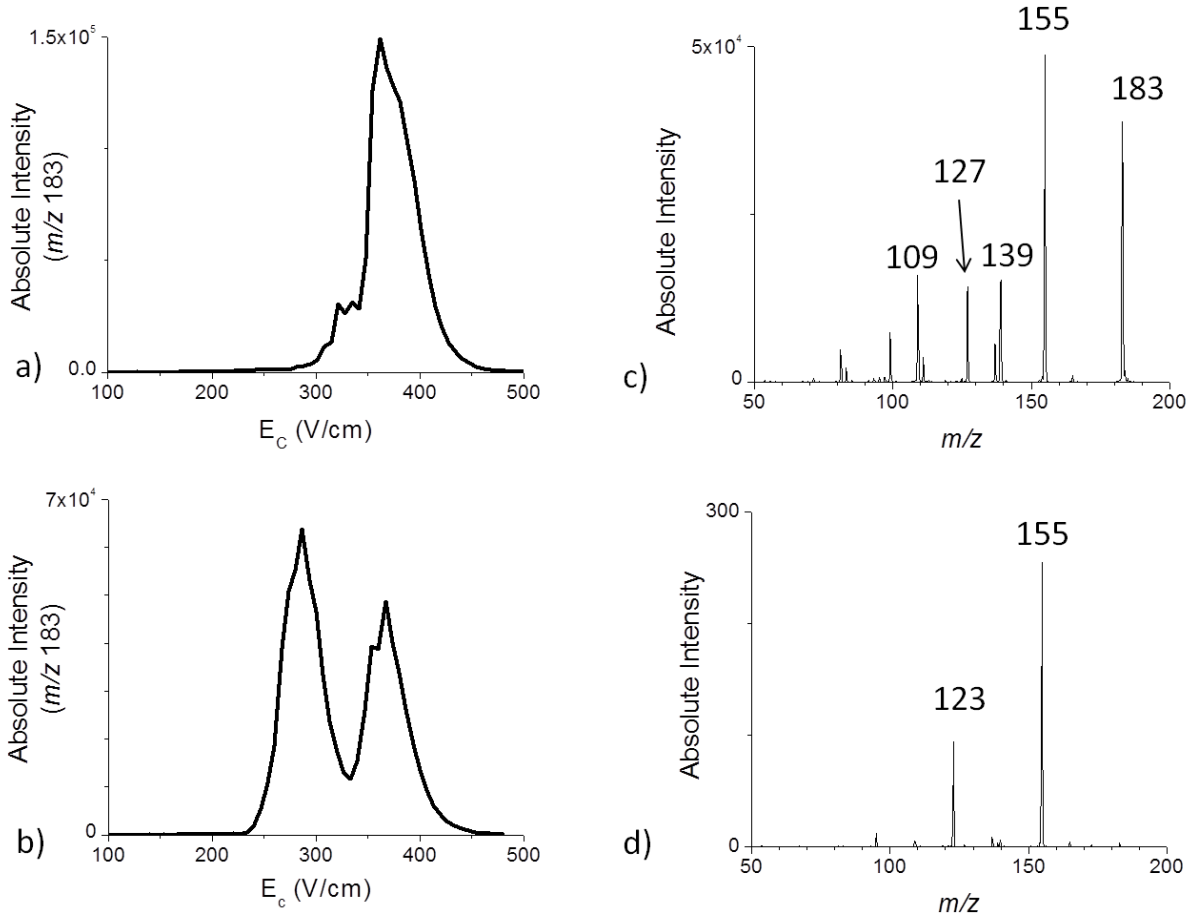

Figure 6.8 DIMS results for the ion observed at *m/z* 183 from the PyLTPI of (a) ethyl cellulose at 40 kV/cm (b) ethyl cellulose spiked with syringaldehyde, and MS/MS spectra obtained (c) without being spiked with syringaldehyde and (d) selecting for spiked syringaldehyde with DIMS.

6.3.3 Trapped ion mobility spectrometry

Collision cross-section information can be helpful in the identification of the compounds present in aerosol particles. To obtain collision cross-sections, trapped ion mobility spectrometry (TIMS, described 2.2.2) can be used. TIMS separates ions based on their low-field ion mobility which is proportional to the collision cross-section (CCS) of the ion (1.2). Using the chemical formulae determined from high-mass accuracy MS, structures can be proposed for a given ion. The energetics and collision cross-sections of the proposed structures can be calculated to determine which structure is most likely present in the sample.

In TIMS, the voltage difference ($\Delta V=V_{exit}-V_{entrance}$) between the entrance and exit lenses is ramped to separate ions based on their collision cross-section. A representative TIMS scan is shown in Figure 6.9, where mass-to-charge ratio is plotted as a function of the mobility spectrum number, which is directly proportional to ΔV. These experiments were carried out on a modified Bruker maXis Q-ToF equipped with a TIMS cartridge. For an ion observed at a given mass-to-charge ratio, the reduced mobility can be determined, which can be converted to the CCS of that ion (as described in section 2.2.2).

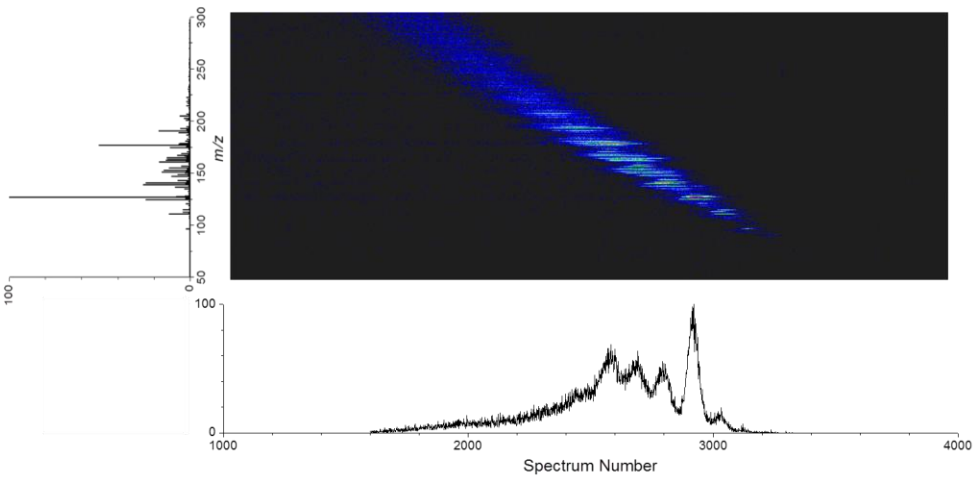

Figure 6.9 TIMS scan for PyLTPI of cellulose at 650°C where mass-to-charge ratio is plotted as a function of mobility spectrum number.

From the TIMS scan, individual mass-to-charge ratios can be selected, and the collision cross-section can be determined (2.3.2). PyLTPI of cellulose at 650°C gives rise to three isobars at *m/z* 163. From high mass accuracy MS using an FTICR, the peaks are can be identified as $C_9H_7O_3$ (*m/z* 163.0388), $C_{10}H_{11}O_2$ (*m/z* 163.0752), and $C_{11}H_{15}O$ (*m/z* 163.1116). With TIMS, each isobar can be differentiated in the ToF spectra, so a collision cross-section can be determined for the protonated molecule of each isobar (Figure 6.10). Additionally, 2 peaks are observed in the TIMS spectra of the ion observed at *m/z* 163.0388 ($C_9H_7O_3$). Although these peaks are not baseline-resolved, two Gaussian peaks were fit to the spectrum to determine the collision cross-section of each isomer.

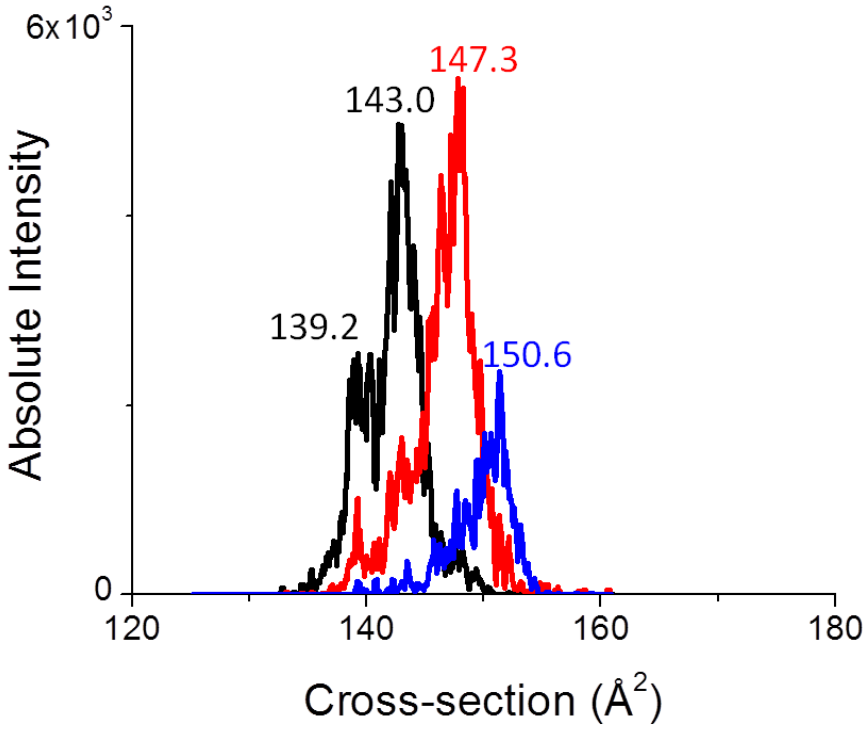

Figure 6.10 TIMS spectra for isobars observed at *m/z* 163: black line represents *m/z* 163.0388, red line represents *m/z* 163.0752, and blue line represents *m/z* 163.1116. Centroid cross-sections are given above each peak.

The ion observed at *m/z* 111 from PyLTPI of cellulose at 650°C has a chemical formula of $C_6H_7O_2$ (*m/z* 111.0439, 6.3 ppm error) determined from high-mass accuracy MS. The experimentally-determined collision cross-section from TIMS is 121.5 ± 5.4 $Å^2$ (n=5). A representative plot is shown in Figure 6.11, where the relative intensity of the ion at *m/z* 111 is plotted as a function of collision cross-section.

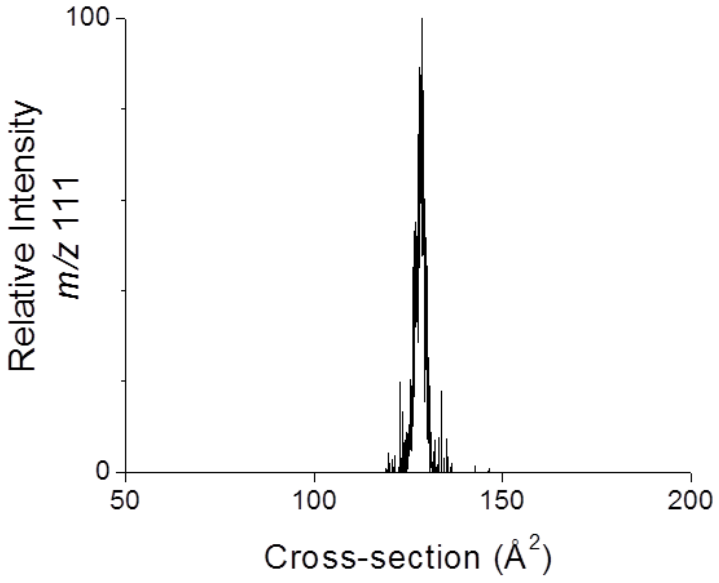

Figure 6.11 Relative intensity of the ion observed at m/z 111 from PyLTPI of cellulose at 650°C as a function of collision cross-section.

From the chemical formula, nine structures were proposed for the protonated molecule observed at *m/z* 111. Input structures were made in GaussView and then energetically minimized, using Gaussian 03.[9] The structures were minimized at four levels of theory as follows: HF/3-21G → B3LYP/3-21G → B3LYP/6-31G → B3LYP/6-31G(d,p). The output from each level of theory was used as the input structure for the next level of theory. The neutral structures were also minimized, and the energy obtained from the highest level of density functional theory (DFT), B3LYP/6-31G(d,p) is reported in Table 6.1. The structure obtained for the protonated ion from the highest level of DFT was used for the

theoretical collision cross-section calculation. Theoretical cross-sections were determined using the trajectory method with MOBCAL.[10] This program was modified for the use of nitrogen as the collision gas rather than helium.[11,12] Ten iterations were performed, and the average cross-section is reported. A summary of the proposed structures, energetically minimized structures, relative energies for the neutral species and theoretical collision cross-sections is given in Table 6.1.

The three lowest-energy structures consist of a phenyl ring with two hydroxyl groups, one of which is protonated. From the experimentally determined collision cross-section, the most likely structures for the ion observed at *m/z* 111 are protonated 3-hydroxyphenol and protonated 4-hydroxyphenol. These structures have theoretical cross-sections of 119.5 and 120.1 $Å^2$, respectively, which is well within the error associated with the experimental cross-section, 121.5 ± 5.4 $Å^2$. Several of the other proposed structures have cross-sections that match up well with the experimentally determined cross-sections for *m/z* 111, but the energy of the neutral compounds relative to the hydroxyphenols are greater than 100 kJ/mol.

Table 6.1. Structures, relative energies for neutrals and theoretical cross-section of the protonated molecules determined from proposed structures for the ion observed at m/z 111 from PyLTPI of cellulose at 650°C.

Starting structure	Energy minimized structure	Relative energy of neutral (kJ/mol)	Cross-section ($Å^2$)
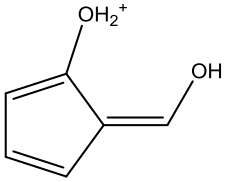	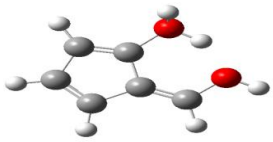	146	114.6
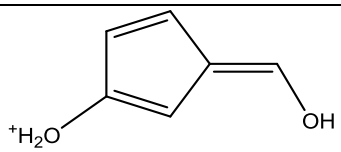	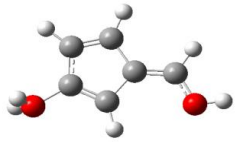	140	117.4
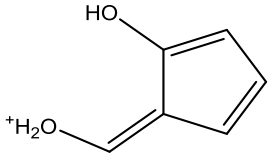	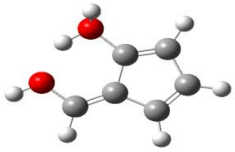	157	114.4
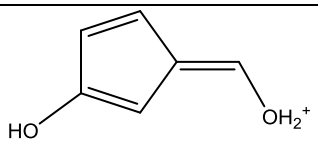	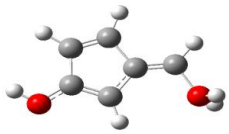	146	122.1
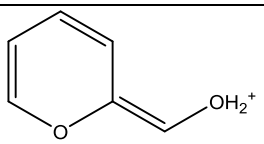	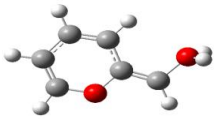	171	119.7
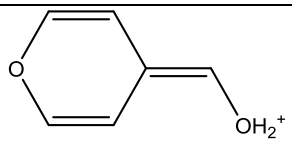	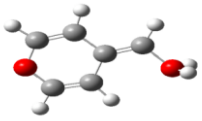	151	119.7
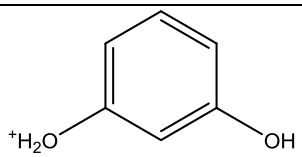	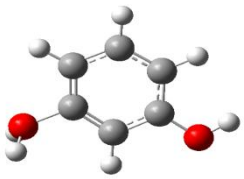	0	119.5
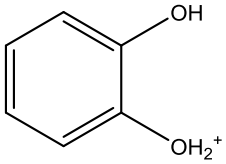	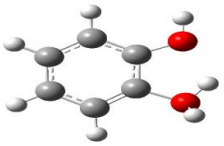	0	115.0
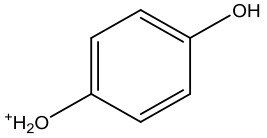	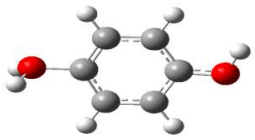	9	120.1

6.4 Summary and conclusions

Ambient ionization techniques for the real-time analysis of aerosols produce complex spectra that require separations due to the presence of isobars and isomers in the aerosol particles. Real-time analysis of aerosols is a goal and therefore chromatographic separations are not an option. Ion mobility separations are expected to provide a fast separation prior to mass analysis to help identify compounds present in the aerosol particles formed by pyrolysis. Both DIMS and TIMS were used to separate ions formed by PyEESI and PyLTPI prior to MS analysis.

DIMS has the ability to resolve isobars and isomers, providing multiple unique MS/MS spectra for a given mass-to-charge ratio observed from PyEESI or PyLTPI. This was demonstrated with the ion observed at *m/z* 199 from PyLTPI of ethyl cellulose, for which high-mass accuracy MS data revealed the presence of isobars, but MS/MS only produced one product ion. With DIMS, three unique MS/MS spectra were obtained by using different compensation voltages. The ability to separate isobars with DIMS was also demonstrated with the ion observed at *m/z* 163 from PyEESI of cellulose, for which nicotine contamination was suspected. A DIMS-scan of the product ions observed from MS/MS of the ion at *m/z* 163 revealed that protonated nicotine, protonated levoglucosan, and an additional unknown compound were all present at *m/z* 163. A DIMS scan of the ion observed at *m/z* 183 from PyLTPI of ethyl cellulose suggested that there was only one species present, for which the MS/MS spectrum did not match the MS/MS spectrum obtained for pure syringaldehyde. Syringaldehyde was spiked into the ethyl cellulose prior to pyrolysis, and an extra peak was observed in the DIMS scan for *m/z* 183. DIMS was shown to have the ability to separate isobars/isomers present in the mass spectra obtained from both

PyEESI and PyLTPI and was shown to be useful as a diagnostic tool to determine the presence or absence of a compound for which the pure compound is available for comparison.

In addition to DIMS, trapped ion mobility spectrometry (TIMS) was employed to help identify compounds present in the aerosol particles by obtaining collision cross-sections. As a proof of concept, TIMS was used to determine the collision cross-section for the isobars and isomers observed at *m/z* 163 as well as the ion observed at *m/z* 111 from PyLTPI of cellulose at 650°C. The experimentally determined cross-section from *m/z* 111 was used to help determine the structure of the ion at *m/z* 111, by comparing the theoretical cross-sections of the proposed structures to the experimental value obtained. Six of the nine proposed structures were within the error of the experimental cross-section, 121.5 ± 5.4 Å^2, so the theoretical relative energies were also considered. This leaves the two most likely structures for *m/z* 111 to be protonated 3-hydroxyphenol and protonated 4-hydroxyphenol. The combination of ion mobility with theoretical calculations could prove to be very powerful for the determination of molecular components formed by pyrolysis and will be discussed further in Chapter 7.

6.5 REFERENCES

1. Poschl, U.: Atmospheric aerosols: composition, transformation, climate and health effects. *Angew. Chem., Int. Ed.* **44**, 7520–7540 (2005)

2. Heyder, J.; Gebhart, J.; Rudolf, G.; Schiller, C.F.; Stahlhofen, W.: Deposition of particles in the human respiratory tract in the size range 0.005-15 m. *J. Aerosol Sci.* **17**, 811-825 (1986)

3. Heal, M.R.; Kumar, P.; Harrison, R.M.: Particles, air quality, policy and health. *Chem. Soc. Rev.* **41**, 6606-6630 (2012)

4. Noble, C.A.; Prather, K.A.: Real-time single particle mass spectrometry: A historical review of a quarter century of the chemical analysis of aerosols. *Mass Spectrom. Rev.* **19**, 248-274 (2000)

5. Nash, D.G.; Baer, T.; Johnston, M.V.: Aerosol mass spectrometry: An introductory review. *Int. J. Mass Spectrom.* **258**, 2-12 (2006)

6. Jayne, J.T.; Leard, D.C.; Zhang, X.; Davidovits, P.; Smith, K.A.; Kolb, C.E.; Worsnop, D.R.: Development of an aerosol mass spectrometer for size and composition analysis of submicron particles. *Aerosol. Sci. Technol.* **33**, 49-70 (2000)

7. Gard, E.; Mayer, J.E.; Morrical, B.D.; Dienes, T.; Fergenson, D.P.; Prather, K.A.: Real-time analysis of individual atmospheric aerosol particles: design and performance of a portable ATOFMS. *Anal. Chem.*, **69**, 4083-4093 (1997)

8. Rodgman, A.; Perfetti, T.A.: *The chemical components of tobacco and tobacco smoke*. CRC Press: Boca Raton, FL, 2009

9. Gaussian 03, Revision C.02, Frisch, M. J.; Trucks, G. W.; Schlegel, H. B.; Scuseria, G. E.; Robb, M. A.; Cheeseman, J. R.; Montgomery, Jr., J. A.; Vreven, T.; Kudin, K. N.; Burant, J. C.; Millam, J. M.; Iyengar, S. S.; Tomasi, J.; Barone, V.; Mennucci, B.; Cossi, M.; Scalmani, G.; Rega, N.; Petersson, G. A.; Nakatsuji, H.; Hada, M.; Ehara, M.; Toyota, K.; Fukuda, R.; Hasegawa, J.; Ishida, M.; Nakajima, T.; Honda, Y.; Kitao, O.; Nakai, H.; Klene, M.; Li, X.; Knox, J. E.; Hratchian, H. P.; Cross, J. B.; Bakken, V.; Adamo, C.; Jaramillo, J.; Gomperts, R.; Stratmann, R. E.; Yazyev, O.; Austin, A. J.; Cammi, R.; Pomelli, C.; Ochterski, J. W.; Ayala, P. Y.; Morokuma, K.; Voth, G. A.; Salvador, P.; Dannenberg, J. J.; Zakrzewski, V. G.; Dapprich, S.; Daniels, A. D.; Strain, M. C.; Farkas, O.; Malick, D. K.; Rabuck, A. D.; Raghavachari, K.; Foresman, J. B.; Ortiz, J. V.; Cui, Q.; Baboul, A. G.; Clifford, S.; Cioslowski, J.; Stefanov, B. B.; Liu, G.; Liashenko, A.; Piskorz, P.; Komaromi, I.; Martin, R. L.; Fox, D. J.; Keith, T.; Al-Laham, M. A.; Peng, C. Y.; Nanayakkara, A.; Challacombe, M.; Gill, P. M. W.; Johnson, B.; Chen, W.; Wong, M. W.; Gonzalez, C.; and Pople, J. A.; Gaussian, Inc., Wallingford CT, 2004.

10. Mesleh, M.F.; Hunter, J.M.; Shvartsburg, A.A.; Schatz, G.C.; Jarrold, M.F.: Structural information from ion mobility measurements: effects of the long range potential. *J. Phys. Chem.* **100**, 16082-16086 (1996)

11. Kim, H.; Kim, H.I.; Johnson, P.V.; Beegle, L.W.; Beauchamp, J.L.; Goddard, W.A.; Kanik, I.: Experimental and theoretical investigation into the correlation between mass and ion mobility for choline and other ammonium cations in N_2. *Anal. Chem.* **80**, 1928-1936 (2008)

12. Campuzano, I.D.G.; Bush, M.F.; Robinson, C.V.; Beaumont, C.; Richardson, K.; Kim, H.; Kim, H.I.: Structural characterization of drug-like compounds by ion mobility mass spectrometry: comparison of theoretical and experimentally derived nitrogen collision cross-sections. *Anal. Chem.*, **84**, 1026-1033 (2012)

CHAPTER 7: SUMMARY AND FUTURE DIRECTIONS

7.1 General Summary

The work presented in this dissertation has described fundamental research as well as applications for differential ion mobility spectrometry coupled to mass spectrometry (DIMS-MS). Fundamental studies are included in Chapters 3 and 4, where results presented in Chapter 3 show the importance of DIMS electrode dimensions and carrier gas parameters for the optimization of DIMS separations. Chapter 4 explores the use of DIMS for the study of ion reactions in the transfer optics of a mass spectrometer, including experiments exploring the origin of multiple peaks in DIMS separations. Following the fundamental work, biological and environmental applications of DIMS are discussed in chapters 5 and 6. The application of DIMS coupled to tandem mass spectrometry (DIMS-MS/MS) as an "electronic immunoassay" for biomarkers in biological matrices is presented in Chapter 5, and Chapter 6 explores the use of ion mobility spectrometry for the separation of compounds present in the aerosols formed from the pyrolysis of natural products. The purpose of this chapter is to summarize the preceding chapters as well as to propose future directions for this work.

7.2 Optimization of DIMS separations

7.2.1 Summary

The electrode dimensions of generation 3 (G3) DIMS were varied to determine the effect on resolving power and ion transmission with DIMS in active mode. As the length of the device

increases, the resolving power (*RP*) improves, but ion transmission (*%T*) decreases because of the increased transit time of ions through the DIMS assembly. Both *RP* and *%T* increase as the gap between the electrodes increases because the transit time increases and the effective analytical gap increases. The temperature of the DIMS carrier gas also has an effect on the separations, where the resolving power improves with increasing temperature for the peptides investigated. The carrier gas temperature can be changed by varying the desolvation gas temperature or by varying the flow rate of the desolvation gas.

DIMS separations with helium added to the nitrogen carrier gas were investigated by comparing the performance at the maximum dispersion field attainable for each *%He*. When the dispersion field is kept constant for each *%He,* an increase in resolving power (*RP*) and a decrease in ion transmission *(%T*) are observed with increasing helium content. When %He is kept constant while varying E_D, the *RP* is also improved. The maximum E_D attainable decreases as *%He* is decreased, and if the maximum E_D for each *%He* is used, the *RP* decreases and the *%T* increases with increasing *%He* for the peptides investigated. Additionally, a linked scan was developed to decrease the helium content in the nitrogen carrier gas as the CV is scanned. The resolving power of the linked scans are consistently greater than those observed for DIMS scans with static helium content.

7.2.2 Future directions

Improvements in ion transmission through DIMS when the device is active are still desired. In the current design, there is no lateral force implemented to reduce diffusion of ions parallel to the electrodes. One option to reduce lateral diffusion to improve the ion transmission is to change the makeup of the electrodes. For example, a resistive material could be used for the

electrodes to create a voltage gradient to focus ions laterally towards the center of the device. Similarly, magnetic electrodes could be used to create a magnetic field to focus ions to the center of the device. Alternatively, two electrodes could be added, electrically insulated from the two planar electrodes. These electrodes would have a small dc voltage applied to them to force the ions back toward the center of the device.

In addition to reducing lateral ion diffusion, a temperature gradient between the two electrodes could be used to cause an ion focusing effect perpendicular to the electrodes. Ion focusing and ion trapping have been reported in cylindrical DIMS assemblies.[1,2] The ion focusing causes an improvement in ion transmission as the dispersion field is increased, but also causes an increase in the peak width observed. A temperature gradient between the two electrodes has been reported to reduce or enhance the ion focusing effect, depending on the direction of the gradient relative to the compensation field.[3] Ion focusing in a planar DIMS has not yet been reported, but theoretically a temperature gradient could be applied to planar DIMS electrodes to impart an ion focusing effect, leading to an increase in ion transmission. Although this is also expected to cause an increase in the observed peak width in the DIMS scan, it would be an interesting variable to investigate.

Organic modifiers can be used to further improve the resolving powers observed from separations with DIMS. Multiple organic modifiers have been shown to improve DIMS resolution,[4-10] but the observed effects are not well understood. A better understanding of separations with gas modifiers could be gained by using small analytes with varying functional groups. The functional groups are expected to affect how the ions interact with the carrier gas modifiers, ultimately affecting the separation in DIMS. Similarly, changing the temperature of the carrier gas might alter these interactions, further improving the increases

in resolution observed by adding the modifiers alone. A linked scan for the modifiers, similar to that developed for helium, may be something to consider in an attempt to improve resolution and ion transmission.

7.3 Investigation of ion reactions using DIMS

7.3.1 Summary

The observation of multiple peaks in a DIMS spectrum is often attributed to multiple ions present at the same mass-to-charge ratio (isobars/isomers) or multiple conformations of the same ion. Investigation of the multiple peaks observed for the protonated peptide GGG and sodiated methyl-α-glucopyranoside lead to the conclusion that some of the peaks in the DIMS scan are observed as a result of multimer formation via ESI. The ion optics of commercial mass spectrometers are designed to minimize the observation of multimers and clusters. Thus, it is important to consider that multimers can be formed via ESI and be separated in DIMS but are broken down into monomers prior to mass analysis, complicating the resultant DIMS spectra.

DIMS spectra can be used to determine whether an ion was formed prior to DIMS or after DIMS but prior to mass analysis. As a proof of concept, myoglobin was electrosprayed using various spray solvents as well as varying ion optics conditions. The protonated heme group was monitored using DIMS, and it was determined that the protonated heme group formed after DIMS in the ion optics is observed at a different CV than the protonated heme group formed prior to DIMS.

Two peaks are observed in the DIMS scan of the 2+ charge state of bradykinin, one of which is suspected to be a result of a charge-reduction of some of the population of

bradykinin^{3+} after DIMS. The peak corresponding to bradykinin^{3+} has the same centroid E_C as one of the peaks corresponding to bradykinin^{2+}. When a basic solvent is added to the spray solution, the bradykinin^{3+} is no longer observed in the mass spectrum and only one peak is observed for the 2+ charge state in the DIMS scan. Utilizing a glass transfer capillary functionalized with trimethylchlorosilane, the ratio of the peak observed from bradykinin^{2+} to the charge-reduced peak decreases. This supports the proposed explanation that a reduction of some of the population of bradykinin^{3+} occurs prior to mass analysis. It is suspected that the negative siloxanes on the surface of the glass transfer capillary contribute to the observed charge-reduction.

7.3.2 Future Directions

The investigation of the charge-reduction reactions of analytes would benefit from experiments with additional analytes to see what other compounds exhibit this type of behavior in the ion optics. It would be interesting to investigate the effect of varying the basic amino acids in a peptide. For example, if a charge-reduced peak were observed for a peptide containing an arginine basic site, it might be expected to undergo a greater degree of charge-reduction if the arginine were replaced with a histidine. Additionally, the results observed with a metal capillary of the same dimensions should be compared to the results observed with a glass capillary. The surface of metal may also induce a charge-reduction and could also be functionalized or passivated for instruments that use a metal transfer capillary.

The functionalization of the glass transfer capillary should be optimized, and the stability of these functionalized capillaries in the source region of a mass spectrometer needs to be determined. For example, the stability of the functionalized capillaries could be limited

by the heat from the desolvation gas or the functional group used. The functionalization of transfer capillaries not only with trimethylchlorosilane, but with other reagents, would be interesting to explore. Reactions used for the functionalization of silica for HPLC particles will be a useful resource, much like the reaction that was used for the original experiment. For example, a reaction used to functionalize silica for ion-exchange chromatography could be used to induce a positive charge on the glass surface rather than a negative charge. This would likely require a secondary reaction with trimethylchlorosilane to "end-cap" the unreacted siloxanes. A positive surface on the glass capillary should prevent charge-reduction within the capillary and may also improve positive ion signal by repelling the ions from the glass surface.

7.4 Detection of biomarkers in plasma

7.4.1 Summary

The specificity of immunoassays for biomarkers is highly antibody dependent, but MS techniques require chromatographic or electrophoretic separations that can add minutes to hours to the total analysis times. Post-ionization techniques coupled to MS, including DIMS-MS/MS, may provide more specific analyses as compared to immunoassays, but a faster analysis method when coupled to mass spectrometry than LC-MS. For example, Brain natriuretic peptide (BNP), a biomarker for congestive heart failure, was used as a model biomarker to determine if DIMS-MS/MS could be used as an "electronic immunoassay". Adding a DIMS separation to the MS/MS method improved the LOD of BNP by about an order of magnitude, but the LOD is still about 3 orders of magnitude greater than the decision limit of BNP immunoassays.

The investigation of BNP in DIMS separations led to an inquiry into the importance of analyte structure in DIMS separations. For example, BNP has a disulfide bond, giving BNP a ring-structure with two tails. When the disulfide bond is reduced, the resolving power of the 5+ charge state in the DIMS scan decreases by greater than 50%. This suggests that the disulfide bond confines the structure of BNP whereas the reduced form does not have a well-defined structure, causing a wider peak to be observed in the DIMS scan. This wider peak shape results in spreading the signal across a wider range of compensation voltages, ultimately reducing the sensitivity when using DIMS.

Another application of DIMS as an "electronic immunoassay" is the identification of cancer antigens. These antigens consist of a 9-10 amino acid peptide fragments derived from cancer associated proteins, that are complexed to a class I human leukocyte antigen (HLA) molecules. Shotgun HPLC-MS approaches are limited due to complicated sample preparation and handling, and these methods preferentially identify the most prevalent peptides, which are not necessarily the most immunogenic. Differential ion mobility spectrometry (DIMS) can be used as a filter to select targeted analytes, making DIMS coupled to tandem mass spectrometry (DIMS-MS/MS) an appealing technique for the detection of cancer antigens predicted by computational algorithms.

The target peptide, known as GLR (amino acid sequence FLSSANEHL) was detected with DIMS-MS/MS at a concentration of 10 pM in a model peptide pool with 94 other peptides present at 1 μM each. Without the DIMS separation, the peptide was not detected at concentrations of 100 nM or below. Each MS/MS scan was obtained using a volume of ≈ 2 μL, meaning the system is able to identify peptides at the low attomole level. In addition to the model peptide pool, DIMS-MS/MS, without the use of HPLC, was used to detect a

previously confirmed cancer peptide antigen[11] in an extract from a leukemia cell line. Five product ions were observed from CG1 (FLLPTGAEA) in the DIMS-MS/MS spectrum that matched MS/MS of the pure peptide. Without DIMS, none of the product ions observed at greater than 5% relative intensity match those observed from MS/MS of CG1.

7.4.2 Future Directions

The best LOD for BNP in human plasma obtained for DIMS-MS/MS is still not low enough to be considered competitive with immunoassays. Improvements in sample preparation to reduce ionization suppression and improvements in mass spectrometer sensitivity in newer designs could improve the detection limit of BNP in plasma. For example, the protein precipitation sample preparation used for the current LOD determination required a 100x dilution to lessen ionization suppression. With improved sample preparation, such as microextraction by packed sorbent (MEPS),[12] this dilution could potentially be avoided, and concentration of the sample may even be possible. Mass spectrometers that employ an ion funnel to transfer ions from atmospheric pressure to the high-vacuum region have been shown to have sensitivities an order of magnitude greater than a capillary/skimmer interface design,[13] With improvements, DIMS-MS/MS could very well be used to reach biologically relevant LODs for BNP in human plasma.

DIMS-MS/MS has been successful in the detection of previously identified antigenic peptides in a leukemia cell line. The next step is to begin work on detecting previously unidentified antigens in the same cell line to determine which antigens predicted by computer algorithms are present in the cell line. Finally, patient samples, including peptide extracts

from whole blood and solid tumors, will be analyzed using DIMS-MS/MS methods optimized for specific antigenic peptides.

7.5 Aerosol analysis

7.5.1 Summary

DIMS separations can be used to help simplify spectra obtained for the analysis of aerosols formed by the pyrolysis of cellulose and ethyl cellulose. Compounds in the aerosol particles can be ionized by extractive ESI (EESI) or low-temperature plasma ionization (LTPI). When coupled to pyrolysis, these ionization techniques are referred to as PyEESI and PyLTPI, respectively. Complicated mass spectra are observed from both PyEESI and PyLTPI, including peaks at nearly every odd mass-to-charge ratio in the spectra. It is also believed that multiple structures could be present at the same mass-to-charge ratio as a result of the presence of isobaric and isomeric species. In some cases one of the isobaric species is present in much greater abundance than the other(s). For example, the ion observed at *m/z* 199 from PyLTPI of ethyl cellulose at 650°C has only one observable product ion (*m/z* 171) in the MS/MS spectra obtained without the use of DIMS. With DIMS-MS/MS, 3 distinct MS/MS spectra were observed by applying 3 different static compensation fields, respectively. The MS/MS spectra that looked most similar to that obtained without DIMS was the most abundant, with the other two being over an order of magnitude lower in intensity.

In addition to DIMS, trapped ion mobility spectrometry (TIMS) was used to separate ions formed by PyLTPI of cellulose based on their collision cross-sections (CCS). The TIMS scan revealed 3 isobaric species at a nominal mass-to-charge ratio of 163 with slightly

different collision cross-sections. Additionally, one of the isobars appeared to have multiple peaks, suggesting the presence of isomers. These data are consistent with data obtained using DIMS with the same sample. The CCS of specific ions can be determined from TIMS spectra. The selected "model ion", observed at *m/z* 111, has an experimental collision cross-section of 121.5 ± 5.4 $Å^2$. Theoretical cross-sections were calculated for nine proposed structures that have the chemical formula obtained for the ion at *m/z* 111 from high mass accuracy MS. Six of the nine proposed structures fell within the experimental error of the cross-section obtained by TIMS. Four of the six structures that fall within the experimental CCS have relative energies higher than 100 kJ/mol, and therefore the most likely structures present are *m/z* 111 are protonated 3-hydroxyphenol and protonated 4-hydroxyphenol.

7.5.2 Future Directions

DIMS can separate several of the isobaric species present in compounds produced by PyLTPI as well as PyEESI of cellulose and ethyl cellulose at 650°C. It would be interesting to look into the pyrolysis of more complex samples and eventually pyrolyzing whole plant leaves. The experiment will become even more complex when combustion is investigated rather than pyrolysis. For combustion experiments, air will be used instead of pure nitrogen to introduce oxygen. Combustion is known to be a more complex process than pyrolysis and is expected to produce more complex mass spectra. DIMS is expected to simplify these spectra and help to elucidate the presence of isobaric structures.

It would be interesting to couple a differential mobility analyzer (DMA) to DIMS. A separation of the aerosol particles based on their size can be achieved with a DMA prior to ionization by EESI or LTPI. In our lab, the mass spectra obtained from PyLTPI have been

observed to change with particle size, so it would be interesting to see how the DIMS spectra change with varying aerosol particle size. Two-dimensional DMA-DIMS separations should help reveal the presence of isobars and isomers with distinct MS/MS spectra by effectively expanding the separation space or peak capacity of the analyses.

7.6 REFERENCES

1. Guevremont, R.; Purves, R.W.: Atmospheric pressure ion focusing in a high-field asymmetric waveform ion mobility spectrometer. *Rev. Sci. Instrum.* **70**, 1370-1383 (1999)

2. Guevremont, R.; Purves, R.W.; Barnett, D.A.; Dang, L.: Ion trapping at atmospheric pressure (760 Torr) and room temperature with a high-field asymmetric waveform ion mobility spectrometer. *Int. J. Mass Spectrom.***193**, 45-56 (1999)

3. Barnett, D.A.; Belford, M.; Dunyach, J.; Purves, R.W.: Characterization of a temperature-controlled FAIMS system. *J. Am. Soc. Mass Spectrom.* **18**, 1653-1663 (2007)

4. Shvartsburg, A. A.; Tang, K. Q.; Smith, R. D. Understanding and Designing Field Asymmetric Waveform Ion Mobility Spectrometry Separations in Gas Mixtures. *Anal. Chem.* 2004, **76**, 7366-7374.

5. Schneider, B. B.; Covey, T. R.; Coy, S. L.; Krylov, E. V.; Nazarov, E. G. Chemical Effects in the Separation Process of a Differential Mobility/Mass Spectrometer System. *Anal. Chem.* 2010, **82**, 1867-1880.

6. Cui, M.; Ding, L.; Mester, Z. Separation of Cisplatin and its Hydrolysis Products Using Electrospray Ionization High-Field Asymmetric Waveform Ion Mobility Spectrometry Coupled with Ion Trap Mass Spectrometry. *Anal. Chem.* 2003, **75**, 5847-5853.

7. Shvartsburg, A. A.;. Tang, K. Q.; Smith, R. D. Differential Ion Mobility Separations with Resolving Power Exceeding 50. *Anal. Chem.* 2010, **82**, 32-35.

8. Shvartsburg, A. A,; Danielson, W. F.; Smith, R. D. High-Resolution Differential Ion Mobility Separations Using Helium-Rich Gases. *Anal. Chem.* 2010, **82**, 2456-2462.

9. Shvartsburg, A. A.; Creese, A. J.; Smith, R. D.; Cooper, H. J. Separation of a Set of Peptide Sequence Isomers Using Differential Ion Mobility Spectrometry. *Anal. Chem.* 2011, **83**, 6918-6923.

10. Rorrer, L.C.; Yost, R. A. Solvent vapor effects on planar high-field asymmetric waveform ion mobility spectrometry. *Int. J. of Mass Spectrom.* 2011, **300**, 173-181.

11. Zhang, M.; Sukhumalchandra, P.; Enyenihi, A.A., et al.: A Novel HLA-A*0201 Restricted Peptide Derived from Cathepsin G Is an Effective Immunotherapeutic Target in Acute Myeloid Leukemia. Clinical cancer research : an official journal of the American Association for Cancer Research **19,** 247-257 (2013)

12. Candish, E.; Gooley, A.; Wirth, H.; Dawes, P.A.; Shellie, R.A.; Hilder, E.F.: A simplified approach to direct SPE-MS. *J. Sep. Sci.* **35**, 2399-2406 (2012)

13. Shaffer, S.A.; Tang, K.; Anderson, G.A.; Prior, D.C.; Udseth, H.R.; Smith, R.D.: A novel ion funnel for focusing ions at elevated pressure using electrospray ionization mass spectrometry. *Rapid Commun. in Mass Sp.* **11**, 1813-1817 (1998)

APPENDIX 1: TABLE OF 94 PEPTIDES

Peptide Sequence	Monoisotopic molar mass (g/mol)
FLVFFLESL	1113.6
FLKNYFTDV	1145.6
SLGFFLVFFL	1188.6
LIISLGFFL	1021.6
IISLGFFLV	1007.6
CILCGLSFV	953.5
ILCGLSFVSL	1050.6
LIISLGFFLV	1120.7
FLVFFLESLA	1184.6
ELIISLGFFL	1150.7
RVFKAVEQV	1074.6
RVFQAVEQV	1074.6
LLLPPSSFM	1003.5
YLFTLEPQTI	1223.6
SLQGFVLMSI	1093.6
YLFTLEPQT	1110.5
TLYWTDCTV	1100.5
LILDAFEEL	1061.5
FLGMAVNTL	964.5
LLILDAFEEL	1174.6
WTLYWTDCTV	1286.5
ILDAFEELEA	1148.5
FIMAAILRI	1046.6
SMFAVGCSV	899.4
LLSLLLLMPV	1110.7
CLLCQPLTSV	1075.5
CLTSLLHTV	985.5
LLLSLLLLM	1027.6
IILSFVFIM	1081.6
TLNIHMTLV	1040.6
LLCQPLTSV	972.5
QLLLSLLLLM	1155.7
SLPRAAEIPV	1051.6
SLLHTVLTMM	1144.6
LLMPVHPQRL	1202.7
IILSFVFIMA	1152.6
SLLHTVLTM	1013.5
ILSFVFIMA	1039.6
TLLNTGLEKL	1100.6
ILSFVFIMAA	1110.6
FVFIMAAIL	1023.6
LLNTGLEKL	999.6
FTQELEWTV	1151.5
AVMAFDLCV	967.4
QLFYFSEENV	1274.6
AMQQQTASV	962.4

TLGIQFIGYV	1109.6
YLAWLAFTT	1084.5
FTTTLNYCV	1060.5
GLHDHTQLL	1032.5
YLAWLAFTTT	1185.6
SAMSYDLYV	1047.4
AMSYDLYVA	1031.4
FILSAMSYDL	1158.5
ILSAMSYDL	1011.5
SAMSYDLYVA	1118.5
AMSYDLYVAI	1144.5
IMFRHVCVPV	1199.6
KIMFRHVCV	1131.6
FIGSKLCPL	976.5
SLPDDDLPEV	1098.5
IMNSCVFGI	982.4
AIMNSCVFGI	1053.5
MLQVFRDISL	1220.6
GLQAIDLVYI	1103.6
LQAIDLVYI	1046.6
AMNGVIFLV	962.5
PQMEIIFFV	1122.6
MVTEFIFMGI	1186.6
NLLGSEPFAM	1077.5
NLLGSEPFA	946.5
LLGSEPFAM	963.5
FMLLIEQSGM	1167.6
VAADCLTNV	904.4
SVAADCLTNV	991.4
FLGTKHNPFI	1172.6
LVLELKNLTV	1140.7
VLPGSSSLNV	971.5
GLADLLEPV	925.5
LLLSDIPSST	1044.6
SLDEASGFNI	1051.5
GMFLMLFYNI	1247.6
TLVESTATA	891.4
KLSWFNHML	1174.6
VLAALVESPV	996.6
SIYTPVVSL	977.5
SVSIYTPVV	963.5
IMIIYWDLI	1178.6
VIMIIYWDL	1164.6
AVFDRYEEV	1126.5
ILAFYIPGL	1005.6
VILAFYIPGL	1104.6
LLLGYAVLRL	1129.7
RLRHWWVIAV	1334.8